FAULT TOLERANT CONTROL OF UNMANNED AERIAL VEHICLES USING NONLINEAR MODEL PREDICTIVE CONTROL

İNSANSIZ HAVA ARAÇLARI İÇİN DOĞRUSAL OLMAYAN MODEL ÖNGÖRÜLÜ KONTROLCÜ KULLANARAK HATA TOLERANSLI KONTROLÜ

UHUT ÇAĞRI ADAMKAYA

ASST. PROF. DR. EMİR KUTLUAY

Supervisor

Submitted to

Graduate School of Science and Engineering of Hacettepe University

as a Partial Fulfillment to the Requirements

for the Award of the Degree of Master of Science

in Mechanical Engineering

2024

ABSTRACT

FAULT TOLERANT CONTROL OF UNMANNED AERIAL VEHICLES USING NONLINEAR MODEL PREDICTIVE CONTROL

Uhut Çağrı Adamkaya

Master of Science, Mechanical Engineering

Supervisor: Asst. Prof. Dr. Emir Kutluay

June 2024, 94 pages

Within the scope of this thesis, a fault tolerant controller is designed to achieve a safe flight of the aircraft under the failure scenarios which might occur during a flight operation. A six degree of freedom aircraft model have been developed. To overcome the different types of failures, nonlinear model predictive control (NMPC) is implemented in the 6-DoF aircraft model. In particular, the thesis focuses on modeling and simulating the UAV model performance under three distinct failure scenarios: aileron jamming, rudder jamming, and a decrease in elevator effectiveness. Statistical data and decision-making rule algorithms are applied to the model to detect failure during the simulation. NMPC is designed separately for longitudinal motion and lateral-directional motion. Extensive simulations have examined the NMPC behavior under the fault scenarios. The outcomes of the thesis exhibit the reliability and robustness of the proposed approach in handling various fault situations, contributing to the progress of unmanned aerial vehicle control systems.

Keywords: unmanned aerial vehicle, 6 degree of freedom, nonlinear model predictive control, fault tolerant, longitudinal control, lateral-directional control

ÖZET

İNSANSIZ HAVA ARAÇLARI İÇİN DOĞRUSAL OLMAYAN MODEL ÖNGÖRÜLÜ KONTROLCÜ KULLANARAK HATA TOLERANSLI KONTROLÜ

Uhut Çağrı Adamkaya

Yüksek Lisans, Makina Mühendisliği

Danışman: Asst. Prof. Dr. Emir Kutluay

Haziran 2024, 94 sayfa

Bu tez kapsamında, uçuş operasyonu sırasında oluşabilecek arıza senaryolarında uçağın emniyetli bir şekilde uçuşunu sağlamak için hata tolere edici kontrolcü tasarlanmıştır. Altı serbestlik dereceli bir uçak modeli geliştirilmiştir. Farklı arıza türlerinin üstesinden gelmek için, 6-DoF uçak modeline doğrusal olmayan model tahmin kontrolü (NMPC) uygulanmıştır. Tez özellikle İHA model performansının üç farklı arıza senaryosu altında modellenmesine ve simüle edilmesine odaklanmaktadır: kanatçık sıkışması, dümen sıkışması ve irtifa dümeni etkinliğinde azalma. Simülasyon sırasında arızayı tespit etmek için modele istatistiksel veriler ve karar verme kuralı algoritmaları uygulanmıştır. NMPC boylamsal hareket ve yanal yönel hareket için ayrı ayrı tasarlanmıştır. Kapsamlı simülasyonlar, arıza senaryoları altında NMPC davranışını incelenmiştir. Tezin sonuçları, önerilen yaklaşımın çeşitli arıza durumlarını ele alma konusundaki güvenilirliğini ve sağlamlığını ortaya koyarak insansız hava aracı kontrol sistemlerinin ilerlemesine katkıda bulunmaktadır.

Keywords: insansız hava aracı, 6 serbestlik derecesi, doğrusal olmayan model tahmini kontrol, hataya dayanıklı, boylamsal kontrol, yanal yönel kontrol

ACKNOWLEDGEMENTS

First of all, I would like to thank my supervisor, Asst. Prof. Dr. Emir Kutluay, for his support and guidance. His feedback during the thesis helped me improve my study and writing skills.

Dear jury members, Prof. Dr. Murat Köksal, Asst. Prof. Dr. Selçuk Himmetoğlu, Prof. Dr. A. Ufuk Şahin, and Asst. Prof. Dr. Ali Emin, I want to thank you from the bottom of my heart for participating on my jury and for the insightful criticism you offered when my thesis was being evaluated.

I also want to extend my profound appreciation to Aslınur Ala for her unwavering support and guidance throughout my master's degree journey. Your constant support has been essential to helping me reach this milestone.

My parents, Necibe Adamkaya and Ünsal Adamkaya, have supported my academic path' unyielding support, who consistently offer direction, encouragement, and sacrifices. Their confidence in me has helped me advance, encouraging me to finish my thesis.

CONTENTS

Page

TABLES

FIGURES

SIGNS AND ABBREVIATION

Signs

α	Angle of attack
A	Aspect Ratio
a	Speed of sound
b	Wing Span
β	Angle of sideslip
$\bar{c}$	Mean aerodynamic chord
C_D	Drag coefficient
C_L	Lift coefficient
C_m	Pitching moment coefficient
C_n	Yawing moment coefficient
C_l	Rolling moment coefficient
C_Y	Side force coefficient
D	Drag force
δ_a	Aileron deflection
δ_e	Elevator deflection
δ_r	Rudder deflection
$\dot{q}$	Pitch acceleration
$\dot{r}$	Yaw acceleration

γ	Flight path angle
g	Gravity
h	Pressure altitude
H	Geopotential altitude
H_p	Horsepower
I_{xx}	Moment of inertia around the x-axis
I_{xy}	Product of inertia with respect to the xy-plane
I_{xz}	Product of inertia with respect to the xz-plane
I_{yy}	Moment of inertia around the y-axis
I_{yz}	Product of inertia with respect to the yz-plane
I_{zz}	Moment of inertia around the z-axis
m	Pitching moment
l	Rolling moment
L	Lift force
M	Mach number
n	Yawing moment
N	Load acting along the y-axis
N_x	Load acting along the x-axis
N_x	Load acting along the y-axis
N_z	Load acting along the z-axis
P	Pressure

p	Roll rate
$\dot{p}$	Roll acceleration
q	Pitch rate
$\dot{q}$	Pitch acceleration
r	Yaw rate
$\dot{r}$	Yaw acceleration
ψ	Yaw angle
R	Gas constant
ρ	Density
S	Area
T	Temperature
F_T	Thrust Force
u	Velocity component in x-direction
V	Velocity
v	Velocity component in y-direction
w	Velocity component in z-direction
W	Weight
Y	Side force
Γ	Temperature Gradient
λ	Taper Ratio

Abbreviations

AC	Adaptive Control
AoA	Angle of Attack
ANN	Artificial Neutral Network
CA	Control Allocation
CAS	Calibrated Airspeed
DOF	Degree of Freedom
EAS	Equivalent Airspeed
EoM	Equations of Motion
FTC	Fault Tolerant Control
FPA	Flight Path Angle
ISA	International Standard Atmospheric
LoC	Loss of Control
MMC	Multiple Model Control
MMS	Multiple Model Switching
MPC	Model Predictive Control
NMPC	Nonlinear Model Predictive Control
PLM	Pseudo Inverse Method
RPM	Revolutions per Minute
SMC	Sliding Mode Control

TAS	True Airspeed
UAV	Unmanned Aerial Vehicle

1. INTRODUCTION

1.1. Motivation

A fault denotes a broken part or system weakness [9], which causes a significant threat to the safety of air vehicles. Ensuring aircraft safety has remained a priority issue since the early days of aviation history. There are many historical examples where unexpected malfunctions led to catastrophic aircraft crashes. The importance of fault-tolerant controllers can be highlighted by examples of past accidents. For instance, some accidents are explained below:

- Air France Flight 447 Accident: In the Air France Flight 447 crash, the pitot tube could not measure the data accurately due to icing. The Pitot tube measures the aircraft's airspeed and then supplies that data to autopilot systems. The pitot tube is directed toward the airflow to capture static pressure and compare it to the ambient pressure. This difference is important for determining airspeed, and this measurement is critical in the control of aircraft, navigation, and safety. The accumulation of the ice on the pitot tube obstructs the airflow into the pitot tube, which leads to incorrect airspeed readings. Thus, the plane's controllers did not work correctly due to improper data gathered from the pitot tube. The pilot pushed the aircraft to stall because of the wrong data, resulting in the accident [10]. This type of accident is classified as a loss of control type fault due to a sensor fault.

- Air Midwest Flight 5481 Accident: After the take-off, the aircraft crashed on January 8, 2003. In this accident, twenty-one people lost their lives. The cables connected to the elevator were incorrectly adjusted on the elevator range, which caused a decrease in the effectiveness of the elevator surface to the given pilot input. The incorrect rigging of the elevator control system prevented the movement of the elevator in the regular range and limited the travel of the elevator in a smaller range. When both pilots pushed forward the control column, the plane failed to respond to

their commands and stalled. Because of that deficiency, the pilot could not control the aircraft properly, which caused an accident [11]. This type of failure is classified as a loss of control type of fault at the pitch axis.

- USAir Flight 427 Accident: The aircraft crashed in Aliquippa on December 8, 1994. One hundred thirty-two people died in this accident. The cause of the crash was a rudder malfunction, specifically caused by the servo valve of the control surface, resulting in the rudder moving in the opposite direction of the pilot input. This rudder malfunction forced an uncontrollable movement of the aircraft. During the approach phase of the flight, the aircraft rolled to the left, which led to a crash. This type of accident is classified as loss of control type faults due to component fault [12]. Figure 1.1 shows that after the crush of aircraft, the catastrophic result of fault can be seen. This fatal aircraft crash emphasizes the importance of using fault control systems.

Figure 1.1 USAir Flight 427 accident remains [5]

Such mentioned faults might be avoided, or the consequences of the accidents can be minimized by implementing fault-tolerant controllers (FTC). Extensive studies have been conducted to predict and proactively prevent faults in flight. An effective approach for this

purpose is integrating fault-tolerant control (FTC) algorithms. These control strategies act as security measures, providing a proactive layer of defense against potential failures and contributing to the overall safety and robustness of the aircraft during flight operations. An unmanned aerial vehicle (UAV) is a type of aircraft that is designed to fly without a pilot in the cockpit. Therefore, a working control algorithm is crucial for the unmanned aerial vehicle due to the absence of an operator in the case of faults. In this thesis, a control algorithm is worked on to avoid faults. In order to carry out fault-tolerant control studies and perform simulations, a controller is implemented in the six-degree-of-freedom aircraft model.

In the literature, many potential control theories can be found. Sliding mode, inverse simulation, nonlinear feedback linearization, dynamic inversion, and nonlinear model predictive control are some of the solutions used for the faults. The advantages and disadvantages of the control algorithms and the objective of the thesis lead to work on nonlinear model predictive control (NMPC). Some of the main reasons for preferring the NMPC are:

- Since the aircraft is a nonlinear system which have multiple inputs and multiple outputs, the controller must be able to handle nonlinear systems with multiple inputs and multiple outputs. The NMPC method allows processing multi-input and multiple-output nonlinear systems. Therefore, the NMPC method is a suitable control method for aircraft.
- Ranges of system inputs and/or outputs can be defined in NMPC. The limitations of the control surfaces should be considered, especially during fault control. Implementing the system limitations and handling the system accordingly during fault control can be easily conducted by NMPC method.
- NMPC is based on predictions regarding the future behavior of the controlled process and performs the controlling accordingly. Therefore, the system effectively aligns the predicted parameter with the desired targets, resulting in improved performance and outcomes [13].

The main objective of this thesis is to implement nonlinear model predictive control to unmanned aerial vehicle models to overcome the different fault scenarios without needing controller gain scheduling. Initially, nonlinear model predictive control is implemented in unmanned aerial vehicle for different fault types. This is called multiple modelling and switching which is active fault tolerant controller. However, initially fault detection is needed. This is done by decision making and statistical data. Then, multiple faults have been simulated to see the performance and robustness of the controller. Within the scope of this thesis, two crucial objectives are attempted to be achieved. The first objective is implementing the nonlinear model predictive control (NMPC) in unmanned aerial vehicles. The second aim is to implement a controller independent of the type of fault scenarios. Thus, regardless of the type of fault, the controller should be able to work without the need for a tuning of the control system. Multiple control theories and solution methods have been investigated to achieve these goals and presented in Section 2..

This thesis aims to show:

- Developing nonlinear six-degree-of-freedom aircraft model on unmanned aerial vehicle by the MATLAB/Simulink program.
- Derivation of the nonlinear model predictive control equations for aircraft in longitudinal and lateral-directional axis.
- Implementing the NMPC equations for the aircraft with ACADO solver for both longitudinal and lateral directional axes.
- Establishing and implementing fault detection algorithm which is based on statistical data and decision making rule.
- Making multiple NMPC's for different failures based on multiple modelling and switching algorithm.
- Combining UAV model as a plant and NMPC model as a controller in Simulink environment.

- Solving the NMPC problem with the ACADO program.
- Examining the NMPC behavior under the multiple fault scenarios.

1.2. Objective

This study will examine and simulate the loss of control type of faults with the nonlinear UAV model. Sensor faults are not evaluated in this study. It is assumed that the model is capable of reading the outputs perfectly without any error. Actuator and component faults will be examined with different combinations and magnitudes of fault degrees within the scope of this thesis.

Actuator and component faults will be simulated within this thesis. Two different scenarios will be examined. One of them is the component fault type. Suppose one of the control surfaces lost its effectiveness to some degree by icing or another reason. In this type of fault, it will be assumed that control power is decreased. This is done by reducing the aerodynamic effects of the control surfaces and seeing that the aircraft can still follow the given trajectory with the decrease in the control power of the control surfaces on the aircraft. This failure will be done on elevator surfaces with different deficiency magnitudes. The second type of fault is selected as the actuator fault. In this type of failure scenario, the control surface is stuck at other positions. For example, the rudder is stuck at zero degrees, five degrees, eight degrees, or negative deflections. Then, the aircraft tries to turn with an aileron, only doing coordinated turn maneuvers. After that, the aileron surface will be stuck at different deflections to see if the rudder can handle the coordinated turn. In this way, the controller can find optimum solutions to varying types of faults and different magnitudes of faults. These failure scenarios have a vital complication, which is control input limits. Effectiveness lost and stuck at rudder/aileron failures results in the controller giving more input. Because of that, the limit of the control surfaces should be considered during the control action. The selection of the controller design is related to handling this constraint.

1.3. Contributions

The primary contribution of this thesis is developing a fault-tolerant control strategy for unmanned aerial vehicles (UAVs) using nonlinear model predictive control (NMPC), examining multiple fault scenarios, and switching the model algorithm according to detected fault type.

1.4. Thesis Overview

The thesis format is designed to provide a comprehensive overview of the research project. It starts by explaining the objective and problem statement, providing a clear base for further discussion. After that, a detailed analysis of the historical background and an in-depth discussion of the theoretical aspects related to the concept under consideration are presented. Next, the thesis discusses a nonlinear six-degree-of-freedom aircraft model in detail, outlining each step of its development for clarity. Then, the thesis discusses the NMPC theory with its basic principles and approaches. In addition, the equations that describe low-fidelity aircraft models are outlined and implemented in NMPC as a predictive model. The last phase of the thesis is a discussion of simulation results that give evidence to support proposed methodologies. Finally, the thesis concludes by outlining essential issues and recommendations for further research work.

The outline of the thesis is as follows:

- **Chapter 1: Introduction** presents the thesis scope, explains the thesis motivation, aims, and contributions, and summarizes the thesis outline.
- **Chapter 2: Background Overview** provides detailed information about fault types, fault-tolerant control theories, and nonlinear model predictive control. This part covers what has been done in fault tolerant control and the advantages and disadvantages of the controllers. The reasons behind the selection of the nonlinear model predictive control are explained.

- **Chapter 3: Nonlinear Aircraft Model** supplies unmanned aerial vehicle properties and a nonlinear model of the aircraft, including aerodynamic, engine, mass, atmosphere, and six degrees of freedom equations of motion models. The trim algorithm of the model is explained. At the end of this section, the UAV model is presented.

- **Chapter 4: Nonlinear Model Predictive Control** introduces the theory of the nonlinear model predictive control. The controller's working principle and the NMPC features are depicted. Low-fidelity model equations, which are used for NMPC, are given in this chapter. Implementation of NMPC and UAV model is described. NMPC is divided into two parts: longitudinal and lateral-directional parts. Step-by-step derivations and implementations of the degree of freedom model are presented.

- **Chapter 5: Fault Tolerant Control** explains the multiple modelling and switching algorithm concept. Statistical methods and decision-making rules are presented to detect the faults in the aircraft.

- **Chapter 6: Result** demonstrates the results of the failure simulations of the study. Failure simulations are conducted with different fault types for longitudinal and lateral directional axes.

- **Chapter 7: Conclusion and Further Studies** shows the contributions of the thesis by the outcome of the study to the literature and gives some recommendations for further studies.

2. LITERATURE SURVEY

2.1. Introduction

In this section, detailed literature review is presented. Fault classifications, fault tolerant controller are mentioned. A fault is an error of a parameter of the system by deviation from the standard condition [14]. The outcome of the fault might be insignificant or crucial to the system, which depends on the significance of the failure type. In the aerospace industry, these faults mostly lead to catastrophic accidents, resulting in many casualties. In the history of aviation, safety measures have been taken with the lessons learned from the detection of security flaws and tragic accidents, and new technologies have been developed, taking into consideration fatal experiences.

Aircraft accidents might be avoided, or the consequences of the accidents can be minimized by implementing fault-tolerant controllers (FTC). Such fatal accidents usually occur as a result of several errors coming together. Failure to notice or late detection of a malfunction in the systems by pilots affects the consequences of accidents. The use of fault-tolerant controllers eliminates human error. This thesis aims to design a fault-tolerant control algorithm to prevent and mitigate the accidents caused by unexpected faults and ensure safer aviation practices for the future.

2.2. Fault Classification

In the literature, aerospace industry faults are classified into several types. Classification of faults in aviation includes critical faults such as loss of control type, runaway faults, system malfunction, fire, collision, and flight into terrain [15]. In the scope of the thesis, loss of control type faults are examined and simulated with FTC. Thus, some of the loss of control type failures can be overcome with the implementation of appropriate controllers for the aircraft. Lost control type faults include component losses, indicating damage in a

surface structure, sensor failure involving wrongly received data and actuator malfunction causing the incorrect movement of a control surface [16].

Loss of control type faults consist of three sub-types:

Components faults: This type of fault is mainly related to structural distortion. This results in changing the aerodynamic characteristics of the aircraft and the mass or inertia of the aircraft. This type of fault is classified as the most difficult to handle. Detecting and managing component failures is crucial to maintaining the security and dependability of aircraft operations. In most aircraft, pilots cannot directly see the wings and tail while sitting in the cockpit under normal flight conditions. However, some larger aircraft may have a design that allows limited visibility of the wings and tail through windows or cameras. Additionally, onboard cameras or other sensors provide a view of the components of many UAVs. Controlling surface damage or breakage of any structure is an example of such failure. The structure may break completely, or some of it may be damaged. In the absence of a FTC, damage may need to be determined visually [17].

Sensor faults: Sensor faults are due to incorrect measurement by the sensors or loss of connection from the sensors. The breakage of a wire connecting a sensor or lack of contact in the cables can lead to a loss of connection and incorrect data in the control cockpit. Disruption of the sensor can result in unreliable data during flight. Ice accumulation on the sensors, like pitot tubes, leads to incorrect measurements. Also, contaminants like dust and dirt cause incorrect data readings. The effects of electromagnetic interference occurring from nearby electronic devices or radio frequency sources can influence the sensory readings, thereby making false data values into being recorded in measured results. These failures result in a partial or false reading on the head on display in the cockpit. These readings can be noise data, bias errors, or downright wrong data. The pilot must realize that there is a failure on the data and intervene for safe flight [18].

Actuator faults: Actuator faults can yield a decrease in the control power of the aircraft or loss of the control surface fully, which results in no controlling authority of the failed axis. Actuators are located at primary and secondary control surfaces: the elevator, rudder,

aileron, flap, spoiler, tabs, and speed brake. That fault might be the result of a decrease in control power by limiting the range of the surface or getting stuck at a specific location, causing a complete loss of control authority. This can lead to difficulties in maintaining stable flight and controlling the altitude, heading, or angle of the bank. When faced with such a fault, the pilot must react to land the plane safely as soon as possible. It may be necessary to turn the aircraft, rotate its heading, control the bank angle, and change altitude in order to land. Pilots may need to use additional control inputs to compensate for the loss of effectiveness in the main related control surfaces of the aircraft. The pilot workload may increase when such failure is encountered. This type of fault causes many accidents, as mentioned in Section 2.1..

2.3. Fault Tolerant Controllers

A fault-tolerant controller (FTC) controls the plant in the case of a failure. FTC is commonly categorized into two primary classifications: passive FTC and active FTC [19]. Passive FTC is a control system which is able to tolerate faults without the need for explicit fault detection or active reconfiguration during a failure [20]. However, passive FTC cannot be convenient for all failure scenarios and can tolerate limited failure cases. Hence, it has limited tolerance capability. Since the failure detection system is not included in passive FTC, failure of the entire system, which can lead to catastrophic accidents, might occur without warning in the case of the failure exceeding the capability of the passive FTC. The advantages of passive FTC are that it takes a very short time to find a solution to the failure, it is computationally cheaper, it is easy to implement in the system, and it is reliable for limited failures. Active FTC actively detects and isolates faults. So that it uses real-time system data, active FTC can handle multiple types of faults by modifying the controller system design. Complex faults can be taken care of with this type of FTC. However, it takes time to find the optimal solution, is computationally expensive, and is more complicated to implement the system.

Regarding aircraft flight safety, it is essential to detect faults and malfunctions by control systems and ensure a safe landing. Therefore, many studies have been carried out on fault-tolerant control systems. This section provides a comprehensive understanding of fault-tolerant control systems to establish the groundwork for the current study by examining the previous studies in this field. Since control systems allow for solving problems with various control methods, literature studies in this field have different methods and approaches. Critical studies in this field, which are based on the different fault-tolerant control system methods, have been examined and formed the basis for the methodology of this thesis study.

There are several methods for active fault controllers to react when a fault of the system is detected. The most common methods are model switching and adaptive control methods. Multiple Model Switching (MMS) method utilizes various dynamic models, each representing the system's behavior under predefined fault scenarios [21]. The models are designed to maintain safe operation or mitigate the effects of the fault. When a system malfunction is detected the control system switches the model according to detected fault and the new control algorithm act to control the system safely according to fault. Adaptive Control method allows the system to self-adjust to adapt to detected fault conditions. Adaptive control algorithms continuously update the parameters or structure of the control system by monitoring parameter changes or uncertainties in the system. Adaptive control is generally achieved through a reference model representing the desired behavior of the system or direct estimate of the unknown parameters or dynamics of the system based on input-output data.

A comprehensive literature review has been conducted to investigate the fault-tolerant control methodologies. Among the extensively used approaches in the literature, several prominent fault-tolerant controllers have been explained. Depending upon their applicability, these controllers vary, with some specifically designed for linear systems while others capable of coping with both linear and nonlinear systems. Each controller method's advantages and disadvantages discussed in detail gives a perspective about the

benefits and limitations. The selection of the controller to handle the failure of a nonlinear aircraft model is based on evaluating the advantages and disadvantages of the controller.

Model Predictive Control (MPC) is a passive control method that works with nonlinear or linear systems with multiple inputs and outputs[22]. With this method, constraints can be defined easily for inputs and outputs. Based on its robustness, the controller can handle the fault problems without needing the fault detection system or specific modeling of the fault type [23]. However, the controller might face fault types or multiple faults at the same time, which it is not able to handle. Moreover, this method takes a long time to find the optimal solution. Liu et al. worked on a trajectory tracking algorithm for Flapping-wing UAVs [24]. Since the MPC method has the drawback of the difficulty to build the predictive model, the high computational complexity, and the poor real-time performance, the authors did not proceed their study with the MPC method and offered the Model-Free Predictive Control (MFPC) algorithm instead. MFPC uses a dynamic linearized model as the prediction model [24]. The simulation results clearly indicate that the MFPC yields the computation time reduction for a certain trajectory of 46% with respect to the classical MPC. On the other hand, it decreases the tracking errors of circular and S-shaped trajectories with over 96% than PID and Model-Free Adaptive Control algorithm [24].

Multiple Model Control (MMC) is an active control method which uses multiple models for the control of the nonlinear systems[25]. It can be used for multiple conditions and uncertainties with good stability and performance. For the control of the fault scenarios, various fault contained systems should be modelled. Multiple tuning is required for each model design based on the fault type. Therefore, complexity of the method is increased because of designing various models. However, the method can be used for multiple conditions and uncertainties with good stability and performance. Also, MMC requires a fault detection systems to switch between case specific control models.

Ahn et al. [26] studied a fault-tolerant flight control system based on an adaptive and sliding mode control scheme. The method employs adaptive control techniques and

sliding mode control to improve the system's robustness and fault tolerance functions. The main advantages of this scheme are the decrease of the sliding mode controller gain and the removal of the need for explicit fault detection and isolation. The control architecture relies on the timescale separation principle to simultaneously deal with the fast inner-loop dynamics and the slow outer-loop dynamics. The stability testing uses the Lyapunov theory and ensures that the control law with the adaptation mechanism will perform relatively reliably. The approach is verified by simulation of push-over and roll maneuver and demonstrates a satisfactory outcome despite the faults in the actuator and the nonlinearities in the aircraft systems. The fault detection and isolation process is not required since the system benefits the robustness of the method.

Ducard et al. [27] presented a fault tolerance module for fast-acting and low computational power, capable of addressing actuator faults while still using the existing control setup. Thus, no controller redesign is required. It computes control surface deflections for aerodynamic moments, particularly for fault-tolerant systems. Advantages include handling the limitations of the actuators, increasing the objective function, and dealing with failures without altering the control law. Fault detection is based on the direct measurement and estimation-derived approach, such as the extended multiple model adaptive estimation. Analytical algorithms are created to diagnose a single actuator problem to ensure that the functional actuators are taking over the control. Simultaneous failures are resolved by re-calibrating equations that include actuators and drives and by considering the actuators' limitations. When a fault is detected, the supervision module starts an implicit law from the specified laws, which governs how functional actuators compensate for the fault. This dynamic self-adjustment can maintain the system's operation efficiency without manual intervention or the redesign of the control law. The model matches the accuracy of the optimization-based techniques and offers much faster computation, making it suitable for applications that require real-time processing and limited computational resources.

Caliskan and Hajiyeva [28] worked on a fault-tolerant UAV flight control system that utilizes Kalman Filters (KF) to detect sensor/actuator faults and a Two-Stage Kalman

Filter (TSKF) for fault isolation. The developed fault-tolerant UAV flight control system does the fault detection and isolation via Kalman filter, with a two-stage Kalman filtering algorithm for sensor and actuator faults handling. The fault isolation algorithm with two states of Kalman filtering is used that in order to detect the sensor-actuator faults and measures the loss of controllability and the magnitude of stuck fault. Control reconfiguration is a process of ongoing the initialization of the feedback controller according to the fault diagnosis. Control inputs are stimulated with pseudorandom noise to achieve estimation of stuck magnitudes and loss of effectiveness. Simulation results demonstrate fault detection, isolation, and identification for both sensor and actuator faults, including partial loss and stuck faults in actuators. To verify the implemented model, the results of simulation exhibit successful determination of faults in the stabilizer states and system parameters (with TSKF) by adapting simultaneously, which help identify stuck states and partial loss of energy. Kalman Filters and Two-Stage Kalman Filters could become computationally heavy processes, especially in real-time applications where the timely response is of importance. This will cause difficulties in terms of processing power and response times, especially for those UAVs that come with a limited computer capacity leading to accelerated request processing.

Zogopoulos-Papaliakos et al. [29] conducted a thorough investigation on fault-tolerant control scheme for fixed-wing UAVs between them, taking into account flight envelope awareness. This is done through different controllers, including Pseudolinear Model Predictive Controller for angular velocity, linear velocity, and position, and path planning, done using Simple Sparse Rapidly-exploring Random Trees (SST). The system combines fail-safe controllers and planer to protect it against combinations of sensor and actuator faults that the unmanned aerial vehicles (UAVs) may encounter. In the design, the loss of efficiency from any control surface, control surfaces stuck, propulsion loss, aerodynamic changes, and loss of sensors such as AoA/AoS sensor, pitot tube, and GPS sensor were assessed. The created fault-tolerant model indicates that the time-separation of control layers and long prediction horizon would be enough to refract most failures. However, in principle, it is impossible to reach complete fault tolerance. On the other hand,

some difficulties, like propulsion losses, exist, but finding a workaround is imperative. The Sparse Stable RRT planning framework is practical, yet not globally optimal, to trash the trade-offs that come with it. Alternative controller schemes are developed for whatever results in an MPC scheme requiring a fault. Though these methods may show different effects in all situations, the designer must consider the possibility of reduced control performance, stability, or even severe consequences. Ultimately, the fault-tolerant control system effectively counters faults causing control loss, typically linked with the out-of-trim point, even when flying far from the trim point.

Dimogianopoulos et al. [30] proposed a statistical approach to the fault detection and isolation (FDI) scheme for aircraft systems based on flight orientation data. Unlike instrumentation data, the attitude makes detecting and identifying failures faster and more cost-effective. The scheme is based on stochastic TFP-NARX representations, which provide consistent models for atmospheric conditions, flight phases, and maneuvers. With the help of relational modeling among data and attitudes, high accuracy is achieved. It discovers the TFP-NARX nominal models in normal conditions and the dynamics under fault conditions, which are compared by applying nominal and current modes for FDI. Assessment of a few high-end flights confirms exceptional operation stability and performance, which is maintained even in turbulent atmospheric conditions. To sum up, the system provides a highly functional approach to FDI targeting. It shows greater accuracy in accomplishing the goals than old system designs and can handle cross variations in fault magnitudes and environment depending on the conditions.

Cieslak et al. [31] applied a signal-based method for detecting jamming failures of aircraft control surface servo-loops, one of the key elements ensuring safety in civil transport airplanes. The method utilizes a sliding-mode differentiator to obtain signal derivatives in a noisy environment and the decision-making rule to identify the jamming data, which is possible even near zero values. The scheme has been tested on Airbus facilities and proven strong enough to adjust various actuator types with minimal change. The study aims to fill the gap between traditional research methods and actual manufacturing needs and thus focus on the practicality and reliability of the results.

In conclusion, the studies presented here offer a comprehensive overview of fault-tolerant control methods, encompassing both active and passive approaches and innovative fault-detection techniques. By studying different forms of control systems and fault detection methods, these studies are in the way of improving fault-tolerant systems, especially in critical fields like aerospace engineering. The findings derived from these research programs provide invaluable resources for creating such robust and fault-resistant controllers, which offer improved protection against system failures by ensuring full functionality in real-world applications.

A summary of the findings is given in Table 2.1. Control methods can be used in linear or nonlinear models. The second column of the table shows the model type that can be used. The third column of the table presents input and output constraint definitions that can or cannot be handled. The last column gives which type of failures can be solved with the controller. In this study, model predictive control is selected to avoid the accident due to failures.

Table 2.1 Fault Tolerant Controllers Comparison [1]

Method	**Linear Nonlinear**	**Constrain**	**Failure Actuator/Component**
Model Predictive Control	Both	Handled	Both
Multiple Model Control	Nonlinear	Partially Handled	Both
Sliding Mode Control	Nonlinear	Handled	Partially Both
Control Allocation	Both	Partially Handled	Actuator
Pseudo Inverse Method	Linear	Not Handled	Component
Adaptive Control	Both	Handled	Both
Artificial Neutral Network	Both	Partially Handled	Partially Both

2.4. Conclusion

The detailed literature review is presented in section 2.. Initially, failure classifications are mentioned, such as loss of control type, runaway faults, system malfunction, fire, collision, and flight into terrain. In the literature, loss of control type failure is found

to be the most common type of fault in aviation history. After that, comprehensive research was done on fault-tolerant controllers, mainly classified as passive and active controllers. Different control types and studies about that are mentioned. After light of the literature review, NMPC is found to be the best adequate controller in this study due to the advantages of the aircraft model.

3. NONLINEAR AIRCRAFT MODEL

3.1. Introduction

This section explains the UAV properties and the aircraft's model. The coordinate system is given to define six degrees of freedom equations. Related coordinate transformations and appropriate angles are defined. The model mainly consists of the atmosphere, forces and moments, and six degrees of freedom models. International standard atmosphere model equations and constants are given. Aerodynamic coefficients and related equations are explained. The engine model equations are derived and simplified. The mass and inertia equations are modeled in the mass block. Equations of motion equations are derived and modeled. The model is implemented using MATLAB/Simulink [32] environment. Lastly, the trim algorithm is explained.

Model consist of below blocks:

- Atmosphere Block
- Aerodynamic Block
- Propulsion Block
- Mass Block
- Equations of Motion Block

3.2. UAV Properties

The model used for the simulations is based on typical general aviation aircraft. The selected aircraft is Ryan Navion general aviation aircraft [2]. The dynamic model is chosen so that open loop characteristics are stable and handling qualities are similar to medium-scale unmanned aerial vehicles. Therefore, the aircraft is assumed to be identical

to Ryan Navion's general aviation aircraft, but it is assumed as an unmanned aerial vehicle for the sake of the thesis work [3]. The specifications of the selected UAV are presented in this chapter. Selected aircraft have stable characteristics, and information about aerodynamics and geometry can be found in Table 3.1, 3.2, 3.3 and 3.6.

The specifications of the UAV wing geometry are shown in Table 3.1. Wing area, span, and mean aerodynamic chord are used to dimensionalize the aerodynamic coefficients.

Table 3.1 Specifications of the wing [2]

Parameter	**Symbol**	**Value**
Wing Area	S_w	17.112 m^2
Wing Span	b	10.18 m
Mean Aerodynamic Chord	$\bar{c}$	1.74 m
Aspect Ratio	A	6.04
Taper Ratio	λ	0.54
Dihedral	-	7.5 deg
Incidence at root	-	2 deg
Incidence at tip	-	-1 deg
Airfoil at tip	-	NACA 6410 R
Airfoil at root	-	NACA 4415 R

The specifications of the UAV horizontal and vertical tail geometry are shown in Table 3.2.

Table 3.2 Specifications of the horizontal tail and vertical tail [2]

Parameter	**Symbol**	**Value**
Area of horizontal tail	S_{HT}	4 m^2
Aspect Ratio of horizontal tail	A_{HT}	4.00
Taper Ratio of horizontal tail	λ_{HT}	0.67
Sweep at leading edge	-	6 deg
Incidence of horizontal tail	-	-3 deg
Airfoil of horizontal tail	-	NACA 0012
Area of vertical tail	S_{VT}	1.163 m^2
Airfoil at root of vertical tail	-	NACA 0013.2
Airfoil at tip of vertical tail	-	NACA 0012.4
Fin offset	-	2 deg

The specifications of the UAV mass and inertia information are given in Table 3.3. For the different center of gravity locations, moment of inertia and product of inertia transferred by using parallel axis theorem [33].

Table 3.3 Mass and inertia of the aircraft [3]

Parameter	**Symbol**	**Value**
Mass	W	1247 kg
Center of Gravity	percent $\bar{c}$	25
Moment of Inertia about X-axis	I_{xx}	1420 kg*m^2
Moment of Inertia about Y-axis	I_{yy}	4067 kg*m^2
Moment of Inertia about Z-axis	I_{zz}	4745 kg*m^2
Product of Inertia about X Z	I_{xz}	0 kg*m^2

The specifications of the UAV control surfaces are given in Table 3.4. Deflection ranges are also defined in the nonlinear model predictive control low-fidelity model. Additional restrictions can be done by decreasing these values for different types of failures.

Table 3.4 Specifications of the control surfaces [3]

Surface	**Area**	**Deflection Range**
Elevator	1.31 m^2	-30 to 20 deg
Rudder	0.558 m^2	-15 to 15 deg
Aileron	0.502 m^2	-20 to 20 deg

3.3. Reference Frames and Sign Conventions

An assumption is needed to be made to define the coordinate axis or reference frames. Earth is assumed as flat in inertial frame [6]. The coordinate system which is attached to the Earth is called an Earth Fixed Coordinate Frame. This frame is used to define the equation of the motion. North, East, and Down convention is used for this frame. North means the positive x-axis of the coordinate system, east means the positive y-axis of the coordinate system, and down represents the positive z-axis of the Earth's fixed coordinate system. Another coordinate system, the body-fixed coordinate system, is defined to show the orientation of the aircraft.

Figure 3.1 shows the body-fixed coordinate system. The positive x-axis of the body-fixed coordinate system is towards the nose of the aircraft, the positive y-axis of the frame is towards the right wing, and the z-axis of the coordinate axis is towards the bottom. Positive sign conventions of the velocities, angular rates, forces, and moments are shown. The velocity of the aircraft is defined as u, v, w, and angular rates are defined as p, q, and r, which are roll rate, pitch rate, and yaw rate, respectively. Forces are X, Y, and Z, and moments are L, M, and N. Aircraft attitude is defined with Euler angles, which are phi, theta, and psi angles (ϕ ,θ, ψ symbol representation, respectively). These angles are used to determine the aircraft's orientation with respect to the earth's fixed coordinate system.

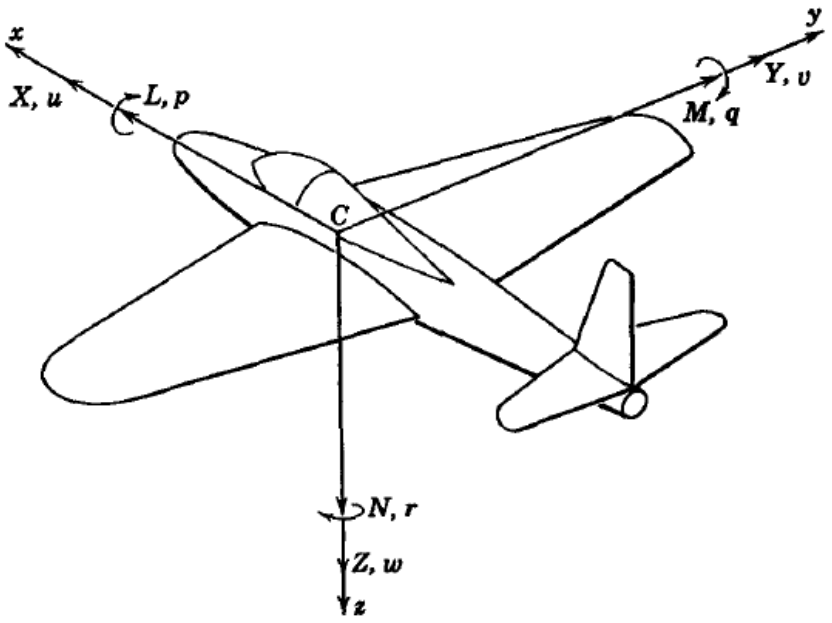

Figure 3.1 Body fixed coordinate system and sign conventions of the velocities, moments, rates and forces [6]

Figure 3.2 shows the control surfaces and motions of the aircraft. Roll motion is rotation concerning the x-axis of the body's fixed coordinate system, which is controlled by ailerons. Ailerons are located at the end of the leading edge of the wings. Positive roll motion means right aileron up, left aileron down. Pitch motion is rotation with respect to the y-axis of the body's fixed coordinate system, which is controlled by an elevator. Elevator is located at leading edge of the horizontal stabilizer/horizontal tail. Positive pitch motion means the elevator deflected up, and a sign of the elevator is negative. Yaw motion is rotation with respect to the z-axis of the body's fixed coordinate system, which is controlled by the rudder. Rudder is located at leading edge of the vertical stabilizer/vertical tail. Positive yaw motion means the rudder deflected right, and a sign of the rudder is negative.

The angle of attack and angle of sideslip serve the purpose of creating forces and moments using aerodynamic data. Both of the angles are defined in the body's fixed coordinate axis. The angle of attack and angle of sideslip can be calculated by Equation 1 and Equation 2, respectively.

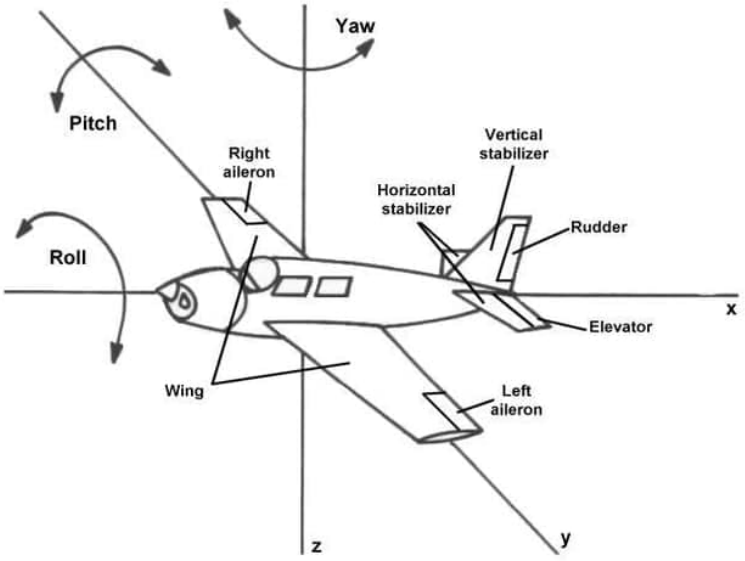

Figure 3.2 Motion of the aircraft and control surfaces [7]

$$\alpha = \arctan\left(\frac{w}{u}\right) \tag{1}$$

$$\beta = \arcsin\left(\frac{v}{V}\right) \tag{2}$$

Where u, v and w are velocity components in body-fixed coordinate axis. Equation 3 shows the relation between pitch angle, angle of attack, and flight path angle. A gamma symbol represents flight path angle (FPA), which shows the aircraft's flight phase. If the FPA equals zero, an aircraft flight without changing altitude is called level flight. FPA is positive, which means the aircraft increases its altitude, which is called the climb phase. FPA is negative, which means the aircraft decreases its altitude, which is called the descent phase.

$$\gamma = \theta - \alpha \tag{3}$$

3.4. Atmosphere Model

This section presents standard and off-standard atmosphere model equations and numerical values to calculate the atmosphere's properties. Pressure, density, temperature, and speed of sound relations are explained. Also, definitions and equations of Mach number, true airspeed, equivalent airspeed, and calibrated airspeed are defined.

The International Standard Atmospheric (ISA) model is defined as a specific altitude where there is a particular value for pressure, temperature, and density. Most of the time, pressure and density decreases with increasing altitude. On the other hand, temperature behavior varies with later. Temperature decreases with altitude at a certain level, then it becomes constant to another certain level. The atmosphere is divided into different layers. Each layer has a different rate of change in the variables. This change is related to the layer constant or is called the temperature gradient. Temperature gradient and layers are defined in Table 3.5.

Table 3.5 Standard atmosphere temperature gradients and parameters at break points [4]

Geopotantial Height, $H_b(m)$	**Temperature Gradient,** $\Gamma\ (K/m)$	**Temperature** T_b**, (K)**	**Pressure** $p_b\ (N/m^2)$
0	-0.0065	288.15	101325
11000	0	216.65	22632
20000	0.001	216.65	5474.87
32000	0.0028	228.65	868.014
47000	-	270.65	110.906

Geometric altitude is defined as a reference point exactly how far from the ground level. Ground level is taken as sea level where pressure altitude is equal to zero. Geopotential altitude is a factious altitude that changes with latitude and gravitational field [34]. The difference between the geometric and geopotential altitudes is minimal. It is an adjustment for the gravity change. Pressure altitude and geopotential altitude are the same for the standard atmosphere model; however, pressure altitude and geopotential altitude are different in the off-standard atmosphere model. Pressure altitude is where the ISA shows

the same pressure. In other words, initially measure the pressure using a pitot- a static tube and find the altitude that gives the same pressure that you measure from the ISA table.

To find the temperature at different pressure altitudes for the standard atmosphere case, Equation 4 can be used.

$$T = T_b + \Gamma(H - H_b) \tag{4}$$

Where T_b is temperature at given geopotential height (H_b) and Γ is temperature gradient. The pressure of the air can be calculated from Equation 5 for temperature gradient is not equal to 0 and Equation 6 temperature gradient is equal to 0, which is a function of the temperature. This formula is used for standard and off-standard models.

$$\frac{p}{p_h} = \left(\frac{T}{T_b}\right)^{(-\frac{g_0}{R\Gamma})} \tag{5}$$

$$\frac{p}{p_h} = e^{-\frac{g_0(H-H_b)}{RT_b}} \tag{6}$$

Where p is pressure, g is gravity and R is gas constant. Similar formulas were used for the density calculation. Density is also a function of temperature. The density of the air can be calculated from Equation 7 for temperature gradient is not equal to 0 and Equation 8 temperature gradient is equal to 0.

$$\frac{\rho}{\rho_b} = \left(\frac{T}{T_b}\right)^{-(1+\frac{g_0}{RL})} \tag{7}$$

$$\frac{\rho}{\rho_b} = e^{-\frac{g_0(H-H_b)}{RT_b}} \tag{8}$$

Using the Equations 4, 6 and 8, the standard atmosphere is modeled up to 10000 meters, which is enough for the thesis scope of the analysis. The variation of air density with altitude is modelled with the Equation 8 and the results are plotted in Figure 3.3. Figure 3.3 shows the density variation with the altitude at ISA is equal to zero degrees.

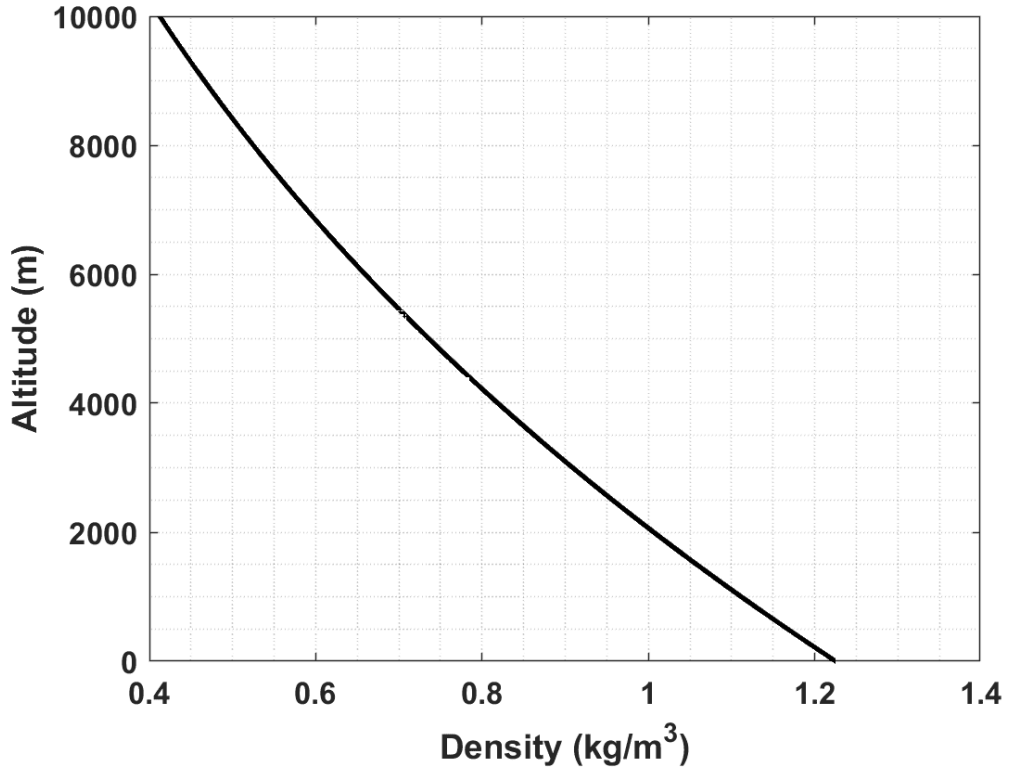

Figure 3.3 Density variation with altitude with respect to ESDU standard atmosphere model

The atmosphere might be different from what ISA assumed or expected it to be. The atmosphere might be hotter or cooler. The difference between them is due to the temperature increment of the air. This temperature difference is the main reason for the off-standard atmosphere. The reference temperature is 288.15K for the standard sea level case. If this value is different, then there is a temperature increment in the atmosphere. Therefore, the mentioned pressure and density formula can be used for the off-standard model, and the temperature formula needs a minor adjustment.

$$T = T_b + \Gamma(H - H_b) + \Delta T \tag{9}$$

With the delta temperature term added, the off-standard atmosphere can be modeled. The equation between the pressure altitude and pressure is the same for the standard and off-standard models. In the pressure equation, the temperature is used as the standard temperature value, not including the temperature increment. As mentioned before, the definition of pressure altitude says that the pressure value is at a specific pressure altitude. Therefore, a change in the temperature of the sea level does not change the pressure altitude and altitude pressure value. However, temperature increment change affects the temperature and density.

The speed of sound can be found at any altitude using Equation 10, which is a function of the temperature.

$$a = \sqrt{\gamma RT} \tag{10}$$

Where γ is adiabatic constant, R is gas constant and T is temperature. Indicated airspeed is measured from a pitot static tube. The main idea is that the difference between the total and static pressure gives dynamic pressure. From the dynamic pressure indicated, airspeed can be found. Calibrated airspeed is the airspeed that indicated airspeed is corrected due to instrumental and position errors. Therefore, CAS is speed that does not contain instrumental and position errors. True airspeed is the speed of an aircraft relative to the air it's flying through. Equivalent airspeed is the speed that gives the same dynamic pressure as the true airspeed at sea level. It is an airspeed corrected for density effects. The relation between equivalent airspeed and true airspeed is given Equation 11.

$$V_{TAS} = \frac{V_{EAS}}{\sqrt{\frac{\rho}{\rho_0}}} \tag{11}$$

Where ρ represents density. Also, true airspeed can be defined as Equation 12 at body-fixed coordinate system components as u,v and w.

$$V_{TAS} = \sqrt{u^2 + v^2 + w^2} \tag{12}$$

Mach number is calculated by true airspeed divided by the speed of sound at a given temperature as shown in Equation 13.

$$M = \frac{V_{TAS}}{a} \tag{13}$$

3.5. Forces and Moments

Equations of the motions (EoM) need forces and moments to simulate the aircraft's behavior. In the EoM block, all forces and moments are calculated by summation of the force and moment sources. Total forces and moments on the aircraft have considered only three different sources for the scope of the thesis in the air.

- Aerodynamic Effects: X, Y, Z forces and l, m, n moments
- Propulsion Effects: X, Y, Z forces and l, m, n moments
- Weight effects: X, Y, Z forces

3.5.1. Aerodynamic Model

Aerodynamic forces and moments are calculated by using aerodynamic coefficients, which are shown in Table 3.6. Aerodynamic forces and moments are related to angle of attack, angle of sideslip, elevator deflection, aileron deflection, rudder deflection, roll rate, pitch rate, and yaw rate. These given coefficients are at flap-up and landing gear-up configurations.

Aerodynamic forces are calculated by using Equation 14. Dynamic pressure and reference area are multiplied by the total lift coefficient, drag coefficient, and lateral force coefficient.

$$
\begin{aligned}
L &= \frac{1}{2}\rho V^2 S\left(C_{L_0} + C_{L_\alpha}\alpha + C_{L_{\delta_e}}\delta_e + C_{L_{\dot{\alpha}}}\dot{\alpha}\frac{c}{2V} + C_{L_q}q\frac{c}{2V}\right) \\
D &= \frac{1}{2}\rho V^2 S(C_{D_0} + C_{D_\alpha}\alpha) \\
Y &= \frac{1}{2}\rho V^2 S\left(C_{Y_\beta}\beta + C_{Y_{\delta_r}}\delta_r + C_{Y_{\delta_a}}\delta_a + C_{Y_r}r\frac{b}{2V} + C_{Y_p}p\frac{b}{2V}\right)
\end{aligned}
\tag{14}
$$

Where ρ is density, V is true airspeed and S is reference area. L represents lift force, drag represents drag force and Y is side force. Lift and drag forces are converted to body axis X and Z forces with Equations 15.

$$
\begin{aligned}
X &= L\sin(\alpha) - D\cos(\alpha) \\
Z &= -L\cos(\alpha) - D\sin(\alpha)
\end{aligned}
\tag{15}
$$

Where α is angle of attack, L is lift force and D is drag force. Aerodynamic moments are calculated by using Equation 16. A similar formula is used as force equations. Span is used for rolling and yawing moments. A chord is used for pitching moment calculation.

$$
\begin{aligned}
l &= \frac{1}{2}\rho V^2 Sb(C_{l_\beta}\beta + C_{l_{\delta_r}}\delta_r + C_{l_{\delta_a}}\delta_a + C_{l_r}r\frac{b}{2V} + C_{l_p}p\frac{b}{2V}) \\
m &= \frac{1}{2}\rho V^2 Sc(C_{m_0} + C_{m_{\delta_e}}\delta_e + C_{m_{\dot{\alpha}}}\dot{\alpha}\frac{c}{2V} + C_{m_q}q\frac{c}{2V}) \\
n &= \frac{1}{2}\rho V^2 Sb(C_{n_\beta}\beta + C_{n_{\delta_r}}\delta_r + C_{n_{\delta_a}}\delta_a + C_{n_r}r\frac{b}{2V} + C_{n_p}p\frac{b}{2V})
\end{aligned}
\tag{16}
$$

Where ρ is density, V is true airspeed, and S is reference area. These equations calculate moments due to aerodynamics, and aerodynamic coefficients are given in Table 3.6. Aerodynamic values are obtained at 0.15M. This aerodynamic data is only applicable to clean configuration, which means flap-up and landing gear-up configuration with subsonic speed region. Also, aerodynamic data is only applicable in linear region where angle of

attack is zero to seventeen degree. Stall value is 54 knot for flap up configuration [35]. Using the relationship between the lift equal to weight in trim condition approximately stall angle of attack is calculated which is seventeen degree. Therefore, this aerodynamic data is only applicable in zero to seventeen degree .

Table 3.6 Aerodynamic coefficients of the unmanned aerial vehicle [3]

Longitudinal		**Lateral-Directional**	
Coefficient	**Value**	**Coefficient**	**Value**
C_{L_α}	4.44 /rad	C_{l_β}	-0.074 /rad
C_{L_q}	3.8 s/rad	C_{l_p}	-0.41 s/rad
$C_{L_{\delta_e}}$	0.355 /rad	C_{l_r}	0.107 s/rad
C_{L_0}	0.41 /rad	$C_{l_{\delta_a}}$	-0.134 /rad
C_{D_α}	0.33 /rad	$C_{l_{\delta_r}}$	0.107 /rad
$C_{D_{\delta_e}}$	0 /rad	C_{Y_β}	-0.564 /rad
C_{D_0}	0.05	$C_{Y_{\delta_r}}$	0.157 /rad
C_{M_α}	-0.683 /rad	C_{n_β}	0.071 /rad
$C_{M_{\dot{\alpha}}}$	-4.36 s/rad	C_{n_p}	-0.0575 s/rad
$C_{M_{\delta_e}}$	-0.923 /rad	C_{n_r}	-0.125 s/rad
C_{M_q}	-9.96 s/rad	$C_{n_{\delta_a}}$	-0.0035 /rad
C_{M_0}	0	$C_{n_{\delta_r}}$	-0.072 /rad

3.5.2. Engine Model

Ryan Navion aircraft has 285 Hp at take-off condition with 2700RPM [2]. Some simplifications have been made in the engine model. One of the critical assumptions is that engine indirect effects, which are p-load, torque, slipstream, and gyroscopic effects, are ignored. This assumption is made to simplify the engine model. An essential requirement of the engine model is that the aircraft should create enough thrust to overcome the drag force. This is the only goal when creating the engine model. Thrust force due to the engine is a function of horsepower and true airspeed. Thrust is calculated by Equation 17

[36]. Calculated thrust and flight test data [2] comparison has been done. Approximately 0.6 is found adequate for the propeller efficiency.

$$T = \frac{550 H_p \eta_p}{V_{TAS}} \tag{17}$$

Where H_p is horse power, η_p is propeller efficiency and V_{TAS} is true airspeed.

3.5.3. Mass Model

Table 3.3 gives aircraft mass and inertia data. In the mass block of the model, two calculations are performed. One of them is changing the inertia data to the input center of gravity location, which is done by using the parallel axis theorem [37]. Secondly, weight is divided into body axis components. From the earth frame to the body frame, a transformation matrix is used, which is shown in Equation 18.

$$T_{BE} = \begin{bmatrix} \cos(\theta)\cos(\psi) & \cos(\theta)\sin(\psi) & -\sin(\theta) \\ -\cos(\phi)\sin(\psi) + \sin(\phi)\sin(\theta)\cos(\psi) & cos(\phi)\cos(\psi) + \sin(\phi)\sin(\theta)\sin(\psi) & \sin(\psi)\cos(\theta) \\ \sin(\phi)\sin(\psi) + \cos(\phi)\sin(\theta)\cos(\psi) & -\sin(\phi)\cos(\psi) + \cos(\phi)\sin(\theta)\sin(\psi) & \cos(\psi)\cos(\theta) \end{bmatrix} \tag{18}$$

Where ϕ is roll angle, θ is pitch angle and ψ is yaw angle representing Euler angles. This transformation matrix is an orthonormal matrix. This type of matrix has a feature that the transpose of this matrix is equal to the inverse of it. Therefore, a transformation matrix can be used for the Earth to body or body to Earth by only taking the transpose of the matrix.

At Earth's fixed coordinate system, total forces due to gravity can be modeled with Equation 19.

$$F^{E}_{Weight} = \begin{bmatrix} 0 \\ 0 \\ mg \end{bmatrix} \tag{19}$$

Where m is mass of aircraft and g is gravity. With the explained transfer matrix and weight components at the earth's fixed coordinate system, body fixed components can be found with Euler angles. Eular angles define the orientation of the aircraft with respect to angles between the earth and body frames. After using the transfer function, weight components can be found as Equation 20.

$$F^{B}_{Weight} = T_{BE} \begin{bmatrix} 0 \\ 0 \\ mg \end{bmatrix} = \begin{bmatrix} -mg\sin(\theta) \\ mg\sin(\psi)\cos(\theta) \\ mg\cos(\psi)\cos(\theta) \end{bmatrix} \tag{20}$$

3.6. Equations of Motion

The motion of the aircraft consists of three translational and three rotational motions. Because of that, aircraft motion is defined with six degrees of freedom. Equations of the motions are given in Equations 21 [37]. Total forces and moments contain aerodynamics, engine, and weight.

$$
\begin{aligned}
m(\dot{u} + qw - rv) &= F_{W_x} + F_{A_x} + F_{E_x} \\
m(\dot{v} + ur - pw) &= F_{W_y} + F_{A_y} + F_{E_y} \\
m(\dot{w} + pv - qu) &= F_{W_z} + F_{A_z} + F_{E_z} \\
\dot{p}I_{xx} - \dot{r}I_{xz} - pqI_{xz} + rq(I_{zz} - I_{yy}) &= l_A + l_E \\
\dot{q}I_{yy} + pr(I_{xx} - I_{zz}) + (p^2 - r^2)I_{xz} &= m_A + m_E \\
\dot{r}I_{zz} + \dot{p}I_{xz} + pq(I_{yy} - I_{xx}) + qrI_{xz} &= n_A + n_E
\end{aligned}
\tag{21}
$$

Where u,v, and w are velocity components, p, q, and r are angular rates, m is mass, F is force, l, m, n are moments, and I represent the aircraft's inertia. Aircraft orientation, which is Euler angles, is obtained by using rates. The matrix form of the equations is shown in Equations 22.

$$
\begin{bmatrix} \dot{\phi} \\ \dot{\theta} \\ \dot{\psi} \end{bmatrix} = \begin{bmatrix} 1 & \sin(\phi)\tan(\theta) & \cos(\phi)\tan(\theta) \\ 0 & \cos(\phi) & -\sin(\phi) \\ 0 & \sin(\phi)\sec(\theta) & \cos(\phi)\sec(\theta) \end{bmatrix} \begin{bmatrix} p \\ q \\ r \end{bmatrix} \tag{22}
$$

Where p,q and r are angular rates and ϕ, θ, ψ are Euler angles. The location of the aircraft can be found using Equations 23, which are in the Earth frame. The trajectory of the aircraft is obtained with the result of these equations.

$$
\begin{bmatrix} \dot{X^E} \\ \dot{Y^E} \\ \dot{Z^E} \end{bmatrix} = T_{BE}^{-1} \begin{bmatrix} u \\ v \\ w \end{bmatrix} \tag{23}
$$

Where u,v and w velocity components and T_{BE} is Earth to body coordinate system transformation matrix. Load factors of the aircraft are obtained by Equations 24, 25,

and 26.

$$N_x = \frac{(X_A + X_W + X_T)}{mg} \tag{24}$$

$$N_y = \frac{(Y_A + Y_W + Y_T)}{mg} \tag{25}$$

$$N_z = \frac{(Z_A + Z_W + Z_T)}{mg} \tag{26}$$

Where X, Y, Z are forces, m is mass and g is gravity. A nonlinear model of the UAV can be obtained by combining all the mentioned equations and the blocks. Atmosphere, aerodynamic, propulsion, mass, and EoM blocks are placed and connected to each other. Figure 3.4 shows the final result of the Simulink model.

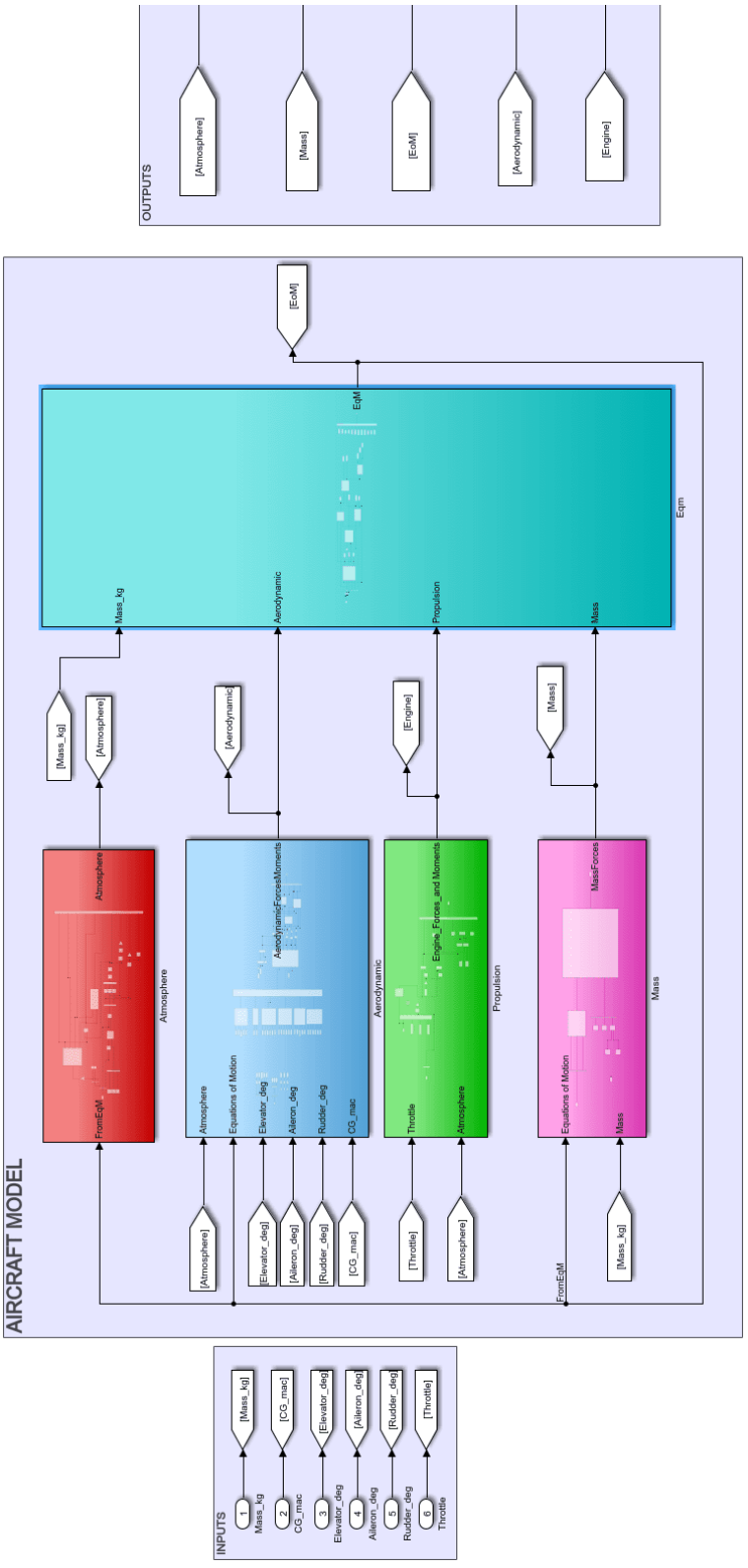

Figure 3.4 6DoF UAV Simulink model

3.7. Trim, Simulation and Verification

Aircraft trim is defined as the equilibrium of the motion. At this trim point, the total forces and moments acting on the aircraft are zero. In this condition, the aircraft continues its motion without change if an external disturbance is not applied. In the trim analysis, Matlab ”findop” code is used [32]. This code finds the steady state point of the model.

Two different trim conditions are used in this study. The only difference between the trims is whether the throttle or flight path angle is input or not. Only one of them can be input, and the other one is unknown.

In the trim analysis, inputs are defined as:

- Mass
- Center of gravity
- Altitude
- Velocity
- ISA
- Flight path angle or Throttle

In the analysis, the wings level trim is used. At this condition, the rates and accelerations of the aircraft are equal to zero. The roll angle phi is also zero degrees. The flight path angle is zero, which means the aircraft is in the cruise flight phase. Aircraft fly without changing altitude. Trim code finds adequate throttle, elevator deflection, aileron deflection, and rudder deflection at given input conditions. Different types of flight phases can be found by changing the flight path angle value. If the FPA is given as positive, then the trim code finds the climb phase. If the FPA is given as negative, then the trim code finds the descending phase.

The results of a wings level trim and simulation are shown in Figures 3.5 and 3.6. Aircraft is trimmed at 125 KCAS and 10000ft altitude with wings level. After running the trim code, the required control surface deflections and throttle percentage are found. An aircraft does not change its equilibrium point if there is no external disturbance. As shown in the figures, all the states and outputs are constant and equal to trim condition values. That verifies that aircraft maintains its equilibrium point without showing any deviation.

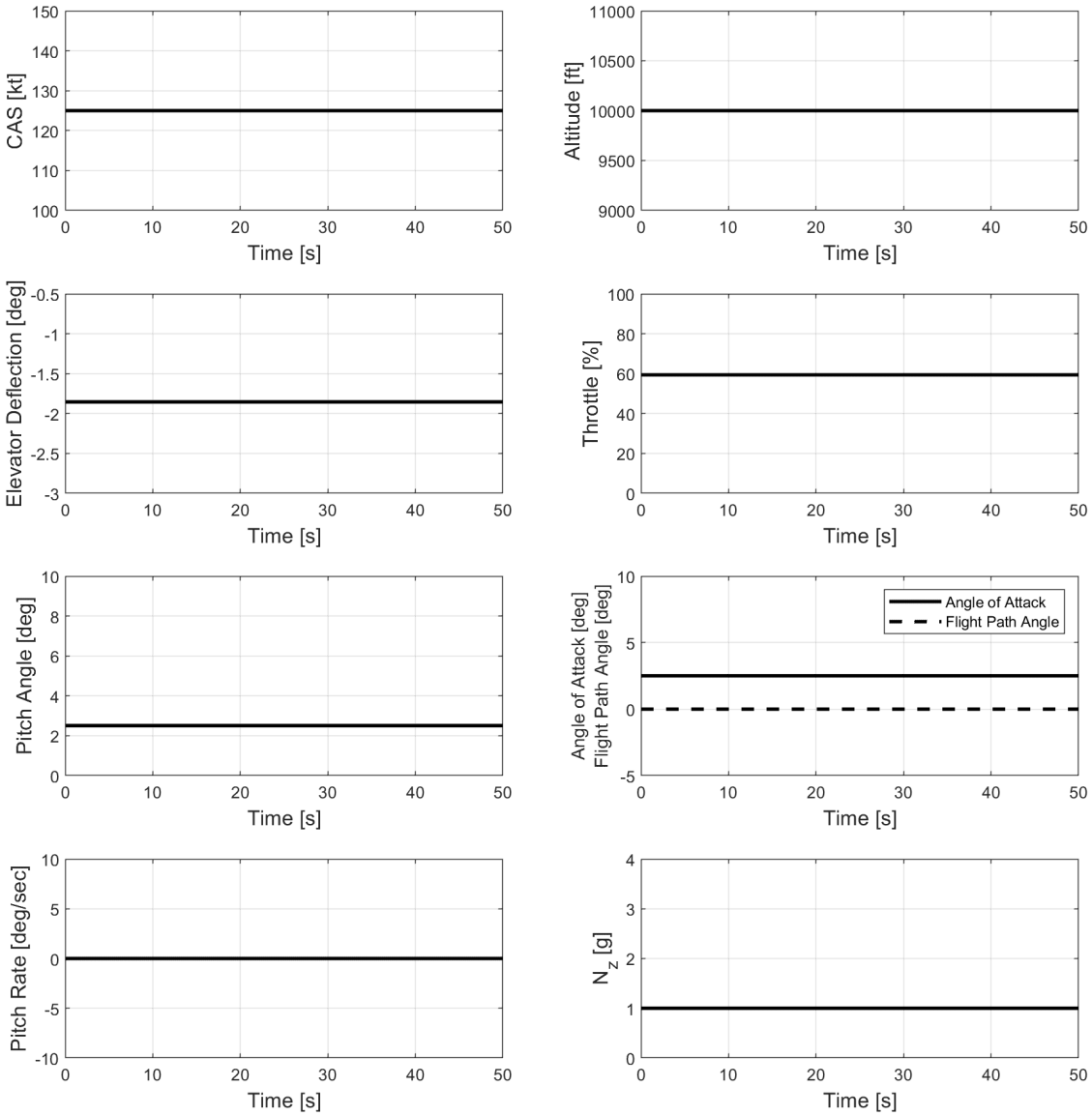

Figure 3.5 Results of wings level trim and simulation longitudinal parameters

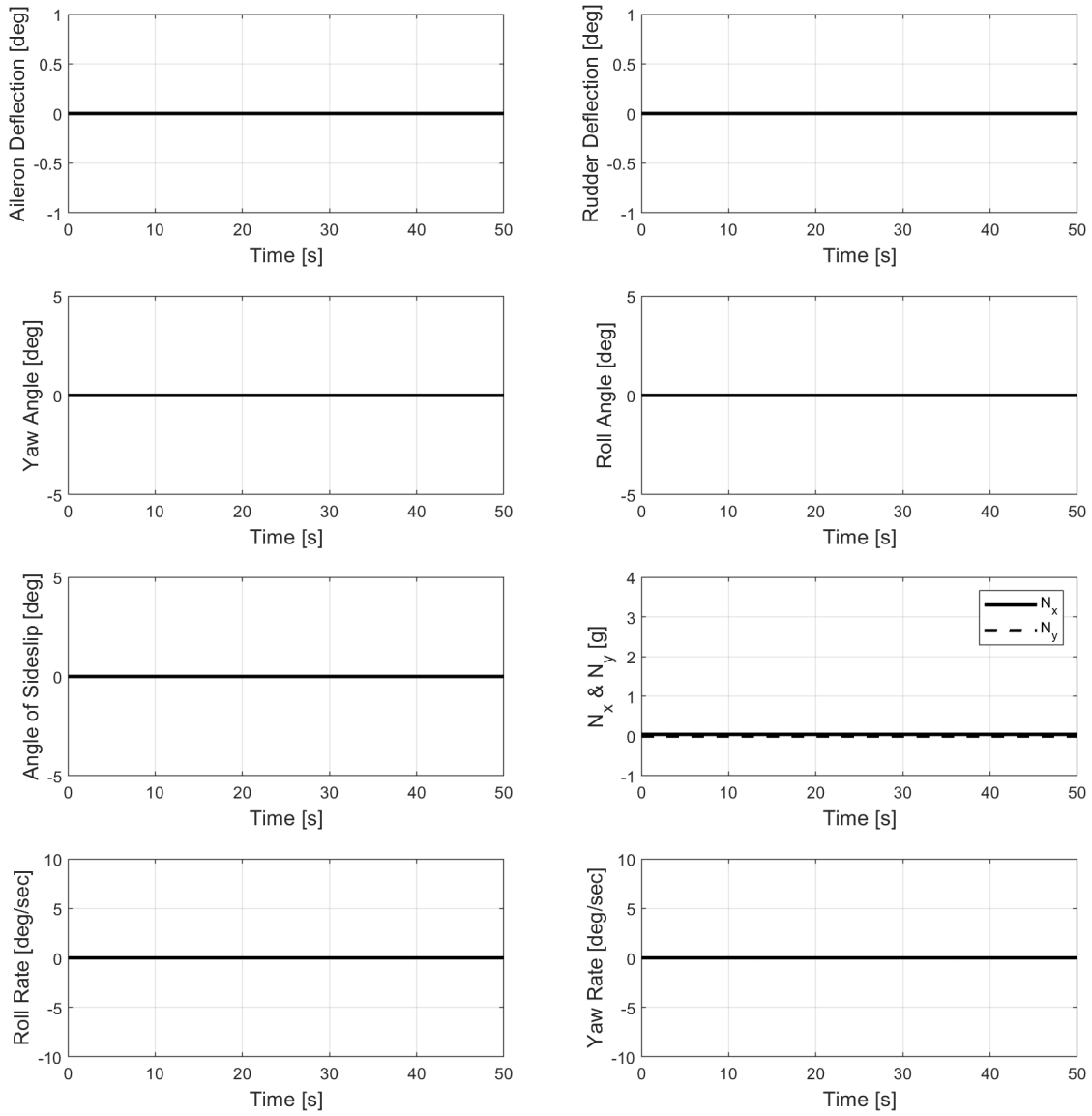

Figure 3.6 Results of wings level trim and simulation lateral and directional parameters

Aircraft have five different dynamic modes. In the longitudinal axis, short-period and long-period modes can be excited. Roll, spiral, and Dutch roll modes can be excited in the lateral and directional axes [37]. In the model analysis, these modes can be found by linearization at a trim point or excitation by an external force at the simulation. Simulations have been performed to examine the longitudinal modes in the lateral directional axis and the lateral directional modes in the longitudinal axis.

The long period is called phugoid mode. This mode is a combination of an aircraft's

climbing and descending oscillatory motion [38]. This mode is generally slower than the other modes. It can be excited by the pilot by giving the elevator application. In the flight test process, the pilot trims the aircraft at the required conditions. Then, the elevator input is applied to decrease its velocity by approximately 15 %. After that, slowly release the pressure on the stick, and the elevators become free to float. Therefore, a long period is excited, and dynamic mode starts. This mode generally has divergent characteristics, and the amplitude of the oscillations increases gradually. Long-period simulation results are shown in 3.7 and 3.8.

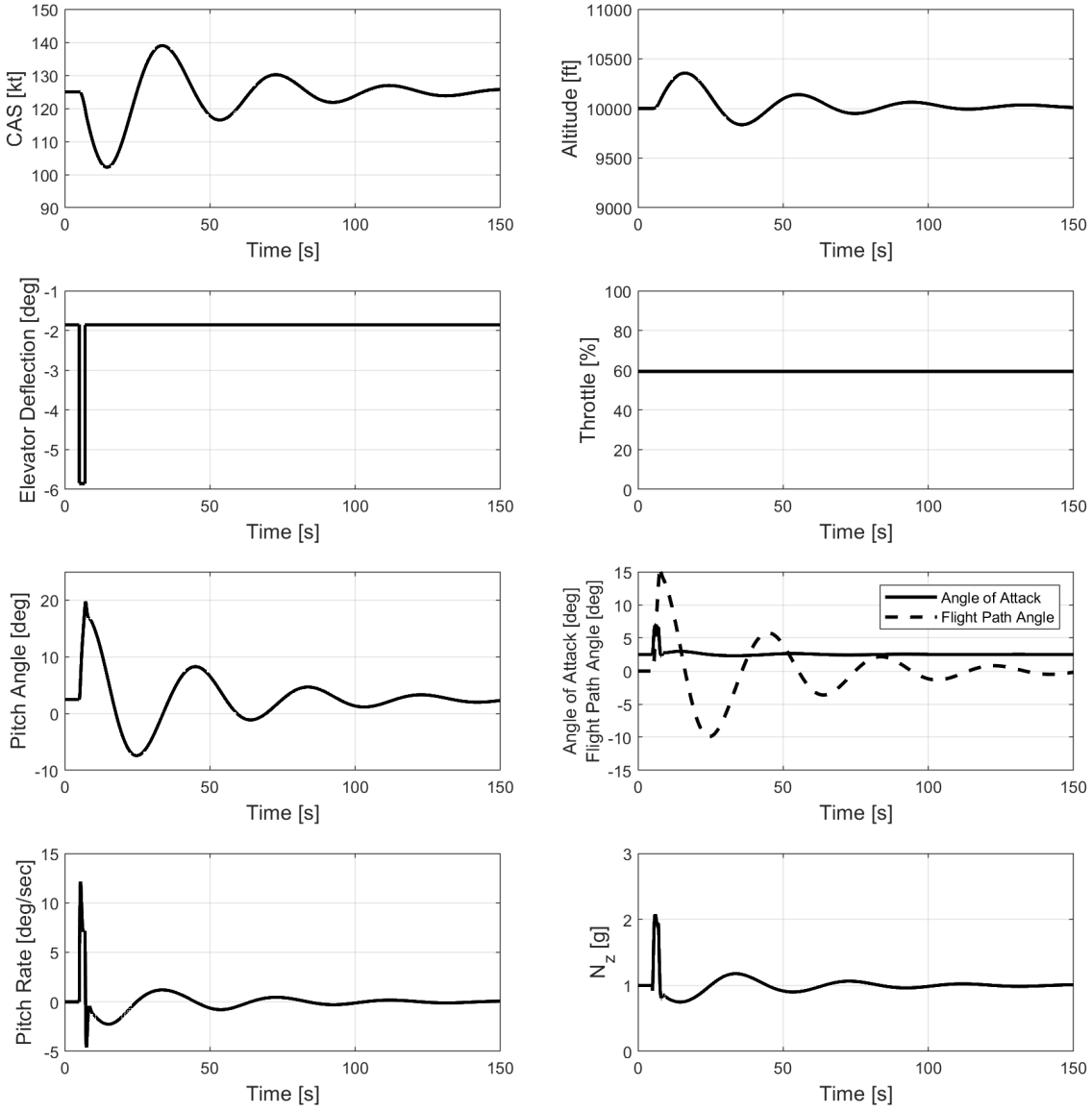

Figure 3.7 Long period simulation results in longitudinal axis

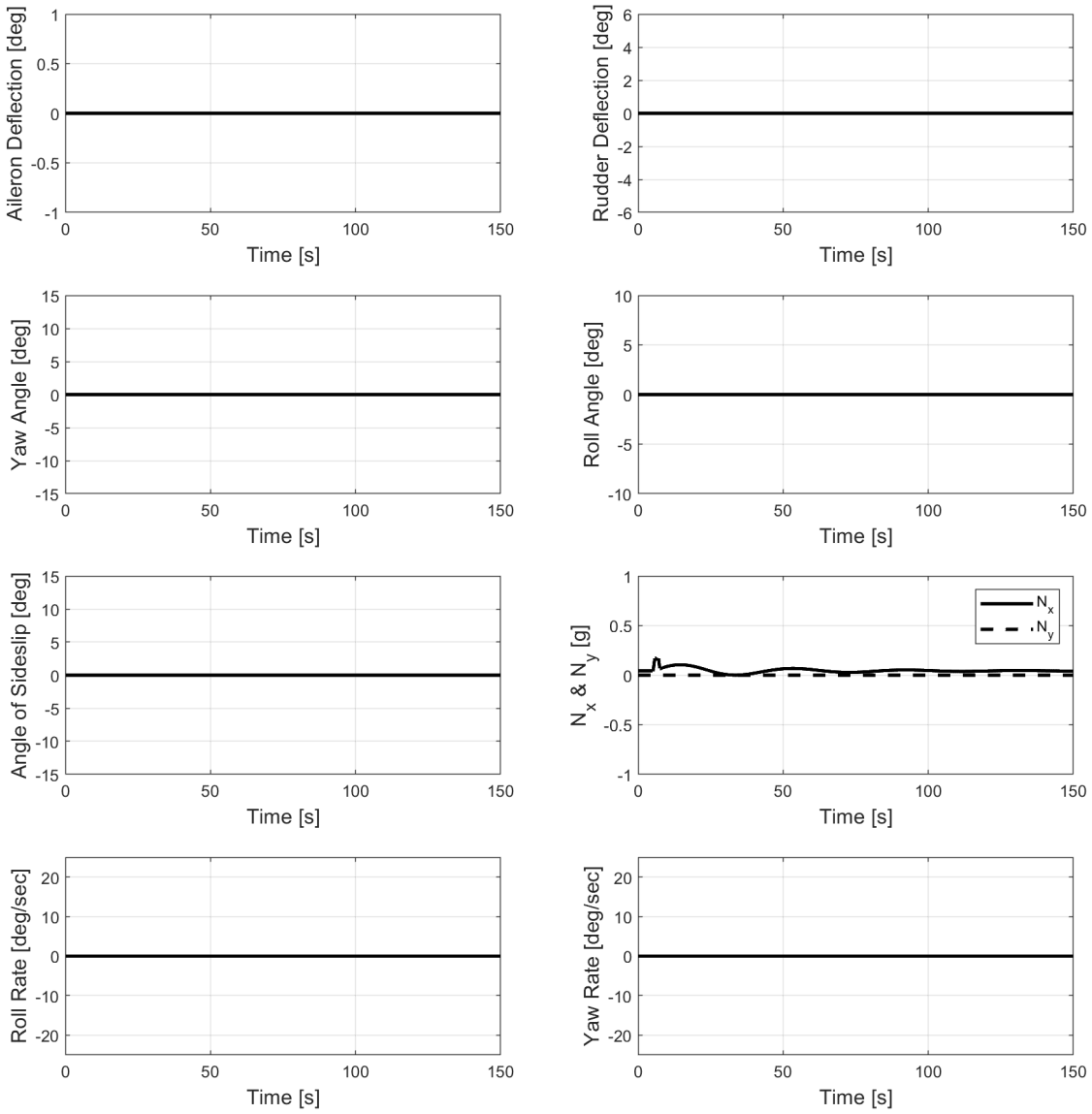

Figure 3.8 Long period simulation results in lateral and directional axes

As shown in these plots, aircraft has convergent long-period characteristics, and longitudinal motion does not affect the lateral and directional axis. This verifies that the UAV model of the aircraft works perfectly in the longitudinal axis with the given input to the model.

Dutch roll mode is an oscillatory yaw and roll motion [38]. This mode is excited by external disturbance or intentional pilot input. In the test procedures, the pilot gives double input to the rudder while not changing the elevator and aileron deflections. After the

rudder input, the aircraft starts the rolling and yawing motion simultaneously.

Figures 3.9 and 3.10 show the Dutch roll simulation results. As mentioned above, the Dutch roll started with the rudder doubled input. The aircraft starts to roll and yaw simultaneously. But it converges to trim the condition as soon as possible. The Dutch roll does not tremendously affect the longitudinal axis parameters. Only minor deviations are observed. That shows that lateral and directional excitation slightly affects the longitudinal motion.

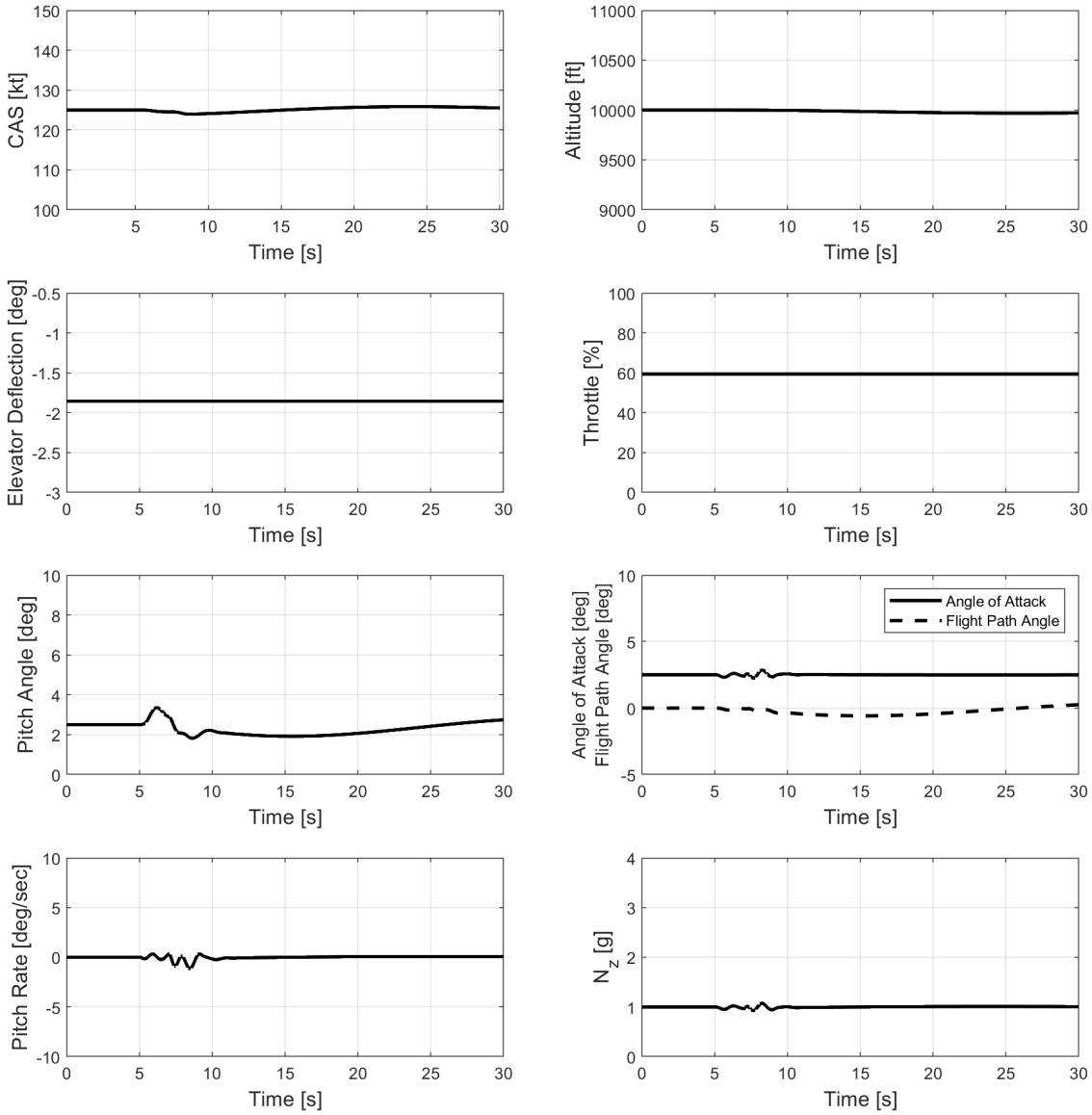

Figure 3.9 Dutch roll mode simulation results in longitudinal axis

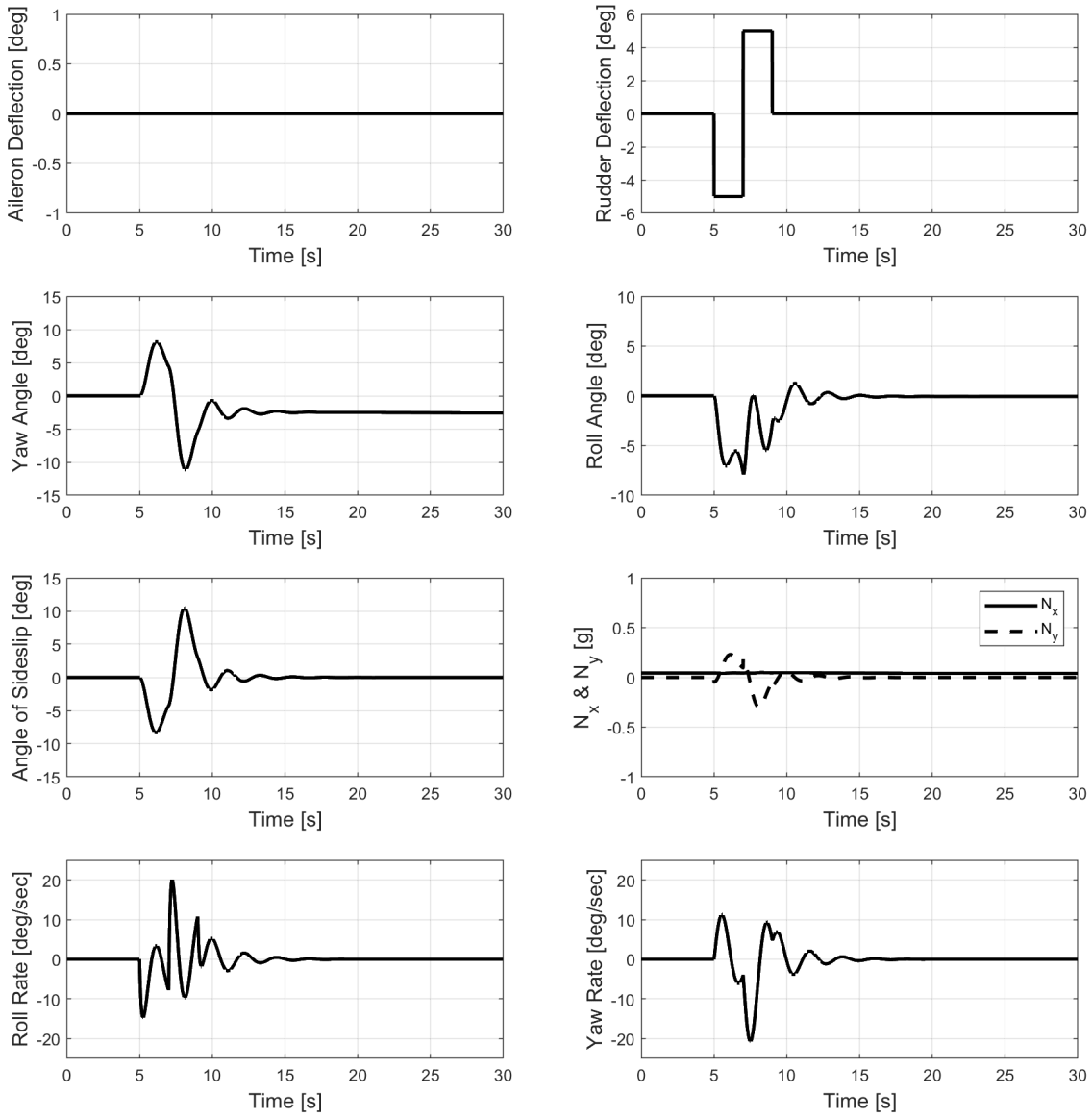

Figure 3.10 Dutch roll mode simulation results in lateral and directional axes

3.8. Conclusion

In this section, UAV properties are presented. Atmosphere, aerodynamics, engine, mass, and equations of motion are derived. All equations are combined and applied to the Simulink environment. Wings level trim is explained, and trim and simulation results are displayed. Long and Dutch roll mode analyses showed that longitudinal and lateral-directional axes are not coupled. They do not affect each other marginally.

4. DESIGN OF NONLINEAR MODEL PREDICTIVE CONTROL

4.1. Introduction

This section aims to explain the theory of the model predictive control and derivation of the MPC model for the aircraft. If the system equations are linear, then the term used for MPC is linear model predictive control. If the system equations are defined as nonlinear, then the term used for MPC is nonlinear model predictive control. In the scope of the thesis, aircraft dynamics are presented nonlinearly. Therefore, nonlinear model predictive control is used in this study. After the explaining the theory of the NMPC and deriving the inner model equations for the aircraft, some verification's have been performed and presented.

Model predictive control (MPC) is an optimal control theory method that finds out the model reaction for a given reference input and, based on the inner model of the system, predicts the required input while minimizing a cost function [23]. Finding the optimal solution to a given problem takes a long time because of the complexity of the system dynamic when solving the MPC problem. Because of that, MPC is generally used for slow processes such as chemical reactions. However, improvements in the optimization methods and improvement of the hardware make it possible to decrease the required time to solve the problem. Even with this disadvantage, MPC can be used in aerospace problems because it handles multi-input systems and makes it easy to give restrictions to inputs and outputs. To analyze the NMPC controller, a high-fidelity six-degree-of-freedom nonlinear aircraft model is needed.

MPC has many advantages that can cause appropriate fault-tolerant control. MPC is a control method that uses an internal model to find optimum input prediction to the main system plant. MPC gives outstanding results in the presence of failure. MPC has a cost

function that is minimized so that prediction input is found with the input and output constraints. This prediction is optimized with the defined prediction horizon.

Figure 4.1 shows the whole model representation. The left block diagram is called a plant or system, the UAV model. This model is as accurate as possible to real aircraft models. MPC consists of a low-fidelity model and optimization tool. Low-fidelity model equations will be derived in Section 4.. In the literature, multiple optimization tools are available such as FORCES, qpDUNES, CasADI, Ipopt, and ACADO are available. ACADO is selected in this study. ACADO is used for optimization and control algorithms [39].

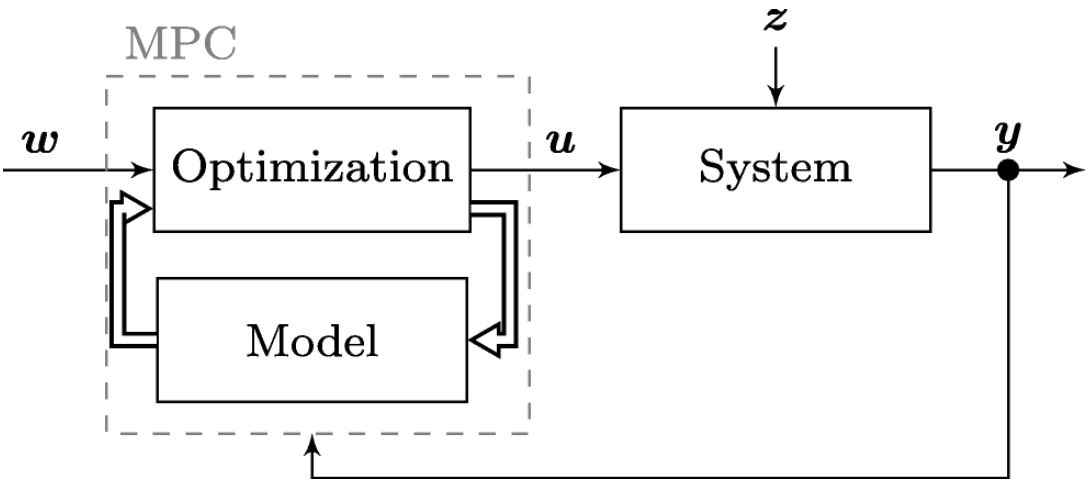

Figure 4.1 Representation of MPC on model [8]

4.2. Theory

Model predictive control is known as receding horizon control [23]. MPC is based on internal model prediction control theory. MPC handles constraints and nonlinear multi-input and output systems, which makes it an efficient control method for aircraft. Inputs and states can be constrained in the MPC algorithm. That allows us to avoid unrealistic input and state output. In this section, the theory of the MPC will be explained. MPC is mainly built upon optimal control methods. Most of the control theories only use the main plant and control algorithms designed on this plant. On the other hand, MPC requires an internal model, which is a part of the model predictive control. This internal

model predicts the future output of the system to find out the inputs required to reach the optimal trajectory for the given prediction horizon.

Figure 4.2 represents the MPC behavior and the theory behind it. As mentioned above, MPC has a model that is used to predict the trajectory of the system at a given prediction horizon Hp at instant time t. This model predicts the behavior of the process. The logic of the controller is to find the best control input that finds out the predicted trajectory. N step times are used during the horizon, and at step time k, the predicted trajectory is as close as possible to the reference trajectory. The cost function is used to optimize the input to reach the given trajectory. Mainly, the quadratic function is used as a cost function for the model predictive control. After finding all the inputs at the prediction horizon, only the first input is given to the system. The prediction horizon shifts to k-step time. Then, calculations are done again. After that, the first inputs are applied to the plant, so the whole cycle continues like that.

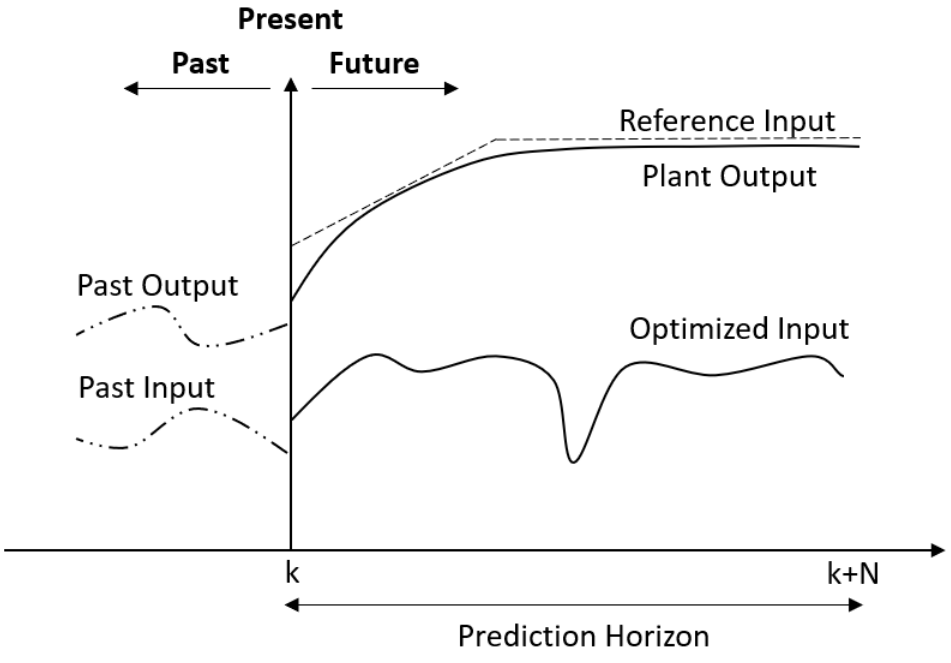

Figure 4.2 MPC theory representation

Shortly, MPC works that initially at time equal to k; the problem is solved by finding the best input u. Then, at time k+1, applying the u-predicted input solves and gets the actual

states of the process. Then the solver continues like that. The horizon shifts by k and predicts new states and required inputs. General MPC formulation of the cost function is shown as in Equation 27. The main idea of the optimal theory is to minimize the cost function so that finding the best control inputs.

$$minimize\ J = \int_{t_0}^{t_N} [\ell(x(t), u(t), t)]dt \tag{27}$$

Nonlinear system dynamics are defined with:

$$x_{k+1} = f(t_k, x(t_k), u(t_k)) \quad \text{System dynamics} \tag{28}$$

the initial values are

$$x(t_0) = x_0 \quad \text{Initial values} \tag{29}$$

the initial constrains are

$$h_u \geqslant h(x_{t_0}, u_{t_0}) \geqslant h_l \quad \text{Constrains} \tag{30}$$

the terminal constrains are

$$r_u \geqslant r(x(t_N)) \geqslant r_l \quad \text{Terminal Constrains} \tag{31}$$

The problem is solved so that control input is found in the range of the restriction or the constraints given initially, and the cost function is minimized. In the ACADO program, the cost function is provided as least square form[39].

ACADO utilizes Sequential Quadratic Programming (SQP) as one of its optimization methods for solving model predictive control (MPC). Sequential Quadratic Programming (SQP) is a numerical technique that involves the iterative solution of nonlinear

optimization problems [40]. The SQP involves solving a sequence of quadratic subproblems in an iterative approach. This is done by means of a quadratic approximation of the original problem, which is a nonlinear optimization problem. SQP proves to be very effective not only for linear but also nonlinear, smooth, objective functions and constraints [41]. SQP has found multiple applications in engineering, economics, and operations research, among others, to solve many types of optimization problems.

4.3. Internal Model

As proved in Section 3., longitudinal motion does not significantly impact lateral-directional motion. Similarly, lateral-directional motion does not have a substantial effect on longitudinal motion. Because of that, to decrease the required time by reducing the number of equations, MPC is divided by two models. Therefore, two different NMPCs are designed to decrease the computational burden. That assumption simplifies the inner model equations. So that longitudinal and lateral-directional can be controlled independently. This section presents derivations of the NMPC low-fidelity inner model.

4.3.1. Longitudinal Dynamics

In the longitudinal motion, the aim is to follow the given reference altitude. This reference altitude might be constant at trim conditions or climb or descend. In the analysis, both climb and descend had been performed to see the reaction of the NMPC. The longitudinal axis is not affected by the lateral directional axis motion. This assumption simplifies the equations. In the longitudinal axis, motion is controlled by the elevator only. Thrust input is taken as a constant parameter in trim conditions. Therefore, all motion in the longitudinal axis is based on elevator behavior. The pitching moment equations were defined in the y-axis as Equation 32.

$$\dot{q}I_{yy} + pr(I_{xx} - I_{zz}) + (p^2 - r^2)I_{xz} = m_A + m_E \tag{32}$$

Where p, q and r are angular rates, I is inertia and m is pitching moment. As mentioned in the propulsion section, propulsion only creates thrust in the axis. Because of that moment, the propeller effect is assumed to be zero. Roll rate and yaw rate terms are also taken as zero due to the coupling assumption. The remaining pitching equation is found as Equation 33.

$$\dot{q} = \frac{m_A}{I_{yy}} \tag{33}$$

Where m_A is pitch moment due to aerodynamic and I_{yy} is moment of inertia in y axis. Due to the coupling assumption, a derivative of the pitch angle is taken as the pitch rate. Because of this equation, the phi angle is taken as zero, which results in the Equation 34. Equation 22 shows the actual pitch rate equation.

$$q = \dot{\theta} \tag{34}$$

Where q is pitch rate and $\dot{\theta}$ is derivative of theta angle. FPA angle was given in Equation 3. Taking the derivative of this equation and using the Equation 34 change of the FPA is found as 35.

$$\dot{\gamma} = q - \dot{\alpha} \tag{35}$$

Where γ is flight path angle, q is pitch rate and $\dot{\alpha}$ is derivative of angle of attack. Total velocity and angle of attack derivative are found as Equation 36 and Equation in wind axis coordinate system, respectively [42].

$$\dot{V} = \frac{T\cos(\alpha) - D - mg\sin(\gamma)}{m} \tag{36}$$

$$\dot{\alpha} = \frac{-T\sin(\alpha) - L - mVq + mgcos(\gamma)}{mV} \tag{37}$$

Where T is thrust, D is drag, m is mass, g is gravity, α is angle of attack, γ is flight path angle, q is pitch rate and V is true airspeed. The aircraft location change is given matrix form in Equation 23 in Earth's fixed coordinate system. Altitude change can be shown in Equation 38.

$$\dot{h} = u\sin(\theta) - v\sin(\phi)\cos(\theta) - w\cos(\theta)\cos(\phi) \tag{38}$$

Where u,v and w velocity components, $\dot{h}$ is altitude change, ϕ is roll angle and θ is pitch angle. Assuming roll angle is zero equation becomes 39.

$$\dot{h} = u\sin(\theta) - wcos(\theta) \tag{39}$$

Longitudinal motion equations are derived from Equation 34 to 39. Combining all the equations is shown in the Equations 40 to 44. These equations are used for the inner model of the longitudinal dynamics of the NMPC. The ACADO toolkit simultaneously solves these five equations. Also, intermediate steps for the lift and drag forces are calculated in the NMPC script.

$$\dot{q} = \frac{m}{I_{yy}} \tag{40}$$

$$\dot{\gamma} = q - \dot{\alpha} \tag{41}$$

$$\dot{V} = \frac{T\cos(\alpha) - D - mg\sin(\gamma)}{m} \tag{42}$$

$$\dot{\alpha} = \frac{-T\sin(\alpha) - L - mVq + mgcos(\gamma)}{mV} \tag{43}$$

$$\dot{h} = u\sin(\theta) - wcos(\theta) \tag{44}$$

4.3.2. Lateral Dynamics

In the lateral directional dynamics, the aim is to turn the aircraft to a given reference yaw angle. This motion is handled by the coordinate turn maneuver. Aircraft banks to the given yaw angle direction so that the y component of the aircraft results in the aircraft's turn without sideslip. The aileron and rudder control surfaces control this maneuver. Hence, NMPC finds the best aileron and rudder input simultaneously for the given yaw trajectory.

Phi and psi derivatives are found by using Equation 22 with the assumption that the pitch rate is zero. Equation 45 is obtained by taking the pitch rate zero and assuming that during the coordinated turn maneuver, the pitch angle is constant. Because of that, the initial pitch angle is used.

$$\dot{\phi} = p + r\tan(\theta_0)\cos(\phi) \tag{45}$$

Where $\dot{\phi}$ is derivative of roll angle, p is roll rate, r is yaw rate and θ_0 is pitch angle. Using the same assumptions, Equation 46 is found.

$$\dot{\psi} = r\frac{\cos(\psi)}{\cos(\theta_0)} \tag{46}$$

Where $\dot{\psi}$ is derivative of yaw angle, r is yaw rate and θ_0 is pitch angle. Equation 21 shows the 6DoF equations of the aircraft. Equations 47 and 48 are obtained by using the fourth and sixth equations and assuming the pitch rate is zero.

$$\dot{p}I_{xx} - \dot{r}I_{xz} = l \tag{47}$$

$$\dot{r}I_{zz} - \dot{p}I_{xz} = n \tag{48}$$

Where $\dot{p}$ is derivative of roll rate, $\dot{r}$ is derivative of yaw rate, I is inertia, l is roll moment and n is yaw moment. Combining these equations, derivative of the roll and yaw rate are found, which are shown in Equation 49 and Equation 50.

$$\dot{p} = \frac{I_{zz}l + I_{xz}n}{I_{xx}I_{zz} - I_{xz}^2} \tag{49}$$

$$\dot{r} = \frac{I_{xz}l + I_{xx}n}{I_{xx}I_{zz} - I_{xz}^2} \tag{50}$$

Where l is roll moment, n is yaw moment, I is inertia, $\dot{p}$ is derivative of roll rate and $\dot{r}$ is derivative of yaw rate. Angle of sideslip derivative is found as Equation 51 and Equation in wind axis coordinate system [42].

$$\dot{\beta} = p\sin(\alpha_0) - r\cos(\alpha_0) + \frac{-T\cos(\alpha_0)\sin(\beta) + mg_y + F_Y^w}{mV} \tag{51}$$

Where $\dot{\beta}$ is derivative of sideslip angle, p is roll rate, r is yaw rate, T is thrust, α is angle of attack, m is mass, g is gravity and V is airspeed. F_Y^w is force y direction of the wind axis which is shown in Equation 52. and g_y is acceleration due to gravitational force in y direction of the wind axis which is shown in Equation 53.

$$F_Y^w = -X\cos(\alpha_0)\cos(\beta) - Y\sin(\beta) - Z\sin(\alpha_0)\cos(\beta) \tag{52}$$

$$g_y = g(\cos(\alpha_0)\sin(\beta)\sin(\theta_0) + \cos(\beta)\sin(\phi)\cos(\theta_0) - \sin(\alpha_0)\sin(\beta)\cos(\psi)\cos(\theta_0)) \tag{53}$$

Where X, Y and Z forces, α is angle of attack, β is sideslip angle, g is gravity and ϕ, θ, ψ are Euler angles. Lateral-directional motion equations are derived from Equation 45 to

51. Combining all the equations is shown in the Equations 54 to 58. These equations are used for the inner model of the Lateral-directional dynamics of the NMPC.

$$\dot{\phi} = p + r\tan(\theta_0)\cos(\phi) \tag{54}$$

$$\dot{\psi} = r\frac{\cos(\psi)}{\cos(\theta_0)} \tag{55}$$

$$\dot{p} = \frac{I_{zz}l + I_{xz}n}{I_{xx}I_{zz} - I_{xz}^2} \tag{56}$$

$$\dot{r} = \frac{I_{xz}l + I_{xx}n}{I_{xx}I_{zz} - I_{xz}^2} \tag{57}$$

$$\dot{\beta} = p\sin(\alpha_0) - r\cos(\alpha_0) + \frac{-T\cos(\alpha_0)\sin(\beta) + mg_y + F_Y^w}{mV} \tag{58}$$

Equations of the internal models are derived from both longitudinal and lateral-directional motion. These equations are modeled with two different blocks so that one of them can be used or both of them can be used in the analysis. Due to the increase in the time when both models are active, studies are performed with only one controller. Figure 4.3 shows the model algorithm. If one of the NMPCs is active, then the other control inputs are taken as a constant value at the trim condition.

The final step is combining the NMPC with the aircraft model. Figure 4.4 represents the final model of the study. The first block is the reference trajectory block. In this block, two different inputs can be given. One of them is altitude input, and the other one is yaw angle. These reference trajectories are connected to the NMPC controller block, whose motion is controlled by the user. Longitudinal or lateral directions or both of them can be selected. In this block, a low-fidelity aircraft model and optimization algorithm are implemented. Lastly, the nonlinear 6DoF high-fidelity model is presented with the AIRCRAFT block. In the analysis, Simulink model step time is selected as 0.10 seconds during the simulations. In the NMPC internal model, step time is chosen as 0.05 seconds. The prediction horizon selected in the longitudinal motion is 2 seconds. In the lateral directional motion, 1 second

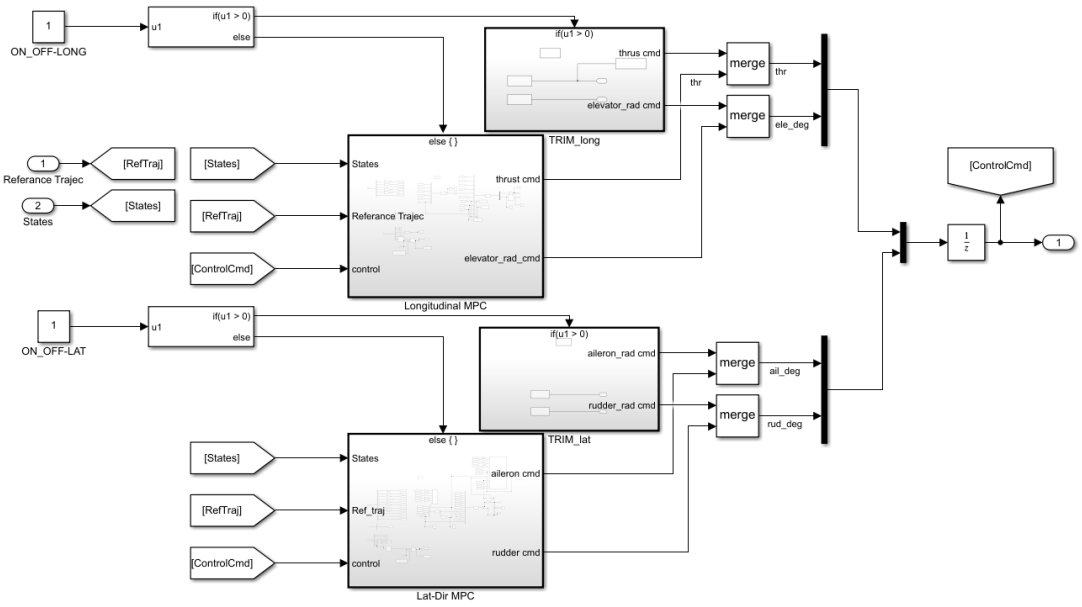

Figure 4.3 Longitudinal and lateral-directional NMPC model in Simulink enviroment

is found to be adequate. As the prediction horizon is increased, the required time to find the optimal solution increases. After some try errors, these values are selected.

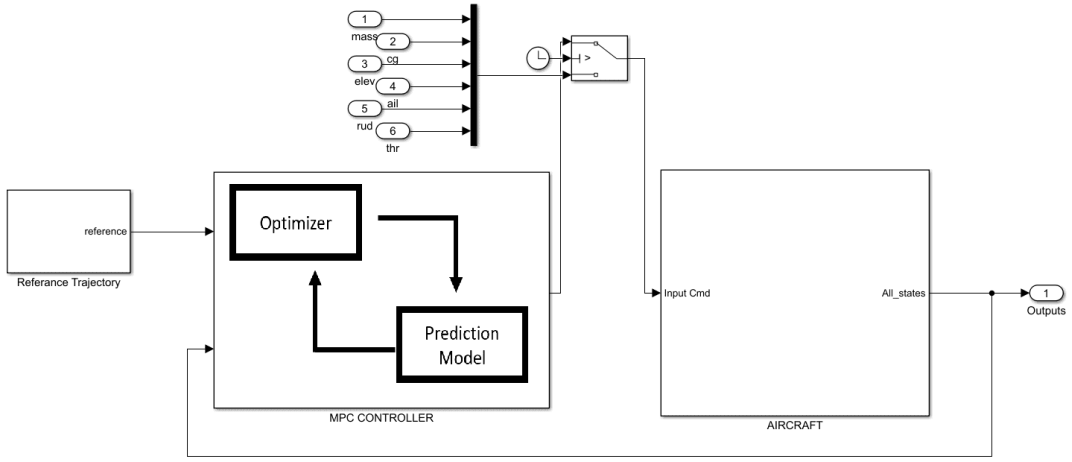

Figure 4.4 Aircraft and controller model

4.4. Verification

To examine the NMPC algorithm behavior, three different analyses were performed without failure. In the first analysis, only longitudinal motion is discussed. In this case, lateral-directional control inputs are taken as constant during the simulation. Altitude is given as a climb and descent phase. The second case is coordinated turn motion. In this case, longitudinal control inputs are taken as constant during the simulation. Only lateral and directional motion are controlled by the NMPC. Reference trajectory is given only a positive yaw angle. As a last case, both trajectories are given, and both NMPC blocks are enabled. Required time to find the optimal control inputs are increased in these case.

Case 1 - Longitudinal Control

Figure 4.5 shows the longitudinal parameters results. The aircraft follows the reference trajectory by changing the elevator angle, which is done by the NMPC algorithm. These graphs show that the aircraft used the elevators without exceeding the control surface limits. The aircraft has no extreme reactions, as demonstrated by pitch rate and normal acceleration. The controller perfectly handled both the climb and descend phases. Also, no oscillatory inputs and outputs are observed.

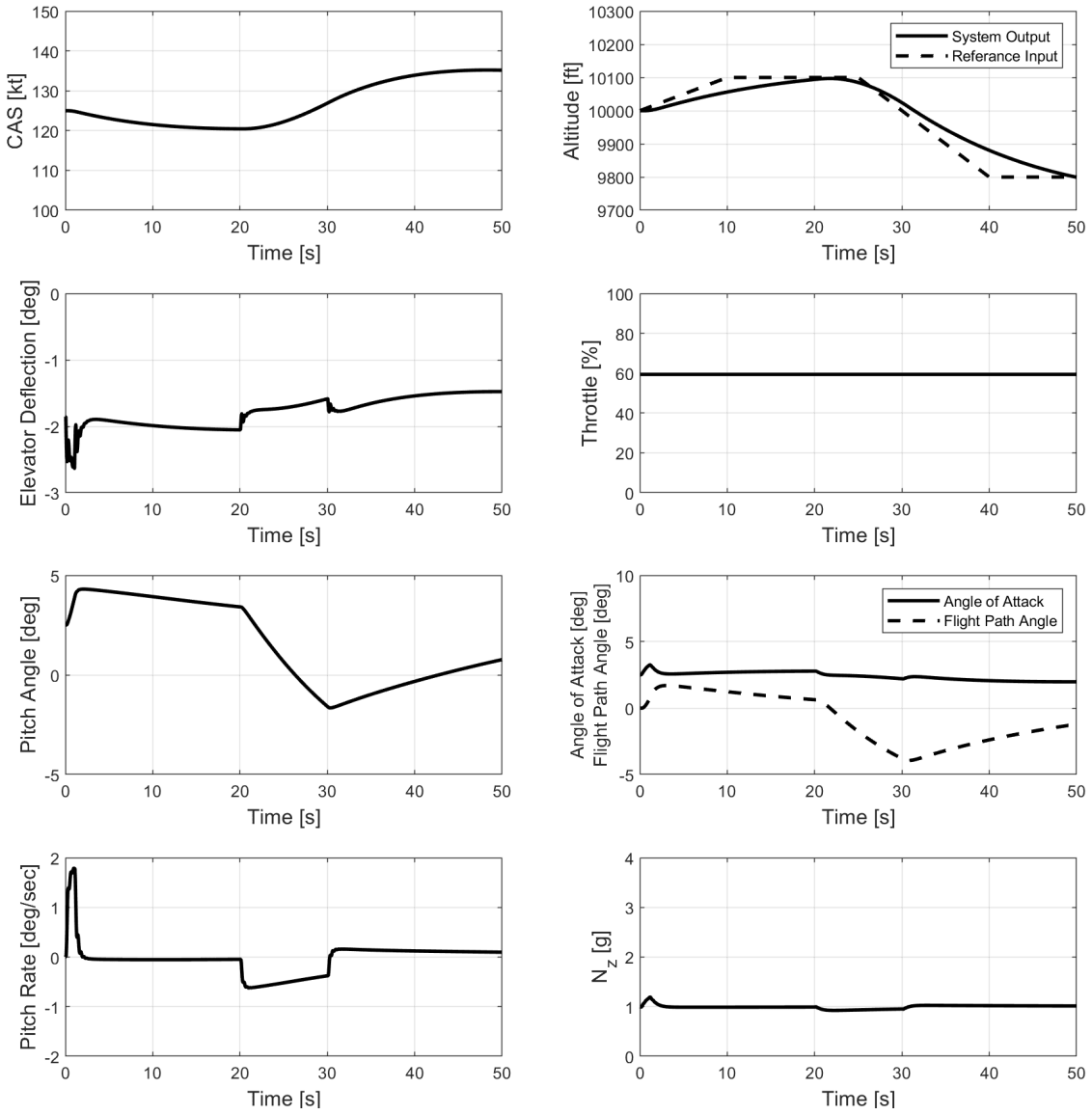

Figure 4.5 Longitudinal control outputs

Case 2 - Lateral-Directional Control

Figure 4.6 shows the lateral-directional results. In this case, aircraft turns to the given reference yaw angle with rolling that direction. Coupled motion is simulated with this case. Both rudder and aileron is used. Aircraft rotates the given yaw angle with little overshoot. However, it reaches steady state value approximately in thirty seconds. There are no oscillatory outputs. Control surfaces are used in the surface limit of the aircraft.

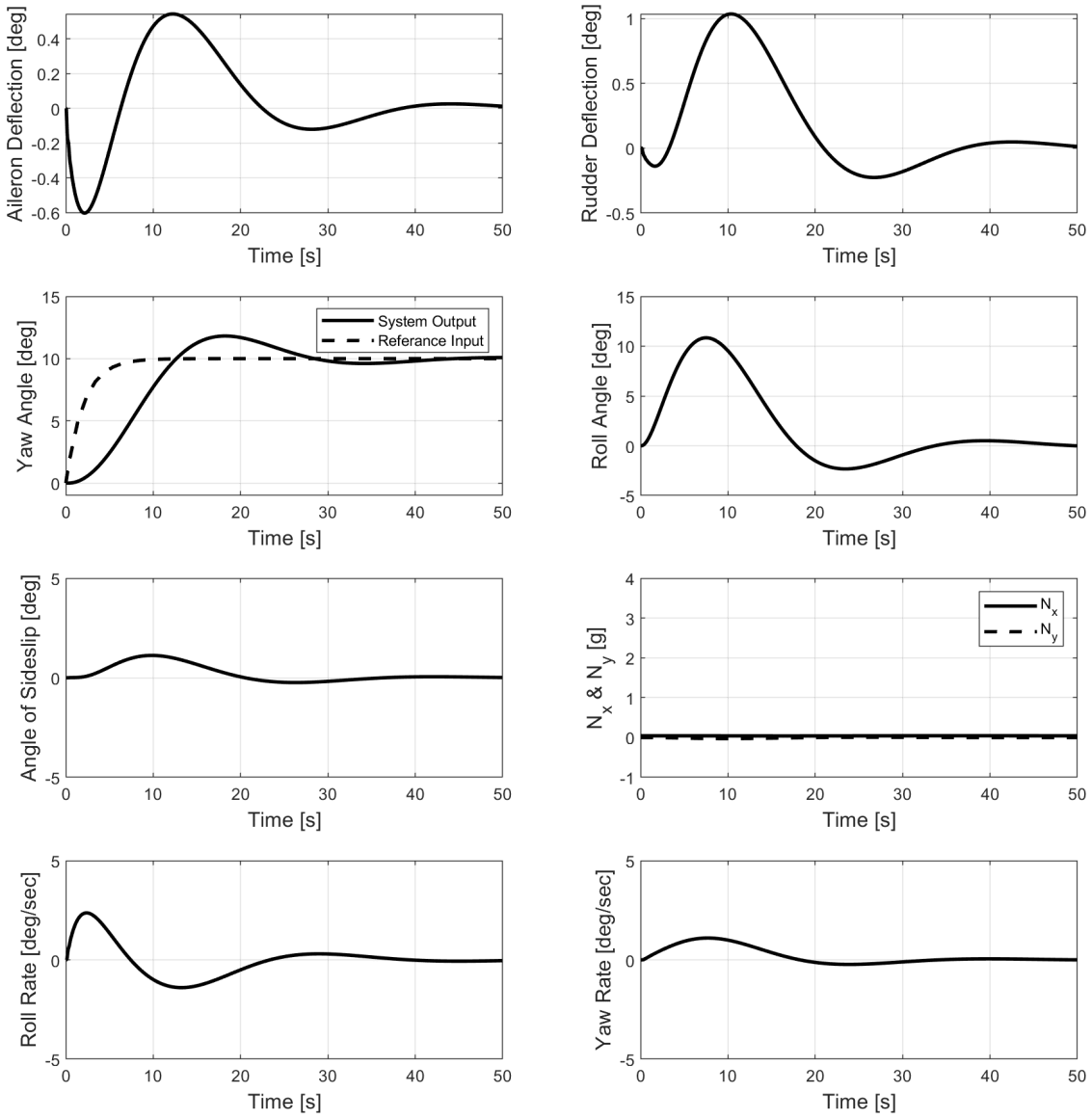

Figure 4.6 Lateral-directional control outputs

Case 3 - Longitudinal and Lateral-Directional Control

In these case, same trajectories are given simultaneously. Aircraft climbs, descends and turns at the same time. In Figure 4.7, longitudinal behaviour is presented with the output parameters. As shown in these graphs, aircraft follows the given attitude reference input without any degradation due to lateral directional motion. Similar results are obtained as Case 1 which proves that longitudinal and lateral directional motion does not affect each other significantly.

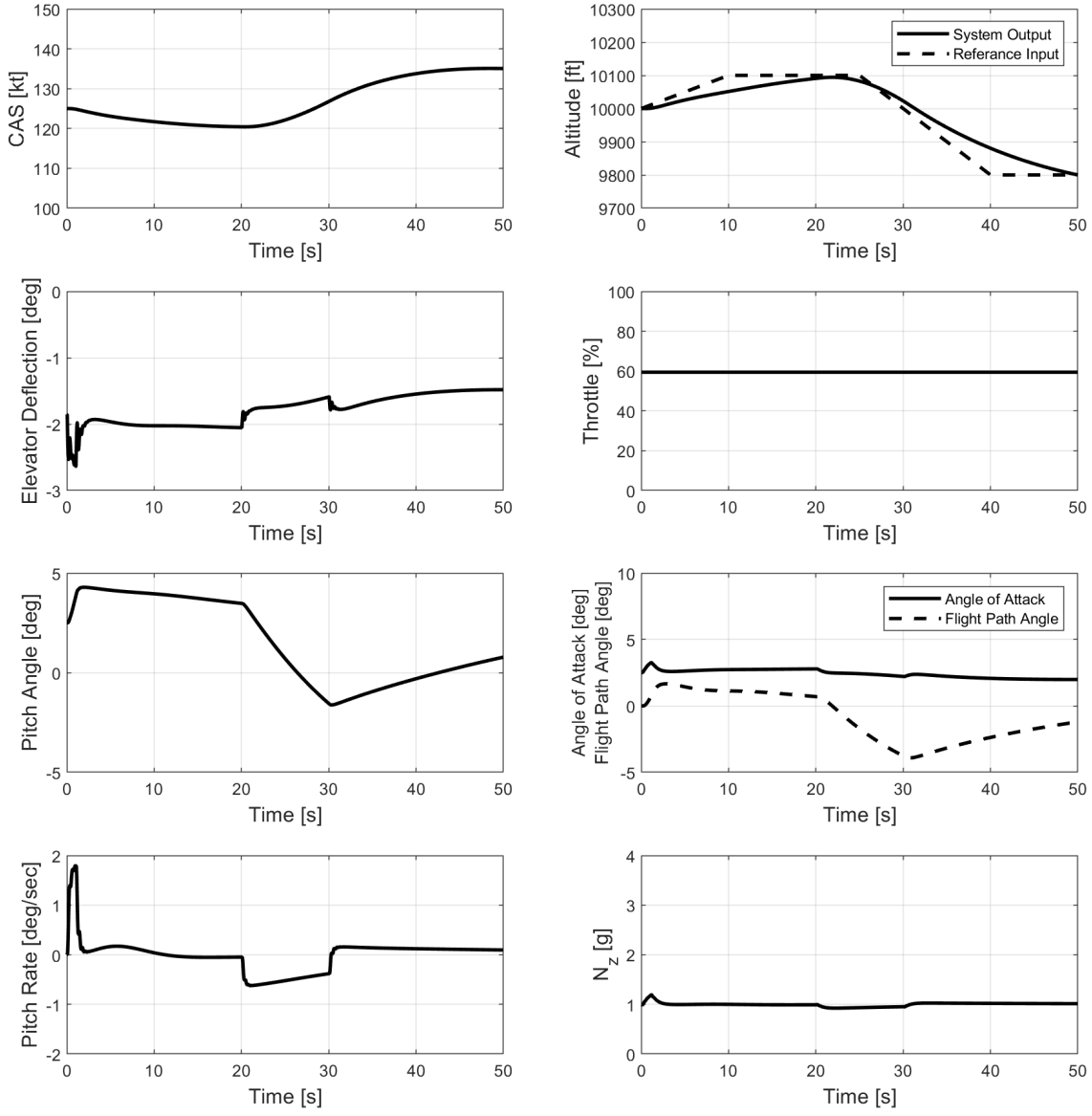

Figure 4.7 Longitudinal results of the NMPC with two axis trajectory

Figure 4.8 shows the lateral directional motion. Same as case 2, aircraft turns the given yaw angle. Controlling longitudinal motion does not changed the lateral directional motion. Aircraft followed the given reference input with predicted rudder and aileron. Overall behaviour is combination of the Case 1 and Case 2. The only big difference is required time is approximately doubled. Therefore, in the failure analysis, only required channel is enabled so that time consumption is minimized.

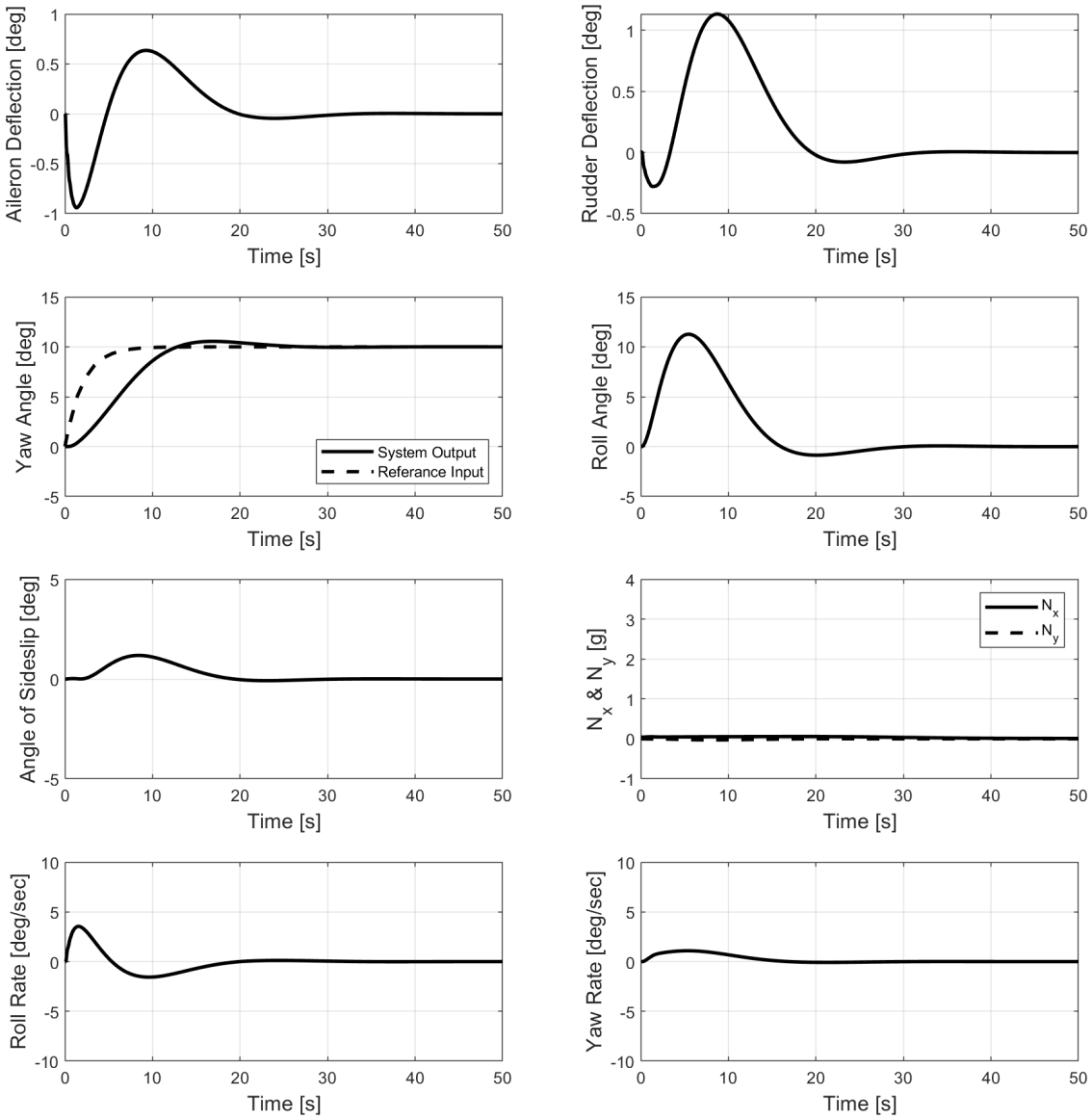

Figure 4.8 Lateral-directions results of the NMPC with two axis trajectory

4.5. Conclusion

In this section, the theory of the NMPC is explained, and the optimization is done by the ACADO program. The internal model of the NMPC equations is derived, and the model is divided into two motions: longitudinal and lateral dynamics. Lastly, some examples are given to show the NMPC results. Longitudinal and lateral directional controllers work without affecting each other. So, the findings of the examples show that only one channel is enough during the simulations, which decreases the required time to solve the simulations.

5. FAULT TOLERANT CONTROL

5.1. Introduction

In this section, a fault detection algorithm is presented. Two different approaches have been used. One is based on statistical data, and the other is the decision-making algorithm. Also, after identifying the fault, an appropriate controller was needed. Some modifications are made to the NMPC inner model to use the best controller. Different NMPCs are developed and integrated into the 6DoF model. This approach is called multiple model switching. The main idea of these concepts is explained in this section.

5.2. Fault Detection System

Multiple methods are found in the literature for fault detection. Mainly, these methods are divided into two: model-based techniques and data-based techniques [43]. In this thesis, two different faults are analyzed. One of them is control surface jamming failure. To detect this type of fault, a decision-making rule algorithm is used [31]. The second fault is control surface effectiveness degrading, and this fault detection is based on statistical data [30].

The decision-making rule is based on model results or aircraft sensor data. The fault is detected if the difference between the aircraft model output of the control surface and the NMPC output is higher than the given threshold. The type of fault is detected if the previous model output is equal to the current model output, which means the control surface is stuck; it is not rotated. Figure 5.1 shows decision-making algorithm representation. This algorithm is done for all the control channels during the analysis: aileron, rudder, and elevator. So that any jamming can be found.

Statistical data is used when the control surface loses its effectiveness. This is only applied to the elevator control surface. In the case of icing or another reason, the control surface might lose its effectiveness. In this thesis, elevator effectiveness is assumed to be

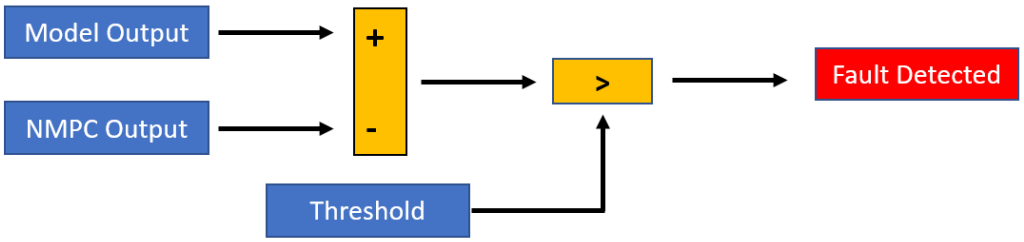

Figure 5.1 Decision making algorithm representation

decreased for some reason. This decrease is directly related to the control power of the elevator. Detection of this type of failure is challenging. To find the fault, statistical data is used in this thesis. Initially, multiple simulations are done with the UAV model without any failure. In this analysis, altitude, velocity, and elevator are changed individually. So that a four-dimensional data set can be created. Multiple breakpoints are selected for the lookup table. These three parameters are used as input in the lookup table, and the output of this data is pitch rate. The pitch rate is selected as statistical data in the longitudinal axis. The first reaction of the aircraft comes in rate, followed by pitch angle when the elevator is deflected. The main idea is that a specific pitch rate must be obtained when these three inputs are given to the lookup table. If the model output pitch rate is not equal to this pitch rate value from the lookup table, then there is a fault. However, similar to the decision-making algorithm, the threshold value is selected. If the difference between the model output and the expected pitch rate output value is bigger than the threshold, then there is a failure in the elevator control surface.

5.3. Multiple Model Switching

After the detection of the fault, the control algorithm switches the fault-free model to the appropriate model with the detected fault. In this section, this algorithm is explained.

When any control surfaces are stuck, decision making rule detects the fault. Then appropriate model is selected by multiple model switching (MMS) algorithm. The NMPC script takes the stuck control surface as constant. In the analysis, longitudinal motion is

controlled by the elevator only. Because of that, jamming failures are not examined in the longitudinal axis. In the lateral-directional motion, a rudder and aileron are used. When one is detected as stuck, NMPC considers that stuck control surface constant after checking the previous and current values. Therefore, fault is detected and appropriate NMPC is selected by multiple model switching algorithm.

In the elevator failure analysis, statistical method is used for detection of the fault. This approach does not answer the magnitude of the decrease, and because of that, two different NMPCs are developed. These NMPCs have different elevator control power values in the internal model—the selection is based on the difference in magnitude. If the magnitude is higher, then the algorithm selects NMPC, which contains the minimum elevator control power; if the magnitude is small, then the algorithm selects NMPC, which includes the maximum elevator control power, to improve the controller's performance. Therefore, multiple modeling is also used in this failure. An important deficiency is that NMPC still does not know the magnitude of the degradation. It only selects the best one for the given failure.

5.4. Conclusion

To sum up, the fault detection algorithm is explained. Two different fault detection algorithms are developed and applied to the UAV aircraft. One is for jamming failures, and the other is to control surface effectiveness degradation. After the fault is detected by the decision-making algorithm or the statistical data, appropriate NMPC is selected to improve the overall performance of the controller. Different NMPCs are developed and integrated into the Simulink model to handle this approach. So, multiple modeling and switching algorithm is used. The found fault type does this selection.

6. SIMULATIONS AND RESULTS

6.1. Introduction

This section performs multiple analyses with the 6DoF aircraft model with NMPC. The summary of the process can be explained in three steps. The first step is developing the 6 DoF aircraft model. The second step is designing NMPC using the ACADO toolkit. The third step is adding a fault detection algorithm and using appropriate NMPC due to selected faults. This adaptive approach helps to follow the given trajectory with reasonable accuracy for different fault scenarios.

Three different types of loss of control fault are examined with varying magnitudes of the fault. In the longitudinal axis, the decrease in elevator efficiency is examined as a fault. This type of fault might occur due to icing problems. Different magnitudes of deficiencies are examined in elevator faults. The main idea is to follow a given altitude change with the available elevator power. Summary of the longitudinal fault scenarios are:

- Elevator Effectiveness Decrease
  - Control Power Deficiency 20%
  - Control Power Deficiency 50%

In the lateral-directional axis, control surface jamming is examined. Rudder stuck, and aileron stuck are simulated separately. In these simulations, the main idea is to follow the given yaw angle by doing a coordinated turn. Different magnitudes of the control surface stuck scenarios are examined. Summary of the lateral directional fault scenarios are:

- Rudder Jamming (stuck)
  - Rudder stuck at 0°, 2°, 5°, 8°, -2°, -5°, -8°
- Aileron Jamming (stuck)

– Aileron stuck at $2°$, $-2°$

6.2. Elevator Efficiency Decrease

In the longitudinal motion, the primary purpose is to follow the given altitude path. Elevator efficiency is decreased when the control power is changed. Three different analyses are performed with varying magnitudes of the deficiency. The effectiveness is reduced step by step so as to examine the effect of the malfunction magnitude on the aircraft and the controller. Each simulation is compared with the fault-free case.

Figure 6.1 shows the reference input, which is given to the NMPC and model result without failure case. The primary objective is to reach as much as possible without failure cases with the failure scenarios. All the analysis have same reference input.

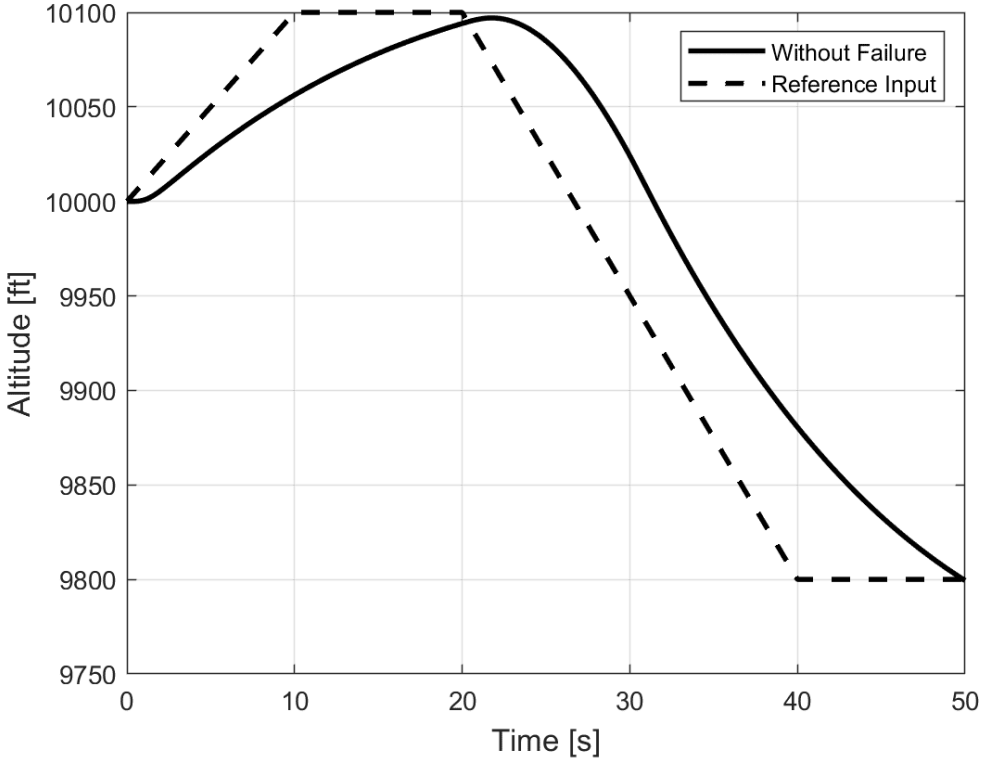

Figure 6.1 Reference altitude trajectory and model result

Fault is given at time is 0.8 seconds. At this time control power of the elevator is multiplied with the deficiency factor. After that point algorithm detects the fault and selects the

NMPC that gives best results. This selection is based on pitch rate difference from the without failure case. When the pitch rate is different than the without case with an threshold, algorithm detects the fault and selects the best NMPC design.

Figure 6.2 shows the pitch rate of the simulation results. 3 different analysis are performed. First one is without failure case, if the pitch rate different from this result that means there is a fault in the aircraft which results an selection of appropriate NMPC. Second and third curves show the fault cases pitch rate. Due to decrease in the elevator effectiveness initial response is that pitch rate is decreases. At this point algorithm detects the difference between the healthy data and the fault data so that knows the failure.

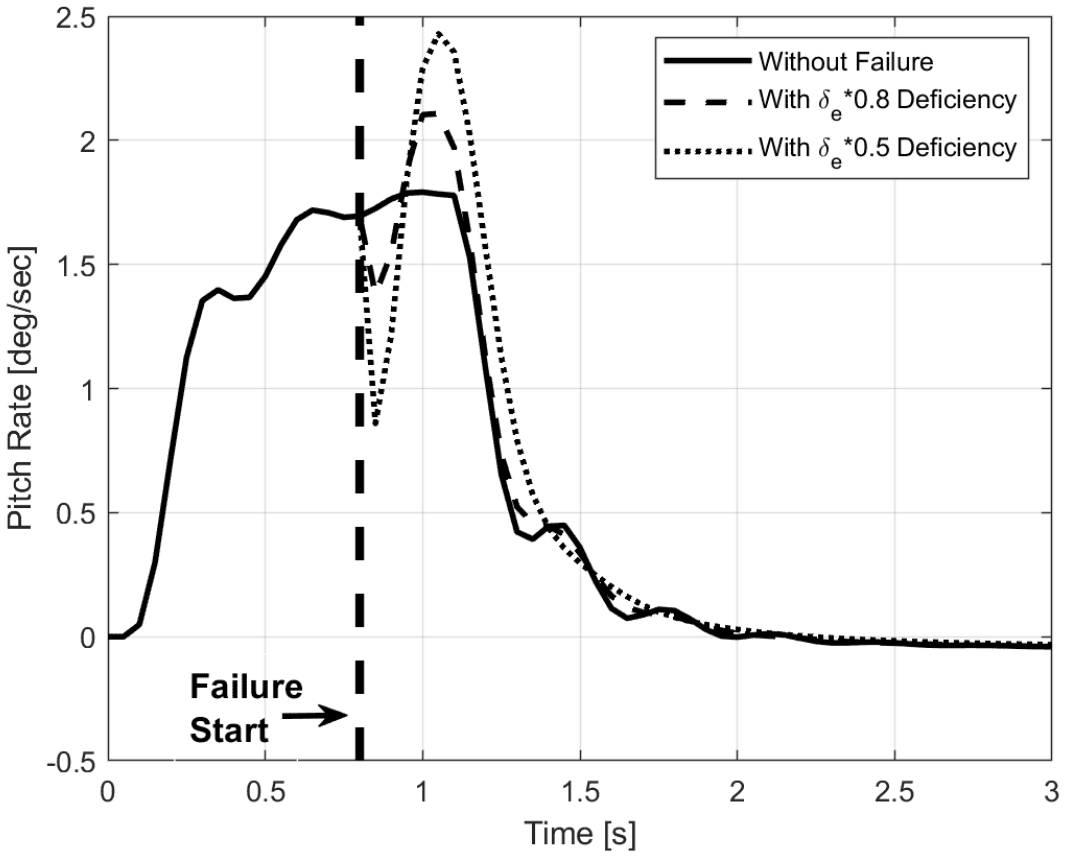

Figure 6.2 Pitch rate results without failure and with failure cases

Figure 6.3 shows the aircraft behavior under the elevator deficiency failure case with a magnitude of 0.2 decreases on the control power. Solid lines refer to a failure case, and dash lines refer to a failure case. As shown in the graphs, altitude is followed with a little deviation in the failure case. These results show that the NMPC algorithm and multiple modeling handle the fault with good performance. Required elevator deflection to follow the given trajectory increased. That result is expected because when the control power is decreased to reach the same flight path angle, the elevator is deflected more than the without failure case. The flight path angle is the same as the without failure case, which shows that the aircraft follows the same path without losing control of the aircraft. The pitch rate difference is mentioned above; in the first 2 seconds, the difference is minimized by increasing the elevator deflection by the NMPC controller.

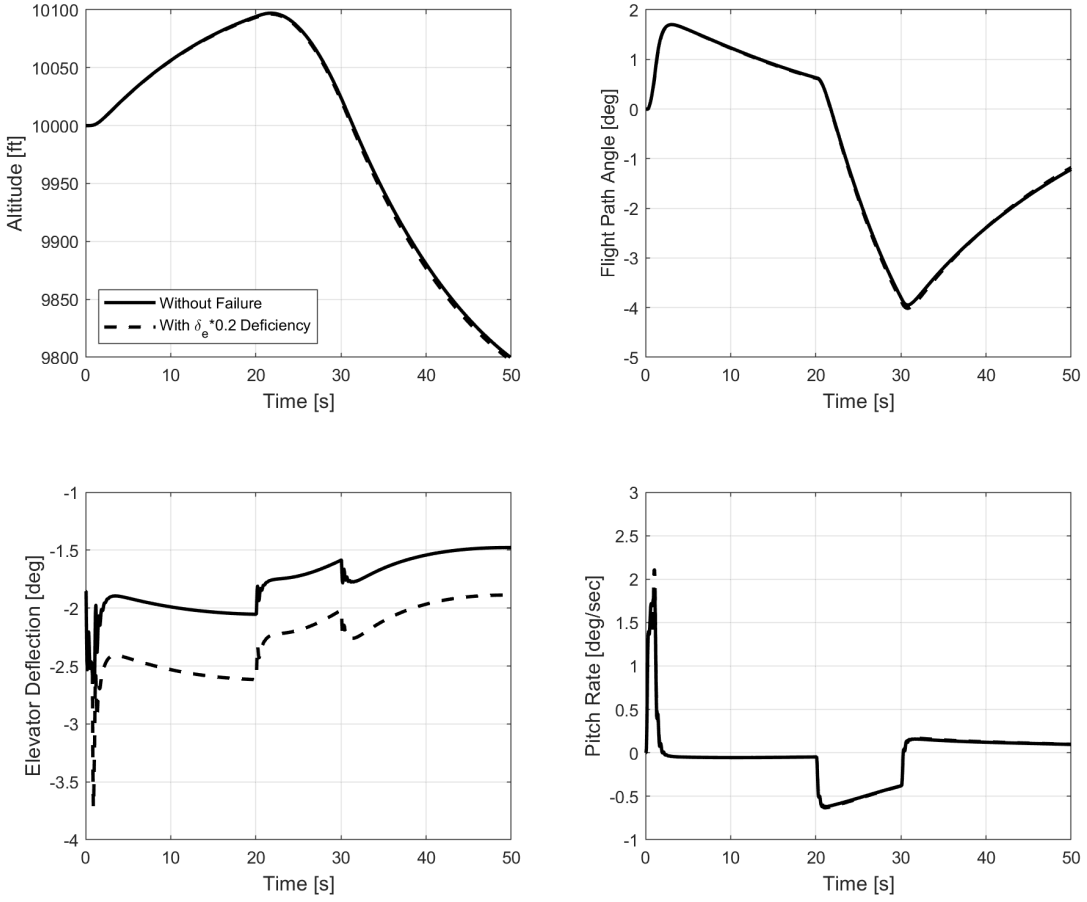

Figure 6.3 Case 1: Longitudinal failure with 0.2 elevator control power deficiency

Figure 6.4 shows the second failure case, which is the 0.5 elevator control power deficiency. This result is similar to Case 1. Aircraft follow the given trajectory as much as possible without any uncontrollable motion. Therefore, the flight path angle is the same as without the failure case. The pitch rate is mentioned above. There is a little deviation that enables the detection of the fault on the aircraft. Elevator deflection magnitude is increased highly due to a decrease in the control power. However, the results are within the control surface limits. Comparing Case 1 with Case 2, the only difference is an increase in the elevator deflection. That result is expected due to a deficiency in the control power. This shows that as the control power decreased, NMPC tried to increase the elevator deflection to reach the same pitch rate and flight path angle.

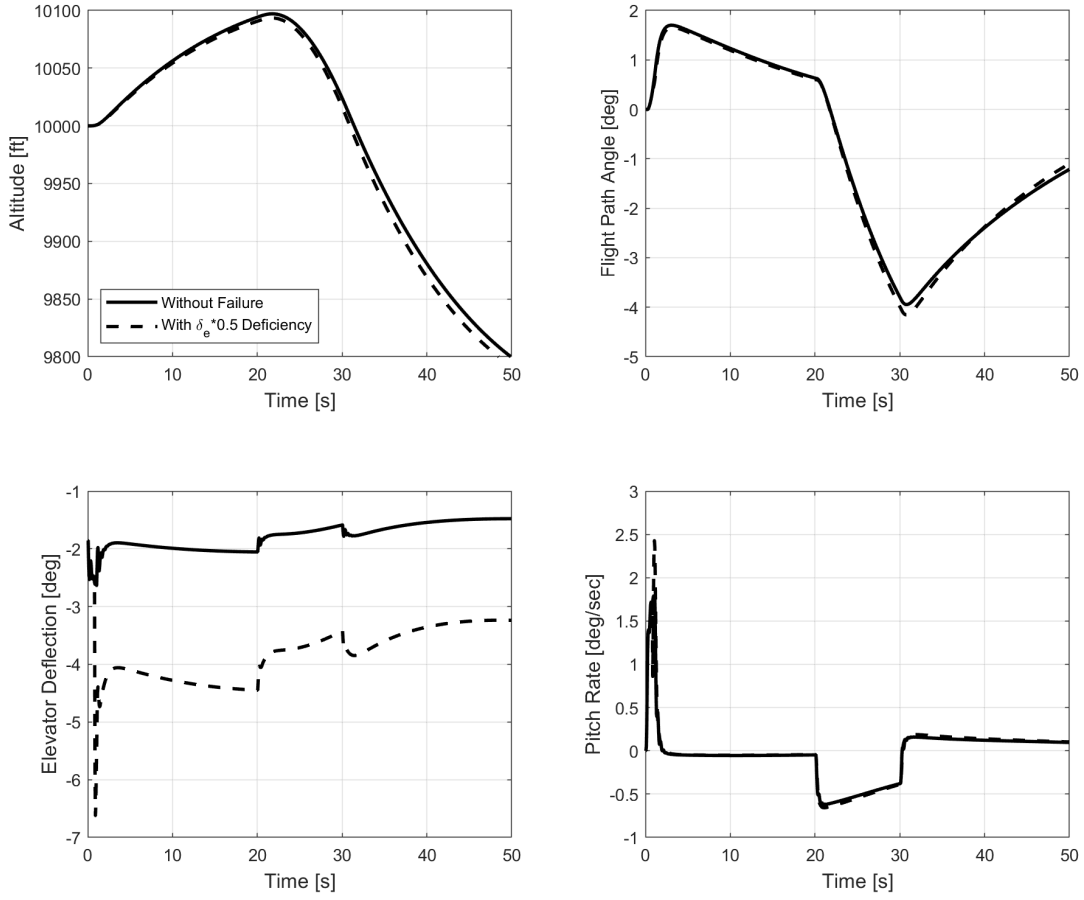

Figure 6.4 Case 2: Longitudinal failure with 0.5 elevator control power deficiency

Figures 6.5 and 6.6 show the aircraft trajectory with different perspectives; figures are obtained with the help of the flypath3d tool [44]. As shown in the figures, aircraft without failure and with failure cases follow the same path. There is no displacement in the y direction. The longitudinal motion does not affect the lateral directional motion. The altitude change is almost the same for all cases. That shows that the NMPC controller can handle the different magnitudes of elevator deficiency without losing the altitude with an elevator deflection range. So that aircraft can be controlled with a controller when there is a fault in the elevator effectiveness.

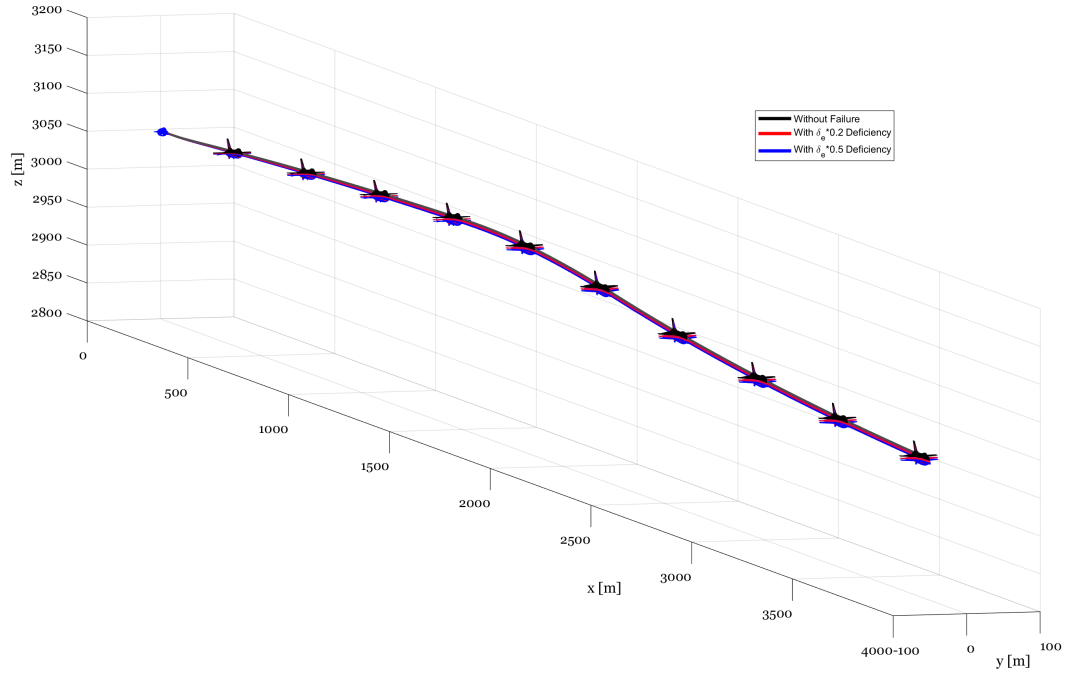

Figure 6.5 3D view of the simulation results

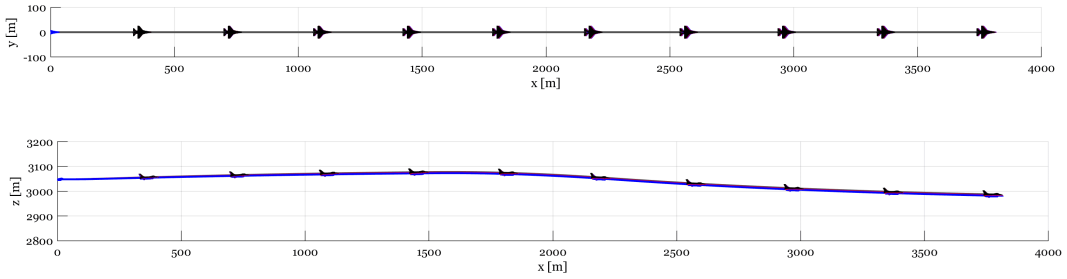

Figure 6.6 Top and side view of the simulation results

6.3. Rudder Jamming

Jamming of a surface means that the control surface is stuck at a specific location due to external forces, actuator, or mechanical problems. In this section, rudder jamming is examined using the 6DoF UAV model. The maneuver is performed and controlled by the NMPC. NMPC found the best aileron and rudder deflections and supplies for the 6DoF UAV model. When the rudder is stuck, aircraft turns become hard to control even with the pilot. Various rudder jamming analyses are performed to examine if aircraft can be turned with an aileron-only configuration. Without the rudder, the only way to control the aircraft is by the aileron control surface. With the scope of the analysis, the effect of the aileron on the coordinated turn maneuver was examined.

The primary purpose is for the aircraft to turn the aircraft to the given yaw rate trajectory by doing coordinated turn maneuvers with the only aileron control surface. Minus eight-degree to plus eight-degree deflection of the rudder is analyzed. So that, step by step, the aircraft behavior and controller performance can be seen. The decision-making algorithm detects the fault and selects the appropriate controller. The main idea is that if the model output, which means sensor output, is not equal to NMPC output, which is input to the 6DoF, the algorithm detects a fault. After that, a suitable NMPC is selected by the decision-making algorithm.

Rudder jamming cases:

- **Case 1:** Rudder deflection is equal to 0°
- **Case 2:** Rudder deflection is equal to 2°
- **Case 3:** Rudder deflection is equal to 5°
- **Case 4:** Rudder deflection is equal to 8°
- **Case 5:** Rudder deflection is equal to -2°
- **Case 6:** Rudder deflection is equal to -5°

- **Case 7:** Rudder deflection is equal to -8°

Figure 6.7 shows the reference input to the model and the model output without failure case. This graph shows that the model output is close to the reference yaw angle. There is a slight overshoot, but it converges in a steady state of approximately 10 seconds. The same reference trajectory is given to the fault case analysis. For the fault cases with the same reference trajectory, expected results follow the same path as much as possible without showing any uncontrollable motion. An important note is that the yaw angle does not mean that the track of the aircraft is the same. Track angle is yaw angle summation with the sideslip angle. With the rudder jamming, there is a sideslip, which results in a different path even though it follows the same yaw angle.

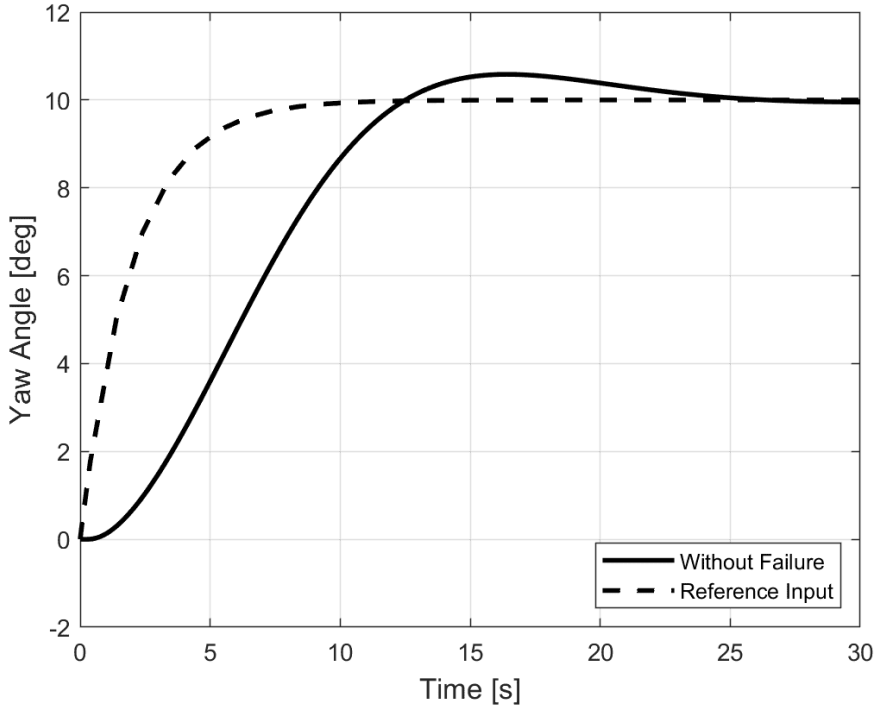

Figure 6.7 Reference yaw trajectory and model result

Figure 6.8 shows the rudder deflections of the 6DoF UAV model output. As shown in these graphs, the rudder initially works without any fault. After five seconds, rudder input is given to the model externally. The scenario is that the actuator or the mechanical reasons rudder rotated to a specific deflection. The left graph shows the positive rudder-stuck

cases; the right graph shows the negative rudder-stuck cases. Without failure case shows that the rudder initially deflected approximately 1° at this point, and the target yaw angle was almost reached. After that, rudder deflection becomes its initial value so that turning is stopped. In the fault cases, in the first five seconds, there is no failure in the aircraft. When the time reaches five seconds, the external rudder deflects different values. The detection algorithm is explained in Section 5.. Mainly, the variance between the model output and the NMPC output is compared. If the variance is higher than the given threshold, related NMPC is selected, and analysis is continued. This algorithm is called a decision-making rule. With the multiple modeling and the fault detection algorithm, numerous analyses are conducted to ensure the performance of the NMPC.

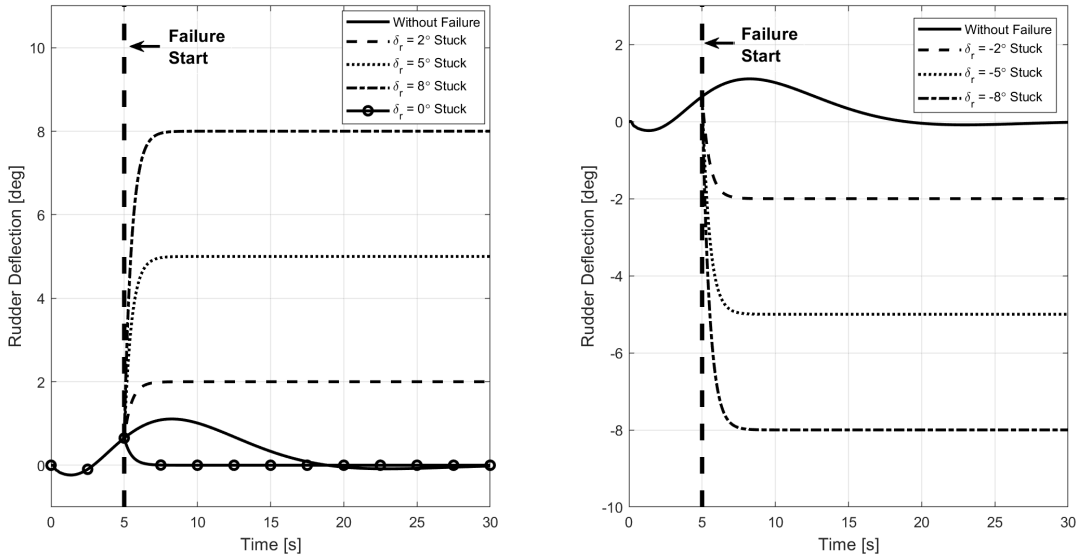

Figure 6.8 Rudder deflections with the different fault cases

Figure 6.9 graph set shows the lateral directional motion of the aircraft with the rudder jamming failure. Solid lines refer to without failure case, and dash lines refer to failure case. In this graph set, aileron deflection, AoS, roll angle, yaw rate, and roll rate are presented. As shown in the yaw angle graph, a similar trajectory is obtained by the NMPC with a failure case. There is a slight deviation after five seconds, which is the time when the failure starts. At this point, to hold the same yaw angle, the aileron is deflected rapidly compared to the without case. In this analysis, the aircraft easily follows the given trajectory because rudder deflection is small in the without failure case, as mentioned

before and seen in Figure 6.8. A similar roll angle is achieved with the failure case. Due to the rapid decrease in the rudder deflection 1° to 0 °, the positive yaw rate increased. Deflecting the rudder trailing edge left, the rudder creates a positive yaw moment, which results in a positive yaw rate. This yaw rate increase affects the yaw angle. Therefore, the reason for this yaw angle deviation is connected to rudder deflection. To follow the same path, NMPC decreases the aileron deflection so that a similar path is followed. With the fault, some of the parameters become oscillatory. However, the magnitude of the oscillation is not too high. Parameters converge to a steady state very quickly.

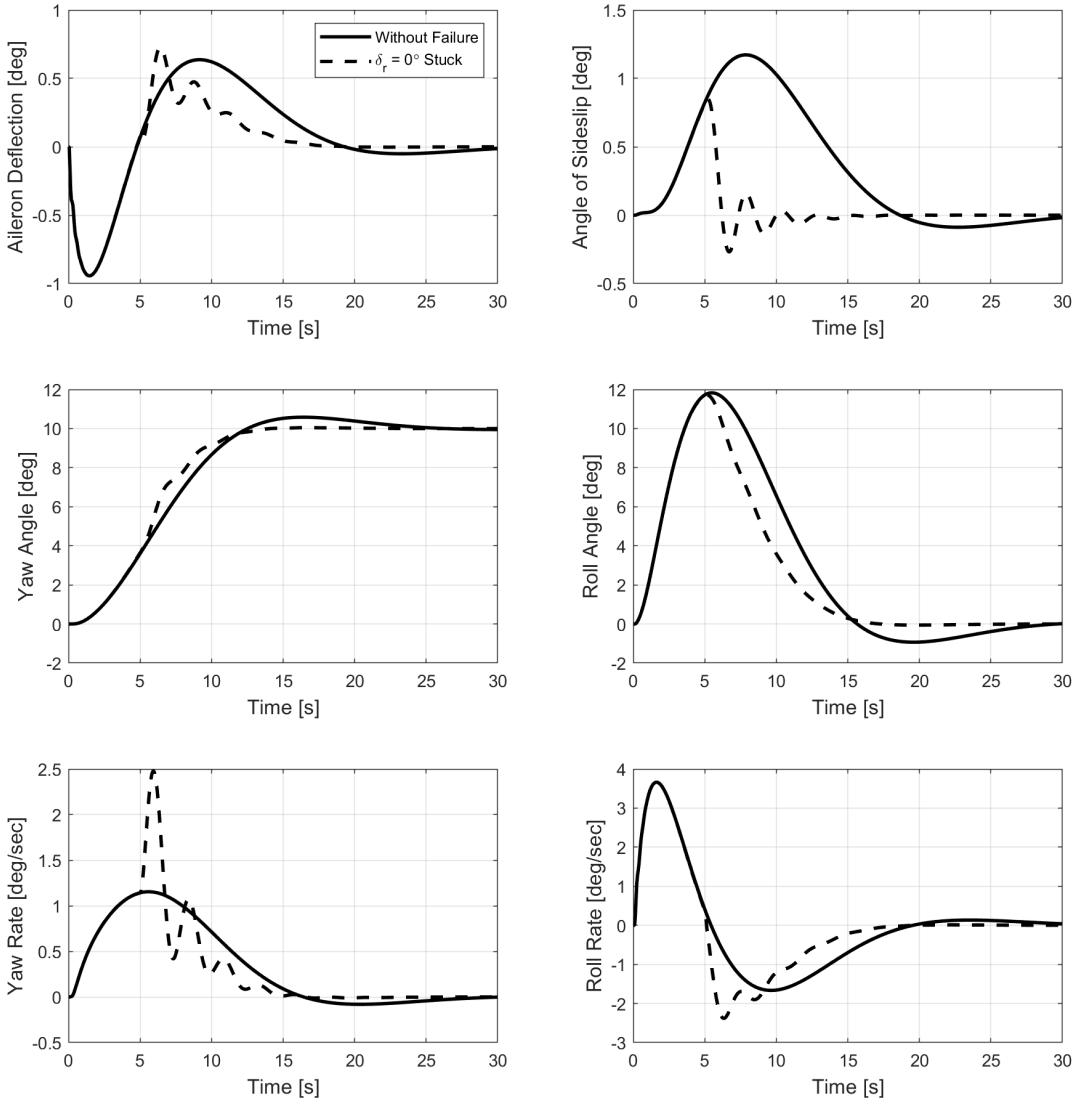

Figure 6.9 Case 1: Rudder jamming at 0° deflection

Figure 6.10 shows the two-degree rudder stuck failure results. Similarly, solid lines show the without the failure case; dash lines show the fail case. The rudder is deflected at a positive two-degree angle at a time of five seconds. At this point, the behavior of the aircraft changed quickly. The initial reaction due to rudder deflection is that the yaw rate changed its sign. Suddenly, the yaw rate changed from positive to negative. That caused to turn the opposite side to the given yaw angle trajectory. To follow the given path, NMPC increased the roll angle by deflecting the aileron more than before. So, given the NMPC follows the yaw reference trajectory with reasonable accuracy without any uncontrollable motion on the aircraft.

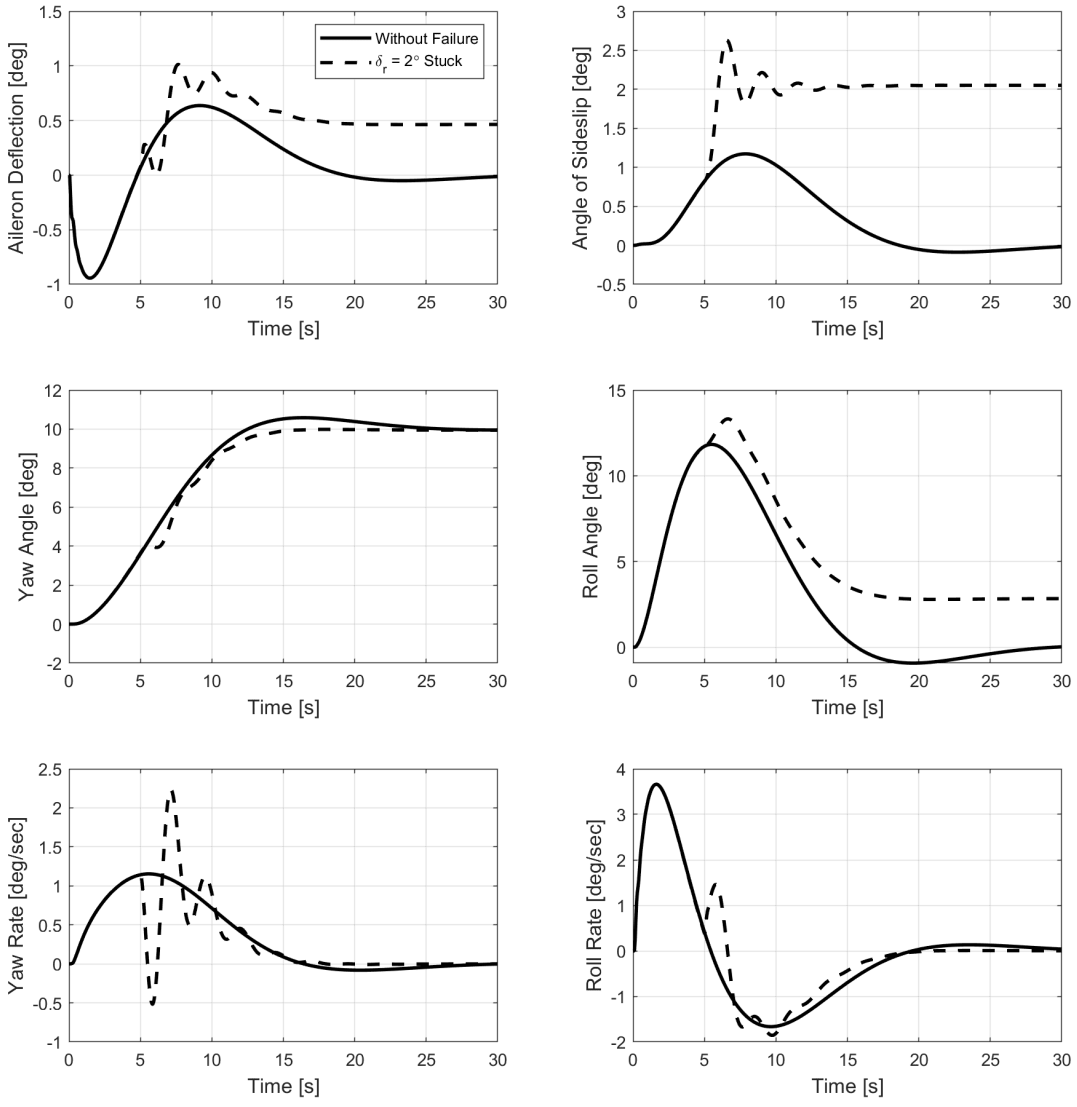

Figure 6.10 Case 2: Rudder jamming at 2° deflection

Figure 6.11 shows the five-degree rudder stuck failure results. Solid lines show the without the failure case; dash lines show the fail case. When the rudder is deflected to five degrees in the five seconds in the simulation, the yaw rate decreases significantly. Therefore, the yaw angle is moved away from the given reference trajectory. NMPC gives higher aileron deflection to turn the aircraft to a yaw angle direction so that the yaw angle increases. These results show that NMPC can handle the different magnitudes of the rudder failure case. As the rudder angle increased, NMPC worked more aggressively to follow the path by deflecting the aileron. A similar time is required to reach the steady state. On the other hand, the magnitude and frequency of yaw rate oscillations are increased.

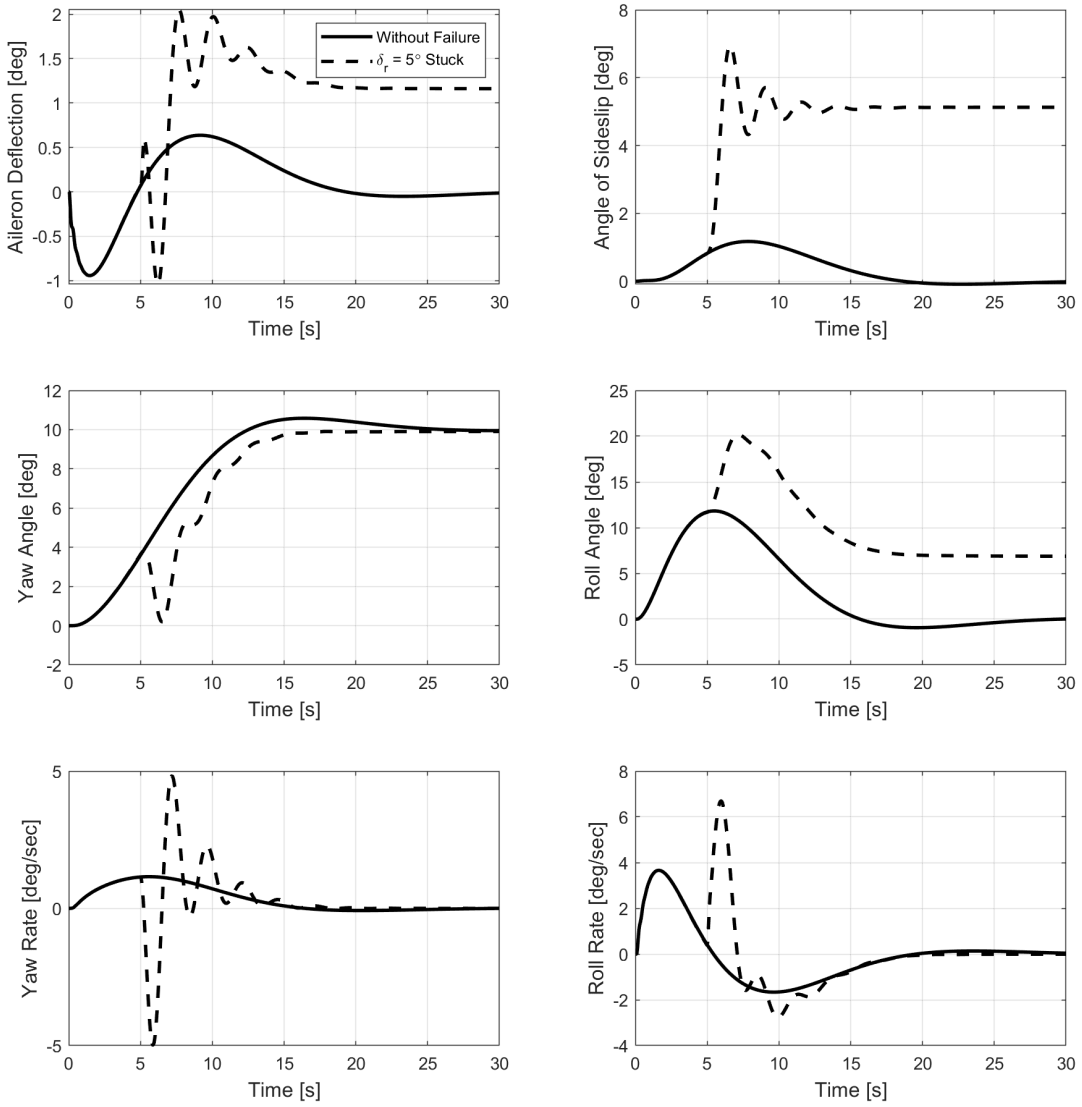

Figure 6.11 Case 3: Rudder jamming at 5° deflection

Figure 6.12 shows the eight-degree rudder stuck failure results. At this time, the behavior of the aircraft is the same as in previous failures. The yaw rate decreased significantly, so the yaw angle changed in the opposite direction from the given reference yaw angle. The aileron is deflected quickly to follow the yaw angle. As the magnitude of the failure increases, the angle of the sideslip increases. At the beginning of the rudder stuck failure, the sideslip was zero degrees. In this case, it converges to eight degrees. That causes the track of the aircraft to be changed because the track angle is the summation of the yaw angle and sideslip angle.

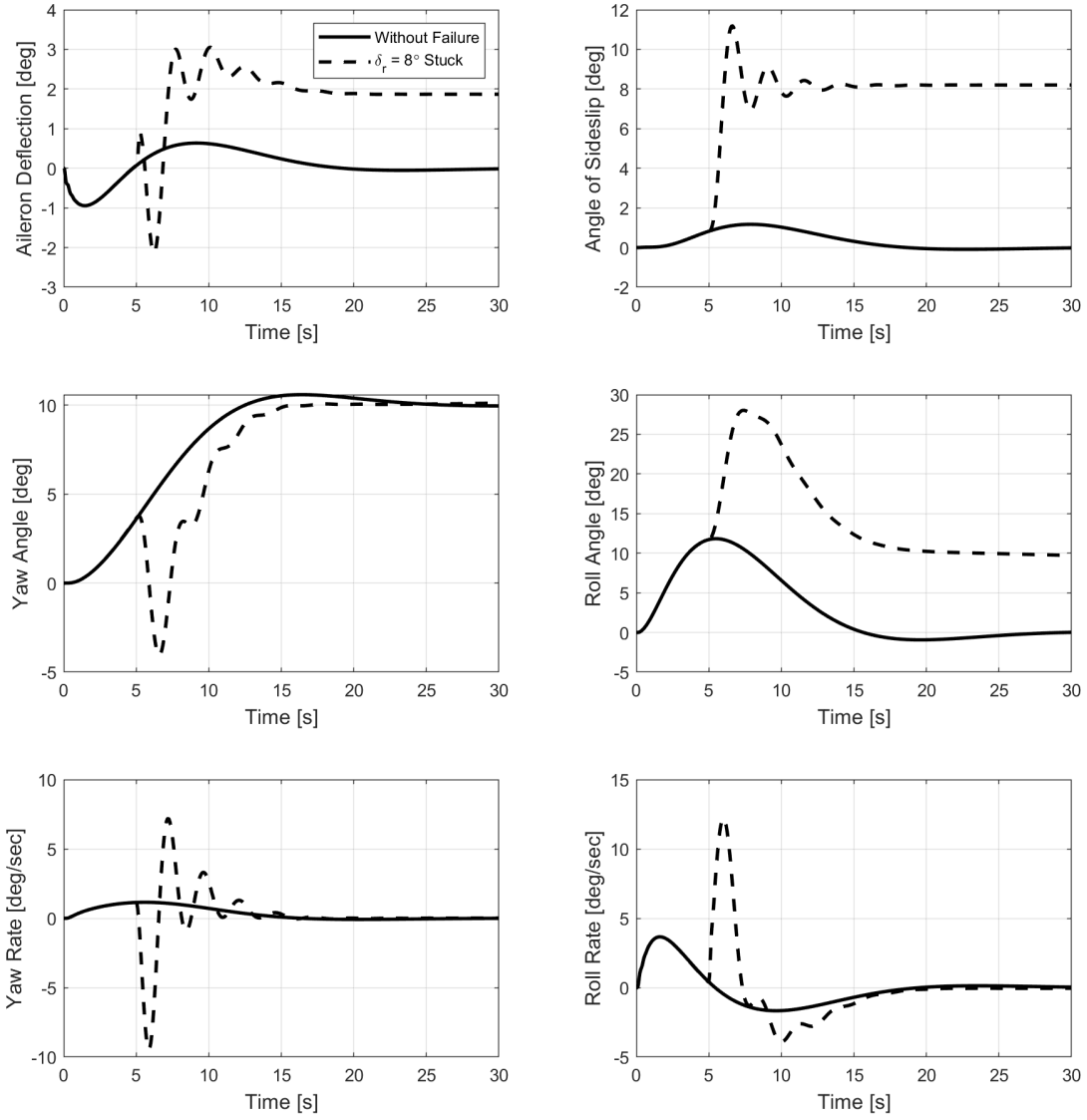

Figure 6.12 Case 4: Rudder jamming at 8° deflection

In figure 6.13, the rudder is deflected to a negative two-degree angle. This time, the aircraft changed its motion. The initial response to failure at five seconds is that the yaw rate is increased the way of the given reference yaw angle. Therefore, the yaw angle is increased from four degrees to ten degrees. Suddenly, the reference trajectory steady state value is reached. To hold the aircraft in the same reference yaw angle, the aileron is deflected to the opposite side of the given yaw angle direction. The angle of the sideslip is changed sigh. That means the track angle is decreased. Almost fifteen seconds into the simulation, all the parameters converged to a steady state value.

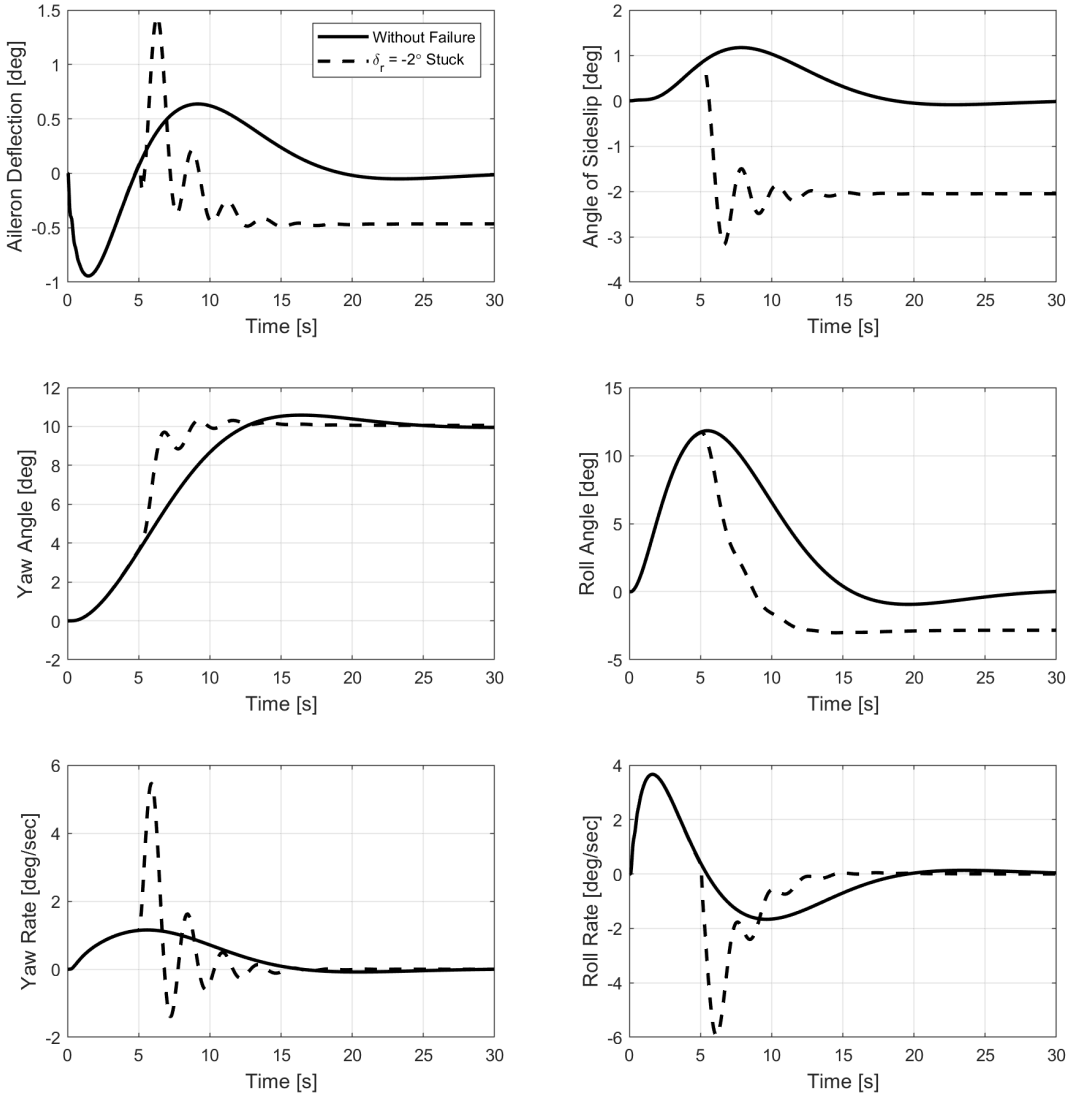

Figure 6.13 Case 5: Rudder jamming at -2° deflection

Figure 6.14 shows the negative five-degree rudder deflection failure case results. The yaw rate increased significantly, which resulted in an increase in the yaw angle. The yaw angle is moved away from the reference trajectory due to rudder failure. The aileron is deflected to the opposite side of the reference yaw angle. That causes the roll angle to become negative. Therefore, the aircraft turns at the given yaw angle due to rudder deflection. However, this turn rate becomes very high; to follow the yaw angle, the aileron is deflected in another direction. Hence, the yaw angle is decreased by the aileron deflection. NMPC handles rudder stuck failure without showing any uncontrollable motion.

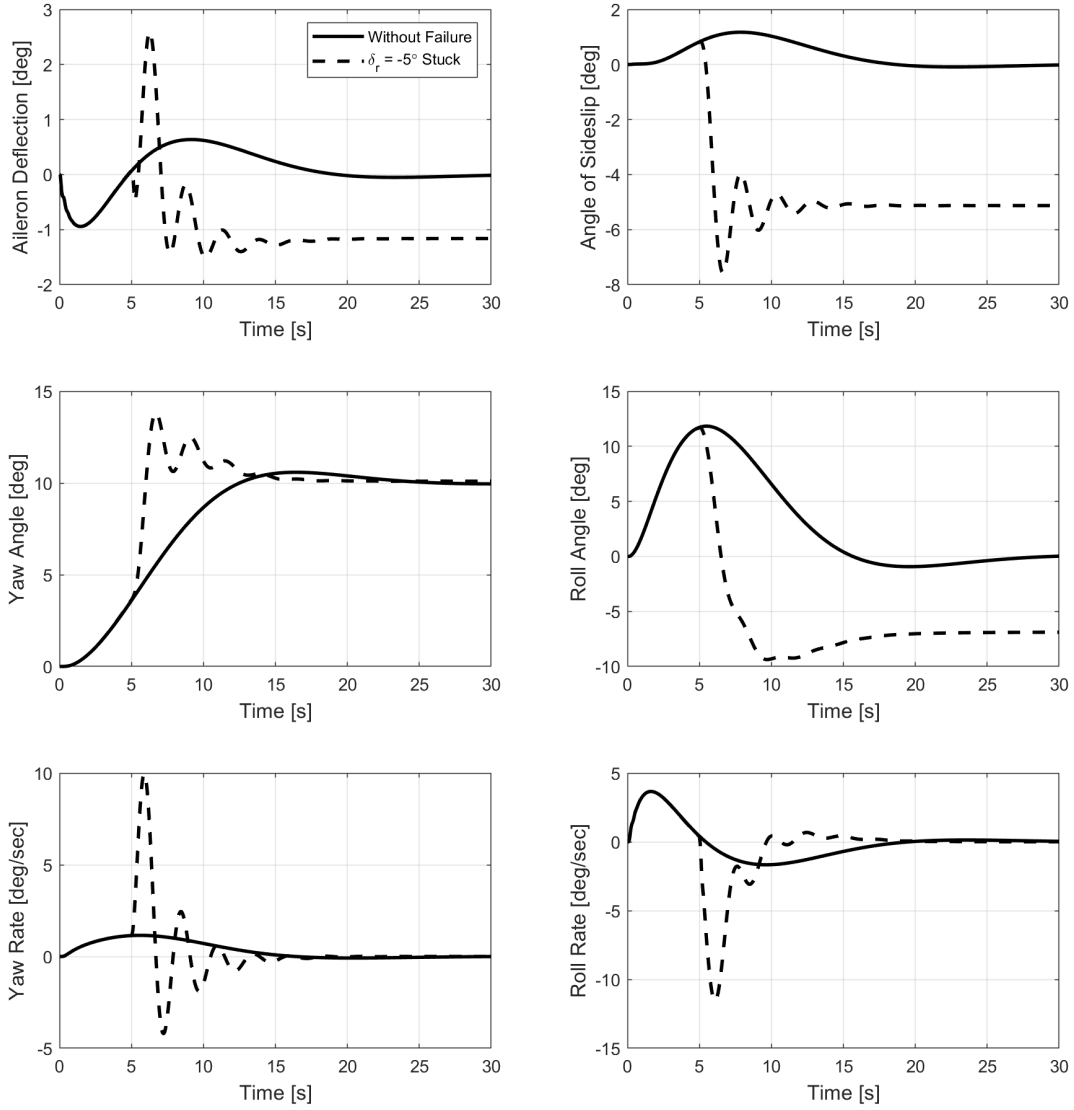

Figure 6.14 Case 6: Rudder jamming at -5° deflection

Figure 6.15 shows the negative eight-degree rudder deflection failure case results. Aircraft motion is the same as in other negative rudder stuck cases. The only difference is the magnitude of the rudder increases the yaw rate, which increases the yaw angle. The aileron deflected more than in the previous failure cases to follow the given yaw angle. Due to this increase, the roll angle magnitude increases. The angle of the sideslip magnitude reached negative eight degrees. That causes a decrease in the track angle. Parameters converged at fifteen seconds, and the amplitude of the oscillations increased. The NMPC input controls the aircraft by following the given yaw angle.

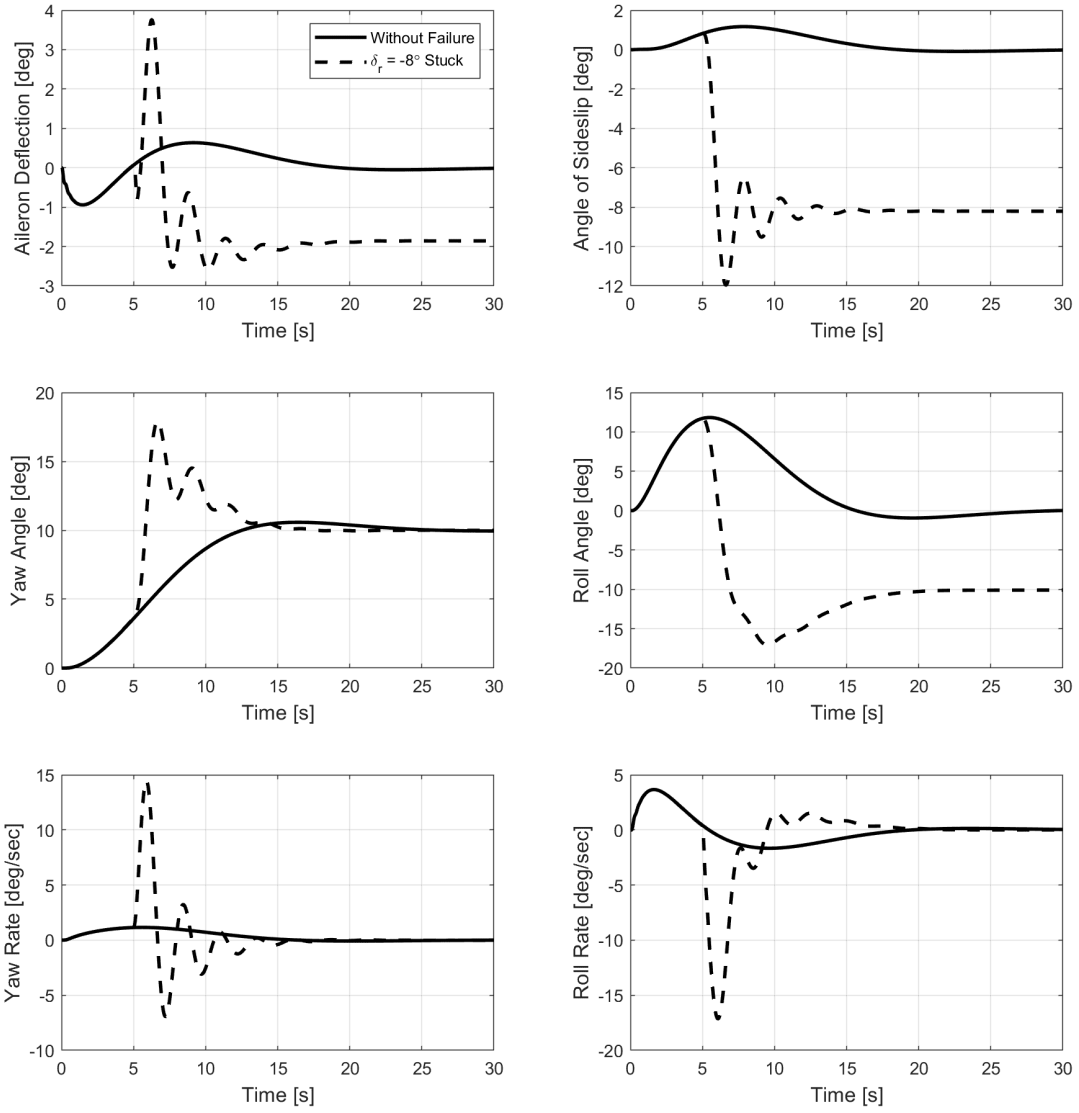

Figure 6.15 Case 7: Rudder jamming at -8° deflection

Table 6.1 shows the rudder stuck results. Three of the performance parameters are compared, and the results are presented. Yaw rate, roll rate, and roll angle results are shown to overshoot value, settling time, and a steady-state value. A comparison can be made by examining the values of the parameters. The first performance parameter is the maximum overshoot value. In the rudder stuck case, there is no fault for the first five seconds; after that, the rudder becomes stuck. Because of that, the first five seconds overshoot or the general behavior is not important. As the magnitude of the failure increased, the maximum overshoot of the aircraft increased, which is expected. Because as the failure increases, NMPC gives higher magnitude inputs to the aircraft model. The table shows that all parameters, yaw rate, roll rate, and roll angle overshoot value increase with the stuck angle magnitude. That indicates that NMPC gives higher, more aggressive input to the model. The -8-degree rudder stuck case especially shows a higher overshoot than others.

Comparison can be made by examining the failure cases with the fault cases. The settling time of the yaw rate, roll rate, and yaw rate are almost similar as the failure magnitude increases; the required time to settle increases. However, this increase is not too marginal. That shows that NMPC tries to follow the given path as soon as possible. However, this increase will be more when the stuck angle increases.

Steady-state values of the rates are similar. The yaw rate and roll rate become zero when the reference yaw angle is reached. That indicates that NMPC tries to follow the same path. The only significant difference is the roll angle. Roll angle steady-state value changes with the failure because the model attempts to follow the given path even though the rudder tries to turn the aircraft. When the rudder is stuck at positive angles, the aircraft attempts to turn left; on the other hand, the reference input is the right yaw angle. To follow the given reference path, the aircraft turns to a positive roll angle. Similarly, when the rudder is stuck at negative deflections, the aircraft turns to the right; however, this turn tendency is higher than the given path. To overcome this situation, NMPC turns the aircraft to the left so that the aircraft can follow the given path.

Overshoot value, settling time, and roll angle show that NMPC can easily control the aircraft in an emergency due to rudder jamming. Maximum overshoot values are not too high, settling time does not increase too much, and steady-state values are similar except for roll angle.

Overall, coordinated turn maneuvers can be performed without danger in rudder-stuck cases. Simulations show that aircraft can be controlled without showing any uncontrollable motion. However, this failure could be a landing maneuver or rapid maneuver situation, and this overshoot or settling time could be a problem. Therefore, this should be considered during the controller's design process.

Table 6.1 Yaw rate, roll rate, and roll angle simulation results, in rudder stuck failure

Parameter	**Cases**	**Maximum Overshoot Value**	**Settling Time [sec]**	**Steady State Value**
Yaw Rate [deg/sec]	Without Failure	1.15	16.5	0.01
	Case 1: $\delta_r = 0^\circ$ Stuck	2.47	15.65	-0.01
	Case 2: $\delta_r = 2^\circ$ Stuck	2.23	16.05	0.01
	Case 3: $\delta_r = 5^\circ$ Stuck	-4.98	17.9	0.02
	Case 4: $\delta_r = 8^\circ$ Stuck	-9.44	18.15	0.01
	Case 5: $\delta_r = -2^\circ$ Stuck	5.46	16.65	0.02
	Case 6: $\delta_r = -5^\circ$ Stuck	9.95	19.6	0.02
	Case 7: $\delta_r = -8^\circ$ Stuck	14.44	21.1	0.01
Roll Rate [deg/sec]	Without Failure	-1.66	18.9	-0.05
	Case 1: $\delta_r = 0^\circ$ Stuck	-2.37	17.9	-0.03
	Case 2: $\delta_r = 2^\circ$ Stuck	-1.85	18.75	-0.03
	Case 3: $\delta_r = 5^\circ$ Stuck	6.68	20.2	-0.1
	Case 4: $\delta_r = 8^\circ$ Stuck	12.22	21.45	-0.05
	Case 5: $\delta_r = -2^\circ$ Stuck	-5.94	18.8	0
	Case 6: $\delta_r = -5^\circ$ Stuck	-11.5	21	0.01
	Case 7: $\delta_r = -8^\circ$ Stuck	-17.14	21.75	0.02
Roll Angle [deg]	Without Failure	-0.9	17	0
	Case 1: $\delta_r = 0^\circ$ Stuck	-0.2	18.85	-0.05
	Case 2: $\delta_r = 2^\circ$ Stuck	13.31	17.85	2.89
	Case 3: $\delta_r = 5^\circ$ Stuck	20.18	19.6	6.9
	Case 4: $\delta_r = 8^\circ$ Stuck	27.9	20	10.2
	Case 5: $\delta_r = -2^\circ$ Stuck	-3	19	-2.84
	Case 6: $\delta_r = -5^\circ$ Stuck	-9.35	20.3	-6.95
	Case 7: $\delta_r = -8^\circ$ Stuck	-17.06	21.8	-10.11

Figures 6.16 and 6.17 figures show the aircraft motion under the rudder stuck failure case. Figure 6.16 shows the 3D view of the motion. The z-axis shows the altitude change, the x-axis shows the forward motion, and the y-axis shows the lateral movement of the aircraft. The aircraft is turning without showing any uncontrollable motion. Altitude is constant during the simulation. The track of the aircraft is not the same; on the other hand, the yaw angle of the aircraft is the same.

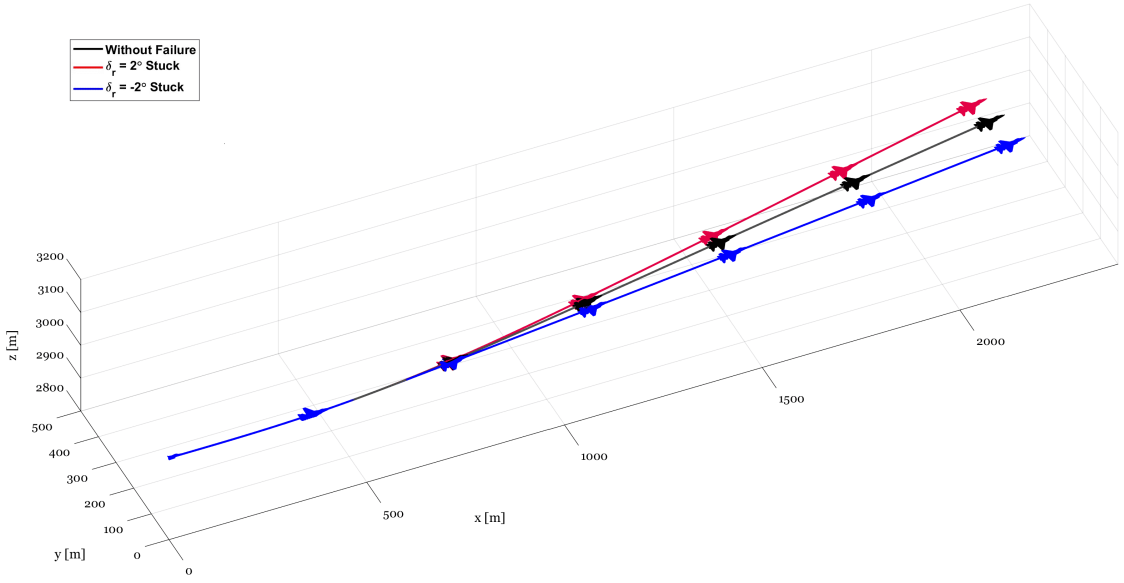

Figure 6.16 3D view of the rudder stuck simulation

Figure 6.17 shows the top view and the side view of the motion. In the top view, the aircraft does not follow the same path in the failure cases. The reason for this is that in the lateral directional analysis, the yaw angle is followed, not the track angle. The yaw angle is the same for all analyses. However, the track angle is the summation of the sideslip and yaw angle. An increase or decrease in the sideslip angle changes the aircraft's track. Also, the side view of the figure shows the aircraft's altitude changes. In the first simulations, the attempt altitude is decreasing due to the roll maneuver. A longitudinal NMPC controller is used to hold the aircraft. Constant altitude value is given during the simulations. Simulation duration is increased; however, altitude becomes constant, as shown in the figure from the side view.

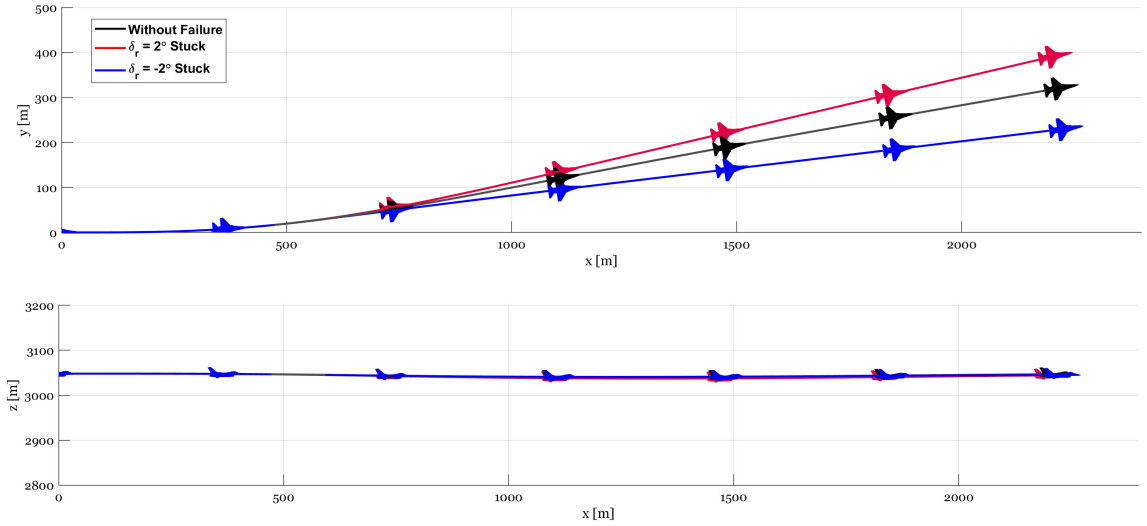

Figure 6.17 Top view and side view of the rudder stuck simulation

6.4. Aileron Jamming

Aileron jamming is simulated with the 6DoF UAV model. A coordinated turn maneuver is used for the analysis. In the analysis, the aileron surface is stuck at different deflections, and NMPC tries to follow the given yaw angle by controlling the rudder deflection. Various aileron jamming analyses are executed. Without the aileron control surface, the rudder is the only control surface to follow the given yaw angle. A decision-making algorithm is used to detect the failure, the same as rudder jamming. When the output of the model is not equal to the output of the NMPC, the algorithm detects the failure and selects the appropriate NMPC controller.

Figure 6.18 shows aileron stuck cases inputs. The solid line shows the without-failure case. Dash and dot lines show the stuck cases. At the time of five seconds in the simulation run, failure starts. At the time of five seconds, aileron deflection is almost zero degrees in the case of without failure. After this point, the aileron is rotated to positive two-degree and negative two-degree deflections in two different analyses. In the aileron jamming failure, two studies are performed. In this analysis, simulations are performed in fifty seconds to show the aircraft motion.

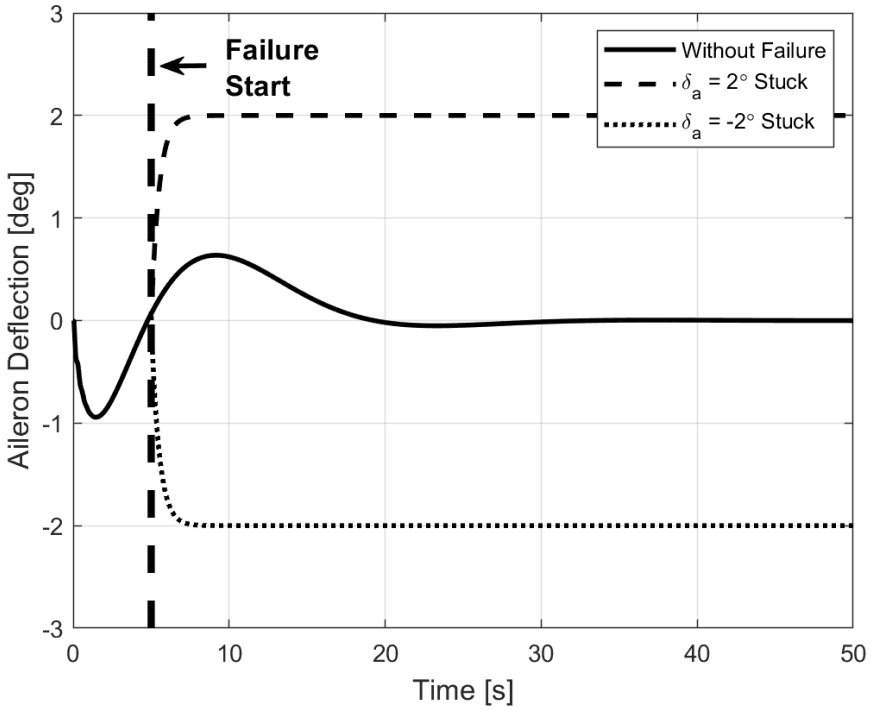

Figure 6.18 Aileron deflections with the different fault cases

Aileron jamming analyses are performed with the 6DoF UAV model with an NMPC controller. Figure 6.19 shows the aircraft motion under the failure cases. Three different analyses are shown in these graphs. The solid line shows the without failure case; the dashed line shows the positive two-degree aileron stuck, and the dotted line shows the negative two-degree aileron stuck failure case. In this simulation, both longitudinal and lateral directional NMPCs are used. A coordinated turn maneuver was tried to perform in the lateral directional motion. Like the rudder jamming case, the yaw angle reference is given as figure 6.7. A ten-degree yaw angle is the reference input for the NMPC. When the aileron is stuck, using the rudder control surface is the only way to control the aircraft on the lateral directional axis. Due to aileron deflection, the aircraft rolls in the given aileron deflected way. The roll angle figure shows that the roll degree increases with time. Because of this increase, aircraft turn to the given aileron direction, which can be seen in the yaw angle graph. On the other hand, this increase is higher than the given reference yaw angle. To overcome this increase in yaw angle, the NMPC deflects the rudder on the other side. Even though the maximum rudder is deflected, fifteen degrees,

the aircraft continues to increase its yaw angle. These two analyses show that with a small aileron stuck cases, aircraft can not follow the given yaw angle with only the rudder control surface. That indicates the rudder-only configuration cannot control aileron stuck failure to perform coordinated turn maneuvers. Different aileron deflection failures are not evaluated due to these uncontrollable results.

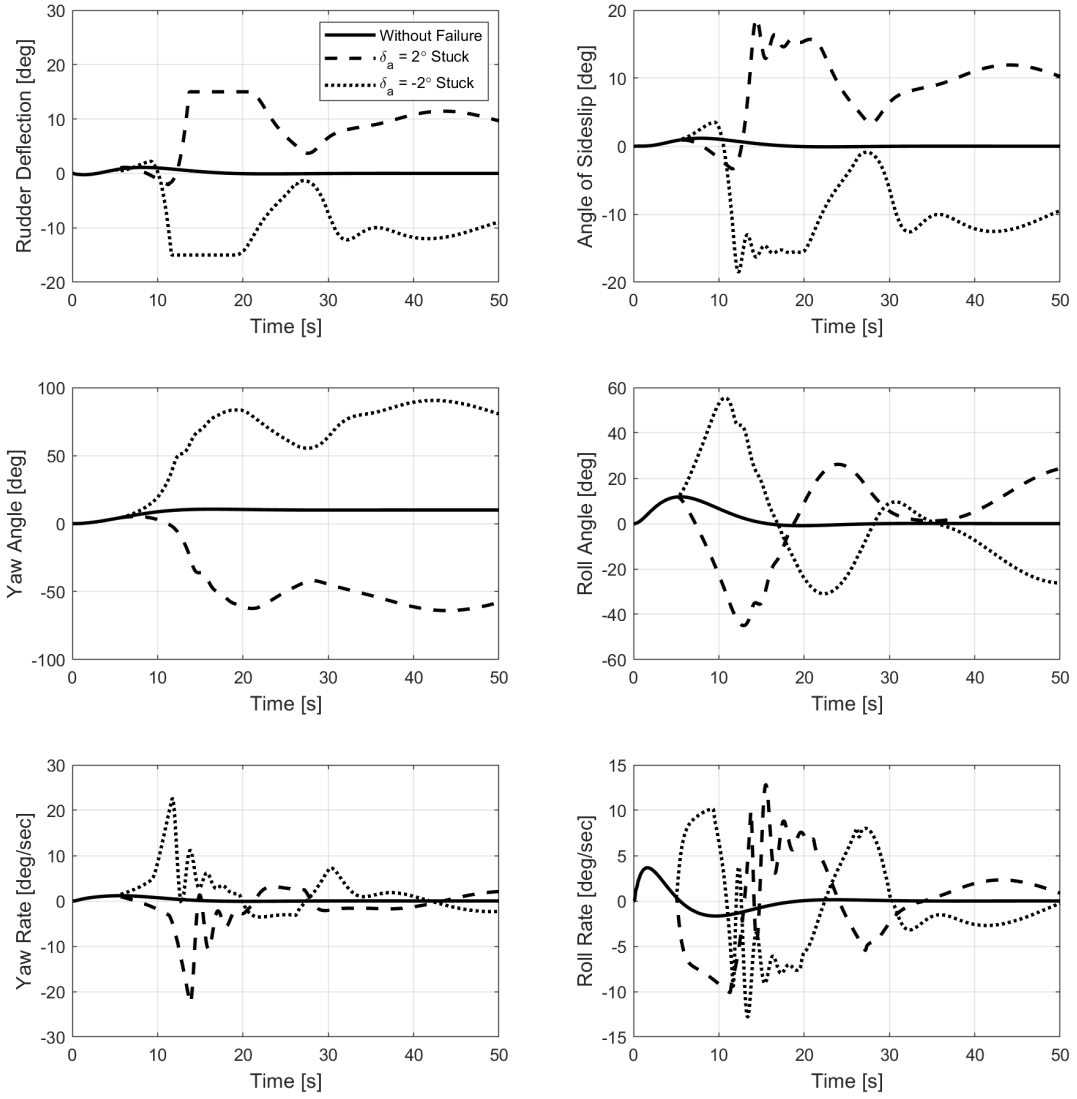

Figure 6.19 Case 1: Aileron jamming at 2° and -2° deflection

6.5. Conclusion

To summarize, various failure scenarios have been analyzed, and results presented. The analysis is mainly divided into two categories. One is effectiveness decrease, and the other is jamming failures. Longitudinal and lateral-directional NMPC are used in these analyses. In the elevator effectiveness case, only longitudinal NMPC is used. In the jamming cases, both controllers are used. The motion of the aircraft is presented in both graphs and 3D views.

Findings of this study can be summarized as:

- **Elevator Effectiveness decrease:** As the elevator's effectiveness is decreased, NMPC gives a higher amplitude of the elevator to follow the given altitude. So that aircraft can follow the given altitude path without showing any uncontrollable motion. All parameters are behaves same except elevator deflection and this is due to deficiency. Figure 6.1 to figure 6.6 are the elevator failure results.

- **Rudder Jamming:** Various analyses have been executed. NMPC handles different failure cases without showing any uncontrollable motion. The coordinated maneuver is performed with the failure cases. Steady-state durations and oscillation of the parameters are presented in Table 6.1. Figure 6.7 to figure 6.17 are the rudder jamming failure results. As the magnitude of the rudder deflection increases in case of failure, the overshoot and settling time of the parameters increase. This situation does not affect the coordinated turn maneuver; however, in the case of landing procedure, could cause problem.

- **Aileron Jamming:** In this failure, the aircraft could not be controlled because the aircraft wanted to turn as much as possible due to the aileron being stuck; the rudder could not overcome this turn tendency. Figure 6.18 and figure 6.19 are the aileron jamming failure results.

7. CONCLUSION

7.1. Conclusion

This thesis applies the Nonlinear Model Predictive Control method in fault-tolerant control for aircraft systems, focusing on various fault scenarios involving control surface jamming and control surface effectiveness degradation as potential failures.

A 6DoF model is developed using Ryan Navion general aviation aircraft aerodynamic and mass data. In the model, aerodynamics, mass, engine, environment, and equations of motion are developed. The simulations use a nonlinear model predictive controller for longitudinal and lateral-directional motion. NMPC is divided into two. One controls the altitude change, and the other controls the coordinated turn maneuver. Internal model equations for the NMPC are derived and integrated into the ACADO toolkit. Control is done by the elevator and the aileron and rudder control surfaces. Also, fault detection is based on statistical data and decision-making algorithms. After detecting the fault, the appropriate NMPC is selected during the simulation using the multiple modeling and switching algorithm. The fault scenarios are decreased elevator control power, rudder jamming, and aileron jamming. Multiple degrees of fault analyses are performed and presented.

The decreased elevator effectiveness is detected by comparing pitch rate data with the statistical data from the fault detection system. The moment a deviation from the expected pitch rate is considered the failure start time. Then, the control model switches to the NMPC model, which is tolerant to decreased elevator effectiveness failure, and the analysis continues with the appropriate model. As the elevator's effectiveness decreases, the elevator surface should be deflected at a higher angle to follow the given altitude trajectory and perform a safe flight. Analysis results show that the NMPC model exhibits similar behavior, and altitude tracking is accomplished with higher deflected elevator inputs. Also, the fault detection algorithm carries out its function efficiently under various

elevator deficiency conditions. NMPC operates successfully through altitude tracking and ensures safe flight under elevator deficiency faults.

The decision-making rule detects rudder jamming failure, and it has been demonstrated that this detection method works successfully in multiple degrees of fault scenarios. When a fault is detected, the model switches to the NMPC model, which is tolerant to the rudder jamming failure. In cases of rudder jamming failure, the aileron surface can assist in tracking the route. Based on the analysis results, when the rudder jamming happens, the NMPC can track the flight path with the help of the aileron. It is observed that as the angle at which rudder jamming occurs increases, aileron deflection also increases. However, as presented in the figures, oscillation is observed in the yaw rate, and the roll rate results in the early moments of the fault. As the angle at the rudder stuck increases, the amplitude of the oscillations increases. Later in the analysis, results that were compatible with the analysis without model errors were obtained. Consequently, the NMPC can operate the aircraft safely with rudder jamming faults.

The final analysis is done with the aileron jamming failure. A fault is detected like a rudder stuck case with the decision-making rule. After the fault is detected, NMPC tries to follow the given yaw angle. Simulation results show that the aircraft cannot controlled due to the rolling motion of the aircraft. A stuck aileron makes the aircraft turn the body's fixed coordinate system x-axis. The rudder is deflected on the opposite side to stop the rolling motion. On the other hand, this causes a change in the yaw direction. Therefore, aircraft can not perform coordinated turn in case of aileron jamming failure.

To summarize, the findings of this study demonstrate the potential of NMPC fault-tolerant control strategies to improve the safety and performance of aircraft systems in the face of unexpected failures during the flight. NMPC handles multiple faults and follows the given trajectory with an outstanding performance.

7.2. Future Work

Future research efforts may be directed toward exploring a broader range of failure scenarios, including scenarios where the control surface can rotate freely. This scenario will bring about a situation where only aerodynamic forces and moments control the movement of the control surfaces in flight, negating any authority over the dysfunctional control surface. Moreover, in the aileron stuck analysis, the aircraft continued to turn in the roll axis, and because of that, the coordinated turn maneuver was not successfully done. However, this might be overcome with the two-engine aircraft so that the engine can be used to control the aircraft's rotation. Also on the list of possible research topics is an investigation into engine failures, another promising line of study. Analyzing failure scenarios associated with crucial phases of aircraft operations like take-off and landing may help make the system more robust. In other aspects, the current six degrees of freedom model also adds the elevator dynamics and interactions with the stick, which makes the fault-tolerant control system more comprehensive. The work in these fields will enhance our current fault-tolerant control strategies and thus ensure the safety and reliability of aerial vehicles in the future.

REFERENCES

[1] Michel Verhaegen, Stoyan Kanev, Redouane Hallouzi, Colin Jones, Jan Maciejowski, and Hafid Smail. Fault tolerant flight control - a survey. *Lecture Notes in Control and Information Sciences*, page 47–89, 2010.

[2] T Suit Wiliam. Aerodynamic Parameters of the Navion Airplane Extracted from Flight Data. Technical Report ADA029345, NASA Langley Research Center, Hampton, Va, 1972.

[3] Nirmit Prabhakar, Andrew Painter, Richard Prazenica, and Mark Balas. Trajectory-driven adaptive control of autonomous unmanned aerial vehicles with disturbance accommodation. *Journal of Guidance, Control, and Dynamics*, 41(9):1976–1989, 2018.

[4] Equations for calculation of international standard atmosphere and associated off-standrad atmosphere. https://www.esdu.com/.

[5] Bill Adair. *The mystery of flight 427: Inside a crash investigation*. Smithsonian Institution, 2004.

[6] Bernard Etkin and Lloyd Duff Reid. *Dynamics of flight: Stability and control*. John Wiley Sons, 1996.

[7] Fikret Caliskan, Youmin Zhang, N. Eva Wu, and Jong-Yeob Shin. Actuator fault diagnosis in a boeing 747 model via adaptive modified two-stage kalman filter. *International Journal of Aerospace Engineering*, 2014:1–10, 2014.

[8] Max Schwenzer, Muzaffer Ay, Thomas Bergs, and Dirk Abel. Review on model predictive control: An engineering perspective. *The International Journal of Advanced Manufacturing Technology*, 117(5–6):1327–1349, 2021.

[9] Cambridge dictionary. Accessed: June 2024.

[10] Interim report on the accident on 1st june 2009 to the airbus a330-203 registered f-gzcp operated by air france flight af 447 rio de janeiro. Available at https://bea.aero/docspa/2009/f-cp090601e1.en/pdf/f-cp090601e1.en.pdf, 2009.

[11] Loss of Pitch Control During Takeoff, Air Midwest Flight 5481. Technical report, National Transportation Safety Board - Washington D.C., 2003.

[12] Aircraft accident report: Uncontrolled descent and collision with terrain: USAir Flight 427 Boeing 737-300. Technical report, National Transportation Safety Board - Washington D.C., 1999.

[13] S.Joe Qin and Thomas A. Badgwell. A survey of industrial model predictive control technology. *Control Engineering Practice*, 11(7):733–764, 2003.

[14] Rolf Isermann and Peter Ballé. Trends in the application of model based fault detection and diagnosis of technical processes. *IFAC Proceedings Volumes*, 29(1):6325–6336, 1996.

[15] A statistical analysis of commercial aviation accidents 1958 - 2023, 2024.

[16] Fly safe: Prevention of loss of control accidents — federal aviation administration, October 2016. `https://www.faa.gov/newsroom/fly-safe-prevention-loss-control-accidents-4?newsId=86688/`.

[17] Loss of control — skybrary aviation safety. `https://skybrary.aero/articles/loss-control/`.

[18] Christine M. Belcastro, John V. Foster, Richard L. Newman, Loren Groff, Dennis A. Crider, and David H. Klyde. Aircraft loss of control: Problem analysis for the development and validation of technology solutions. *AIAA Guidance, Navigation, and Control Conference*, Jan 2016.

[19] Jin Jiang and Xiang Yu. Fault-tolerant control systems: A comparative study between active and passive approaches. *Annual Reviews in Control*, 36(1):60–72, Apr 2012.

[20] Isabelle Fantoni Hassan Shraim Clovis Francis Majd Saied, Benjamin Lussier. Active versus passive fault-tolerant control of a redundant multirotor uav. *Aeronautical Journal-New Series*, 124(1273):385–408, 2019.

[21] Kumpati S Narendra, Jeyendran Balakrishnan, and Kemal M Ciliz. Adaptation and learning using multiple models, switching, and tuning. *IEEE Control Systems*, 15(3):37–51, Jun 1995.

[22] Reza Kamyar and Ehsan Taheri. Aircraft optimal terrain/threat-based trajectory planning and control. *Journal of Guidance, Control, and Dynamics*, 37(2):466–483, Mar 2014.

[23] L. Grüne and J. Pannek. *Nonlinear model predictive control: Theory and algorithms*. SPRINGER INTERNATIONAL PU, 2018.

[24] Xuguang Liu, Yuean Wu, Changping Du, Jiahao Yu, and Yao Zheng. Trajectory tracking control for flapping-wing uav based on model-free predictive control. *2023 IEEE International Conference on Mechatronics and Automation (ICMA)*, Aug 2023.

[25] Ciprian Lupu. Switching solution for multiple-models control systems. *2006 14th Mediterranean Conference on Control and Automation*, Dec 2006.

[26] Chae-Ik Ahn, Youdan Kim, and Hyounjin Kim. Adaptive sliding mode controller design for fault tolerant flight control system. *AIAA Guidance, Navigation, and Control Conference and Exhibit*, Jun 2006.

[27] Guillaume Ducard, Hans P. Geering, and Emil Dumitrescu. Efficient control allocation for fault tolerant embedded systems on small autonomous aircrafts. *2006 International Symposium on Industrial Embedded Systems*, 2006.

[28] Fikret Caliskan and Chingiz Hajiyev. Active fault-tolerant control of uav dynamics against sensor-actuator failures. *Journal of Aerospace Engineering*, 29(4), Jul 2016.

[29] George Zogopoulos-Papaliakos, George C. Karras, and Kostas J. Kyriakopoulos. A fault-tolerant control scheme for fixed-wing uavs with flight envelope awareness. *Journal of Intelligent amp; Robotic Systems*, 102(2), May 2021.

[30] D.G. Dimogianopoulos, J. Hios, and Spilios Fassois. Aircraft fault detection and identification by stochastic functionally pooled modelling of relationships among attitude data. *Proceedings of The Institution of Mechanical Engineers Part G-journal of Aerospace Engineering - PROC INST MECH ENG G-J A E*, 222:801–816, 09 2008.

[31] J. Cieslak, D. Efimov, A. Zolghadri, A. Gheorghe, P. Goupil, and R. Dayre. A method for actuator lock-in-place failure detection in aircraft control surface servo-loops. *IFAC Proceedings Volumes*, 47(3):10549–10554, 2014. 19th IFAC World Congress.

[32] Mathworks. MATLAB R2021a. https://ch.mathworks.com, 2021.

[33] Ferdinand P. Beer, E. Russell Johnston, Phillip Cornwell, Brian Self, and Sanjeev Sanghi. *Vector Mechanics for Engineers: Dynamics*. McGraw-Hill Education, 2020.

[34] R A Minzner, C A Reber, L G Jacckia, F T Huang, A E Cole, T J Kantor, T J Kenesbea, S P Zimmerman, and J M Forbes. Defining Constants, Equations and Abbreviated Tables of the 1975 U.S. Standard Atmosphere. Technical report, National Aeronautics and Space Administration - Washington D.C., 1976.

[35] Staff, Plane Pilot, Desiree Kocis, Isabel Goyer, and Bill Cox. Ryan navion, Feb 2016.

[36] Daniel P. Raymer. *Aircraft design: A conceptual approach*. 1992.

[37] Marcello R. Napolitano. *Aircraft Dynamics: From modeling to simulation*. J. Wiley, 2012.

[38] Robert C. Nelson. *Flight stability and automatic control*. McGraw-Hill Education (India) Private Limited, 2010.

[39] D. Ariens, B. Houska, H. Ferreau, and F. Logist. *ACADO for Matlab User's Manual*. Optimization in Engineering Center (OPTEC), 1.0beta edition, May 2010. `http://www.acadotoolkit.org/`.

[40] Jorge Nocedal and Stephen J. Wright. *Numerical optimization*. Springer, 2006.

[41] J Frédéric Bonnans, Jean Charles Gilbert, Claude Lemaréchal, and Claudia A Sagastizábal. *Numerical Optimization: Theoretical and Practical Aspects*. Springer, 2003.

[42] Brian L. Stevens and Frank L. Lewis. *Aircraft Control and Simulation*. John Wiley Sons, 2016.

[43] Youmin Zhang and Jin Jiang. Bibliographical review on reconfigurable fault-tolerant control systems. *IFAC Proceedings Volumes*, 36:257–268, 06 2003.

[44] Witold Bużantowicz. Matlab script for 3d visualization of missile and air target trajectories. 5:419–422, 09 2016.